Swiss J Geosci (2011) 104:367–408
DOI 10.1007/s00015-011-0072-2

Aalenian to Cenomanian Radiolaria of the Bermeja Complex (Puerto Rico) and Pacific origin of radiolarites on the Caribbean Plate

Alexandre N. Bandini · Peter O. Baumgartner · Kennet Flores · Paulian Dumitrica · Cyril Hochard · Gérard M. Stampfli · Sarah-Jane Jackett

Received: 27 March 2010 / Accepted: 30 July 2011 / Published online: 8 November 2011

Abstract The study of the radiolarian ribbon chert is a key in determining the origins of associated Mesozoic oceanic terranes and may help to achieve a general agreement regarding the basic principles on the evolution of the Caribbean Plate. The Bermeja Complex of Puerto Rico, which contains serpentinized peridotite, altered basalt, amphibolite, and chert (Mariquita Chert Formation), is one of these crucial oceanic terranes. The radiolarian biochronology presented in this work is mainly based by correlation on the biozonations of Baumgartner et al. (1995) and O'Dogherty (1994) and indicates an early Middle Jurassic to early Late Cretaceous (late Bajocian–early Callovian to late early Albian–early middle Cenomanian) age. The illustrated assemblages contain about 120 species, of which one is new (*Pantanellium karinae*), and belonging to about 50 genera. A review of the previous radiolarian published works on the Mariquita Chert Formation and the results of this study suggest that this formation ranges in age from Middle Jurassic to early Late Cretaceous (late Aalenian to early–middle Cenomanian) and also reveal a possible feature of the Bermeja Complex, which is the younging of radiolarian cherts from north to south, evoking a polarity of accretion. On the basis of a currently exhaustive inventory of the radiolarite facies *s.s.* on the Caribbean Plate, a re-examination of the regional distribution of Middle Jurassic sediments associated with oceanic crust, and a paleoceanographic argumentation on the water currents, we come to the conclusion that the radiolarite and associated Mesozoic oceanic terranes of the Caribbean Plate are of Pacific origin. Eventually, a discussion on the origin of the cherts of the Mariquita Formation illustrated by Middle Jurassic to middle Cretaceous geodynamic models of the Pacific and Caribbean realms bring up the possibility that the rocks of the Bermeja Complex are remnants of two different oceans.

Keywords Radiolaria · Radiolarites · Jurassic · Cretaceous · Caribbean Plate · Bermeja Complex

Résumé L'étude des radiolarites rubanées est capitale pour la détermination de l'origine des terrains océaniques allochtones mésozoïques et peut être utile pour parvenir à un compromis général concernant les principes basiques de l'évolution de la Plaque Caraïbes. Le complexe de Bermeja à Puerto Rico qui est constitué de péridotites serpentinisées, de basaltes altérés, d'amphibolites et de cherts (Formation des Cherts de Mariquita), est l'un de ces terrains océaniques déterminants. La biochronologie des radiolaires présentée dans ce travail est basée par

Editorial handling: Elisabetta Erba & Daniel Marty.

A. N. Bandini · P. O. Baumgartner · K. Flores · P. Dumitrica · C. Hochard · G. M. Stampfli
Institut de Géologie et de Paléontologie, Université de Lausanne, bâtiment Anthropole, quartier Dorigny, 1015 Lausanne, Switzerland

A. N. Bandini (✉)
School of Earth and Environment, The University of Western Australia, 35 Stirling Highway, Crawley, WA 6009, Australia
e-mail: alexandre.bandini@uwa.edu.au

K. Flores
American Museum of Natural History, Central Park West at 79th Street, New York, NY 10024-5192, USA

S.-J. Jackett
Integrated Ocean Drilling Program, Texas A&M University, 1000 Discovery Drive, College Station, TX 77845-9547, USA

correlation essentiellement sur les biozonations de Baumgartner et al. (1995) et d'O'Dogherty (1994) et indique un âge Jurassique Moyen inférieur à Crétacé Supérieur inférieur (Bajocien supérieur-Callovien inférieur à Albien inférieur supérieur-Cénomanien moyen inférieur). Les assemblages illustrés contiennent environ 120 espèces, parmis lesquelles une est nouvelle (*Pantanellium karinae*), et appartenant à environ 50 genres différents. Une révision des travaux publiés précédemment sur les radiolaires de la Formation des Cherts de Mariquita, ainsi que les résultats de cette étude suggèrent que cette formation a un âge allant du Jurassique moyen au Crétacé Supérieur inférieur (Aalénien supérieur à Cénomanien moyen inférieur) et révèle aussi une caractéristique éventuelle du Complexe de Bermeja qui est le rajeunissement des radiolarites du nord au sud, évoquant une polarité d'accrétion. Sur la base d'un inventaire actuellement exhaustif du facies radiolaritique rubané *s.s.* sur la Plaque Caraïbes, d'un nouvel examen de la distribution régionale des sédiments du Jurassique Moyen associés à de la croûte océanique et d'une argumentation paléocéanographique, nous arrivons à la conclusion que les radiolarites et les unités tectoniques océaniques du Mésozoïque associées de la Plaque Caraïbes sont d'origine pacifique. Finalement, une discussion sur l'origine des cherts de la Formation de Mariquita illustrée par des modèles géodynamiques du Jurassique Moyen au Crétacé moyen des régions pacifique et caraïbes, fait poindre la possibilité que les roches du Complexe de Bermeja proviennent de deux océans différents.

Mots-clé Radiolaria · Radiolarites · Jurassique · Cretacé · Plaque Caraïbes · Complexe de Bermeja

1 Introduction

Geodynamic models describing the Mesozoic history of the Caribbean realm (Fig. 1) can be divided into two main categories. The simplest model consists of an in situ origin of the actual Caribbean plate or *Inter-American Origin Model* (e.g., James 2009). In opposition, a "non-fixist" hypothesis proposes an eastward transport relative to the Americas of oceanic fragments from the Pacific s.l., the *Pacific Origin Model* (e.g., Pindell and Kennan 2009). In this debate, the study of the paleoceanography of radiolarites is a key in determining the origins of Mesozoic oceanic terranes of the Caribbean plate.

The advances in radiolarian biochronology of the last 20 years has allowed to date radiolarites throughout the world which has greatly enhanced our understanding of ancient remnants of ocean floor found in many orogenic settings on land. The Bermeja Complex in south-western Puerto Rico is one of these enigmatic terrane, where elements of oceanic upper mantle, crust and oceanic sediments—mainly radiolarian ribbon chert—are jumbled together in a heavily tectonized mélange.

In this study, we present new radiolarian biochronological data form 16 samples of the Mariquita Chert Formation collected in the Sierra Bermeja. Our data and a review of the previous radiolarian published works (Mattson and Pessagno 1979; Montgomery et al. 1994b) tend to show an early Middle Jurassic (late Aalenian, ca.172 Ma according to Gradstein et al. 2004) maximum age for the Mariquita Formation and the Bermeja Complex, which a priori would be compatible with a Proto-Caribbean or central Atlantic origin of these sediments.

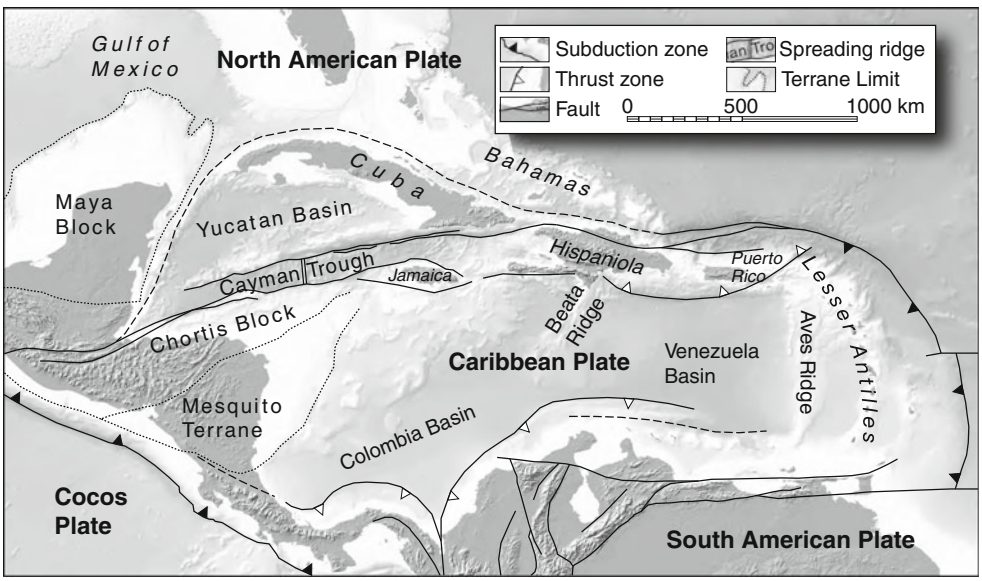

Fig. 1 Circum-Caribbean region map modified from Baumgartner et al. (2008), and Pindell and Kennan (2009) with plate-boundaries and bathymetry, showing important tectonic features

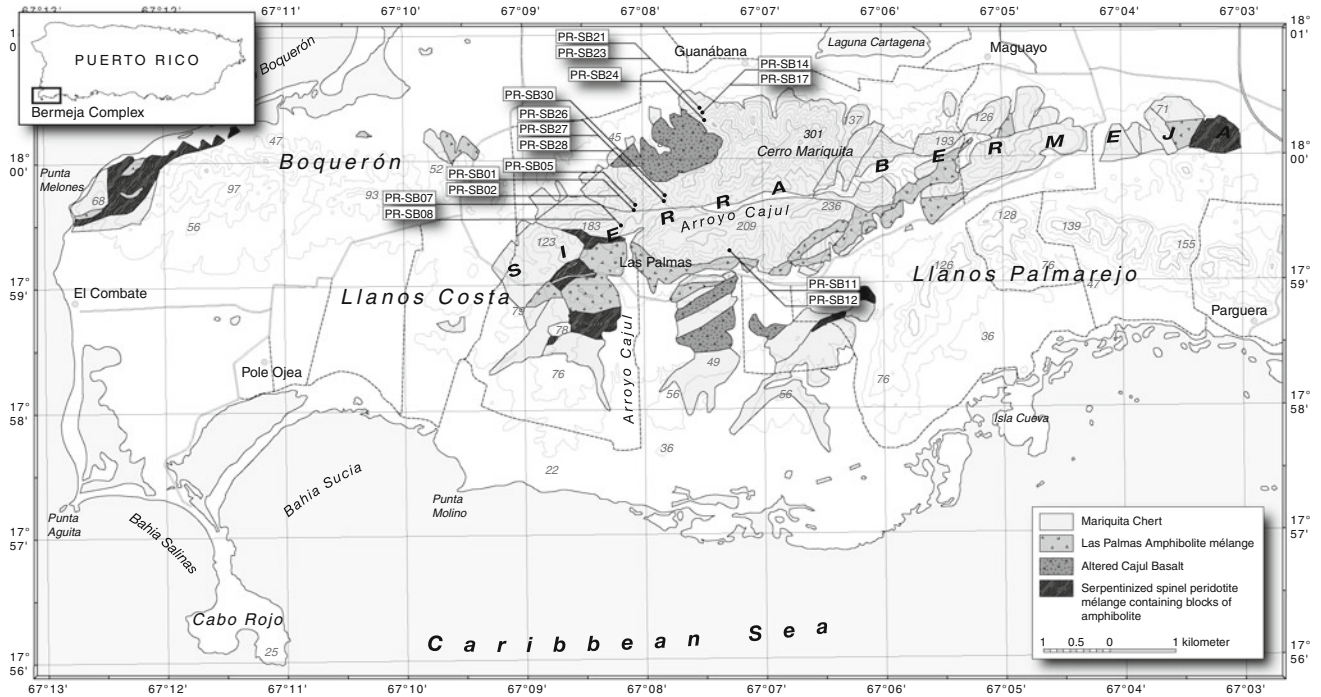

Fig. 2 Geological map of the Sierra Bermeja Complex, which forms a tectonized chaotic mélange containing serpentinized peridotite, altered basalt (Cajul Basalt), amphibolite (Las Palmas Amphibolite) and chert (Mariquita Chert) (modified from Jolly et al. 1998). *Numbers* indicate location of radiolarite samples. The topographical informations are based on the Puerto Real, San German, Cabo Rojo, and La Parguera USGS 1:20,000 quadrangles

The previous argument for a Pacific origin of the Bermeja Complex presented by Montgomery et al. (1994b), based on their radiolarian age and their estimation of the oldest Proto-Caribbean oceanic crust, is nowadays seriously questionable, owing to the recent progresses in radiolarian biostratigraphy and new discoveries on the age of the first oceanic crust spreading between the Americas. Furthermore, we reassess the meaning of the radiolarian *Parvicingulidae*-rich assemblages in the low-latitude Caribbean context as potential indicators of upwelling or land nutrients inputs, instead of indicators of paleolatitudes, as firstly stated by Pessagno and Blome (1986).

Finally, we discuss the emplacement of the cherts of the Bermeja Complex from their supposed Pacific origin to their late Early Cretaceous position based on Middle Jurassic to middle Cretaceous geodynamic models of the Pacific and the Caribbean realms.

2 Geological setting

The Bermeja Complex (Fig. 2) of the Sierra Bermeja in the southwestern part of Puerto Rico was first described by Mattson (1960). It forms a tectonized chaotic mélange, which contains serpentinized peridotite, altered basalt (Cajul Basalt), amphibolite (Las Palmas Amphibolite) and chert (Mariquita Chert). This mélange could clearly be separated from other geological units of the island because of its lithology, tectonic history and age. As noted by Montgomery et al. (1994b), the extensive deformation in the Sierra Bermeja has destroyed most primary textures and bedding. Moreover, stratigraphic relationships between rock types or even between adjacent boulders are difficult to reconstruct in the jumble of floating blocks that comprise the serpentinite mélange. The lack of continuity of stratigraphic contacts and the inclusion of blocks of diverse size, lithology, and age (ranging through 80 Ma) with many adjacent to or floating in serpentinite have suggested to previous workers an ophiolitic mélange (e.g., Mattson 1973; Mattson and Pessagno 1979) forming part of an accretionary complex (Burke 1988).

2.1 The serpentinized peridotite

The serpentinized peridotite is an intensely sheared green, greenish-white, blue-green, or brownish-black rock, in some cases with visible green pyroxene crystals (Mattson 1960). The depleted rare earth patterns of these ultramafic rocks are typical of upper mantle peridotite (Jolly et al. 1998).

2.2 The Cajul Basalt

The Cajul Basalt (Mattson 1960) in the central part of Sierra Bermeja complex and at the type section along Arroyo Cajul exhibits MORB-like Sr, Nd and Pb isotope ratios and depleted normalized REE patterns (Jolly et al. 1998). In the central Sierra Bermeja, the Cajul Basalt is interlayered with the Mariquita Chert suggesting this suite represents the upper part of the transition zone from oceanic basalt to pelagic sediment within the original oceanic crust (Jolly et al. 1998). If this interpretation is correct, the Cajul Basalt could be similar in age to the associated radiolarites.

2.3 The Las Palmas Amphibolite

The Las Palmas Amphibolite (Mattson 1973) has a medium-grade metamorphic paragenesis of green hornblende and calcic plagioclase, sometimes with relics of clinopyroxene, brown hornblende, and plagioclase (Schellekens et al. 1990). Two varieties of amphibolite can be distinguished based on the texture: foliated and non-foliated, there is, however, no difference in mineralogy between the two varieties (Schellekens et al. 1990). In several locations, the presence of chlorite could be an evidence of retrograde metamorphism (Schellekens et al. 1990). The Amphibolite has yielded whole-rock K–Ar ages of hornblende that range from 126 ± 3 and 110 ± 3.3 Ma to 86.3 ± 8.6 and 84.9 ± 8.5 Ma (Mattson 1964, 1973; Tobisch 1968; Cox et al. 1977). These ages are much younger than the ages of associated radiolarian chert and the variations probably reflect multiple periods of metamorphism rather than the actual time of MORB volcanism (Jolly et al. 1998).

2.4 The Mariquita Chert

The Mariquita Chert (Mattson 1973) was named after Cerro Mariquita, the highest peak of the Sierra Bermeja. It is a faulted formation, which overlies the peridotite, volcanic rocks and amphibolite. Lenses of sheared serpentinite mark a somewhat brecciated subhorizontal contact at the base of the chert (Mattson and Pessagno 1979). The chert is a fine-grained greenish-gray, greenish-white, red or dark grey radiolarian ribbon chert rock that generally weathers reddish, and greenish-black chert interlayered with tuffs. Previous radiolarian studies have given ages of chert from the Bermeja Complex that range from Early Jurassic (Montgomery et al. 1994b) and Late Jurassic to Early Cretaceous (Mattson and Pessagno 1979).

3 Radiolarian biochronology

We collected 32 samples in the Sierra Bermeja, of which 16 yielded identifiable radiolarians. In total, about 120 species, of which 1 is new (*Pantanellium karinae*, see systematic paleontology in Appendix A), belonging to about 50 genera, were present in these samples, ranging in age from the early Middle Jurassic to the early Late Cretaceous (late Bajocian–early Callovian to late early Albian–early middle Cenomanian). Apart from radiolarians, no other biogenic constituents were found in the residues. This part includes a brief lithological description and biochronological ages of each localities, which are sorted alphanumerically. Faunal contents are listed in Tables 1, 2, 3, 4, 5, 6, 7, 8, 9, and could also be found with description of the localities in Appendix B.

The dominant radiolarian-bearing lithology of the studied samples is chert. The procedure described by Bandini et al. (2008, p. 6) was used for the extraction of siliceous radiolarians. The remaining material and SEM stubs are stored in the collection of the Musée de Géologie de Lausanne, Université de Lausanne, Switzerland (MGL no. 97008–97023).

The supraspecies taxonomy used in this work follows De Wever et al. (2001) and O'Dogherty et al. (2009a, b). The radiolarian biostratigraphy is mainly based on the Middle Jurassic–Early Cretaceous radiolarian zonation of the InterRad Jurassic-Cretaceous Working Group (Baumgartner et al. 1995) and the middle Cretaceous zonation of O'Dogherty (1994). Both zonations have been established using the Unitary Association method (Guex 1991). Moreover, in order to better constrain age ranges, several assemblages have been compared with radiolarian faunas illustrated by previous authors.

3.1 Samples PR-SB01 and PR-SB02

The decimeter bedded radiolarite is a 6 m thick greenish-white chert sequence that weathers dark grey to black (Fig. 3a, b). This radiolarite is embedded in a massive and intensely brecciated greenish-gray siliceous rock that weathers reddish and composes most of the Sierra Bermeja (Fig. 4). Two of 4 processed samples give radiolarian ages.

3.1.1 PR-SB01 (Table 1; Plate 1)

The species *Emiluvia chica* Foreman, *Svinitzium depressum* (Baumgartner), and *Obesacapsula bullata* Steiger are present in the Tethys zonation of Baumgartner et al. (1995)

Table 1 List of Late Jurassic to Early Cretaceous radiolarian species of samples PR-SB01 and PR-SB02 from the Mariquita Chert Formation of the Bermeja Complex with ranges for the species considered important for the biostratigraphy (see Sect. 3 for detailed discussion)

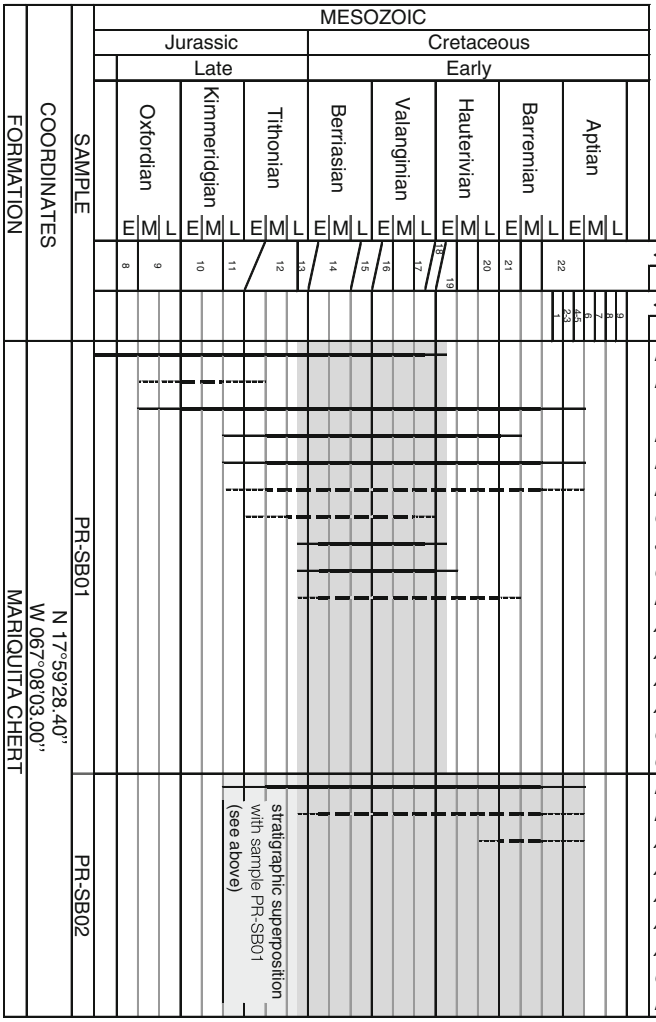

< Unitary Association Zones of BAUMGARTNER et al. 1995

< Unitary Association of O'DOGHERTY 1994

SPECIES	ILLUSTRATIONS
Emiluvia chica FOREMAN	Pl. 1 Fig. 13
Emiluvia cf. *ordinaria* OZVOLDOVA	Pl. 1 Fig. 14
Tethysetta boesii (PARONA)	Pl. 1 Fig. 7
Pseudodictyomitra carpatica (LOZYNIAK)	Pl. 1 Fig. 9
Pantanellium squinaboli (TAN)	Pl. 1 Fig. 17
Hiscocapsa cf. *kitoi* (JUD)	Pl. 1 Fig. 11
Cinguloturris cf. *cylindra* (KEMKIN & RUDENKO)	Pl. 1 Fig. 6
Svinitzium depressum (BAUMGARTNER)	Pl. 1 Fig. 8
Obesacapsula bullata STEIGER	Pl. 1 Fig. 15
Hiscocapsa cf. kaminogoensis (AITA)	Pl. 1 Fig. 10
Amuria sp.	Pl. 1 Fig. 16
Archaeodictyomitra cf. *tumandae* DUMITRICA	Pl. 1 Fig. 3
Archaeodictyomitra pseudomulticostata (TAN)	Pl. 1 Fig. 2
Archaeodictyomitra spp.	Pl. 1 Figs. 4 and 5
Caneta (?) sp.	Pl. 1 Fig. 1
Cryptamphorella sp.	Pl. 1 Fig. 12
Pantanellium squinaboli (TAN)	Pl. 1 Figs. 28-30
Homoeoparonaella cf. *irregularis* (SQUINABOL)	Pl. 1 Fig. 31
Archaeodictyomitra cf. *chalilovi* (ALIEV)	Pl. 1 Fig. 18
Acanthocircus sp.	Pl. 1 Figs. 26 and 27
Archaeodictyomitra cf. *tumandae* DUMITRICA	Pl. 1 Fig. 19
Archaeodictyomitra mitra gr. DUMITRICA	Pl. 1 Fig. 20
Archaeodictyomitra sp.	Pl. 1 Fig. 21
Cryptamphorella spp.	Pl. 1 Figs. 23-25
Pseudodictyomitra cf. *suyarii* DUMITRICA	Pl. 1 Fig. 22

Thin lines are used for first and last appearance intervals and dashed lines for ranges of uncertain determination species ("cf."). The samples are given with their geographic coordinates (WGS 84, °) (see also Fig. 2). The numbers of illustrations in this table correspond to those in Plate 1

and this assemblage corresponds to UAZ 13–18 of latest Tithonian–earliest Berriasian to latest Valanginian–earliest Hauterivian age. This fauna is comparable with the Berriasian assemblages PF28.80 to PF41.75 described by Dumitrica-Jud (1995), Préalpes médianes plastiques, Switzerland). In the same publication, the early Valanginian assemblage PI95.50 from the Umbria-Marche Apenines (Italy) is comparable with our fauna. Our assemblage also bears some resemblance with sample 565 presented by Dumitrica et al. (1997, Maghilah Unit, Oman), which is correlative with the zones E1a and E1b of Jud (1994) of late Berriasian–early Valanginian. A comparable late Berriasian–early Valanginian assemblage from Svinita (Romania) has been observed by Dumitrica (1995, samples Mo17 and Mo22).

3.1.2 PR-SB02 (Table 1; Plate 1)

The occurrence of *Pantanellium squinaboli* (TAN) also present in the zonation of Baumgartner et al. (1995) indicates a late Kimmeridgian–early Tithonian to late Barremian–early Apian (UAZ 11–22) age without further precision. However, it seems to be restricted to the latest Tithonian to late Barremian–early Aptian interval by stratigraphic superposition with sample PR-SB01 (see above).

Table 2 List of Middle Jurassic radiolarian species of sample PR-SB05 from the Mariquita Chert Formation of the Bermeja Complex with ranges for the species considered important for the biostratigraphy (see Sect. 3 for detailed discussion)

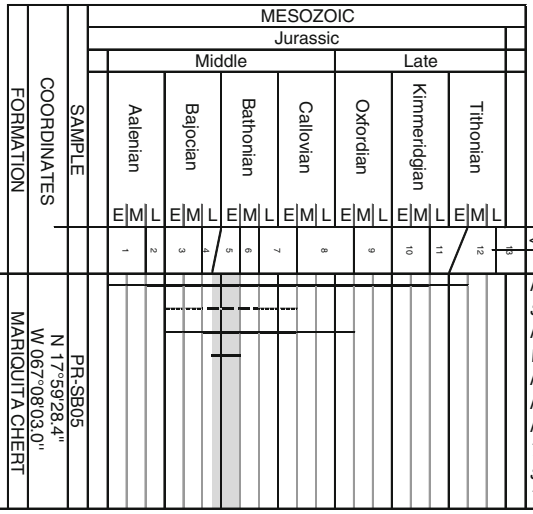

< Unitary Association Zones of BAUMGARTNER et al. 1995

SPECIES	ILLUSTRATIONS
Praewilliriedellum convexum (YAO)	Pl. 2 Figs. 5 and 7
Svinitzium cf. *kamoense* (MIZUTANI and KIDO)	Pl. 2 Fig. 1
Praewilliriedellum japonicum (YAO)	Pl. 2 Fig. 6
Williriedellum tetragona (MATSUOKA)	Pl. 2 Fig. 10
Hexasaturnalis nakasekoi DUMITRICA & DUMITRICA-JUD	Pl. 2 Fig. 11
Hiscocapsa lugeoni O'DOGHERTY, GORICAN & DUMITRICA	Pl. 2 Fig. 4
Parahsuum sp.	Pl. 2 Fig. 3
Triversus (?) sp.	Pl. 2 Fig. 2
Striatojaponocapsa synconexa O'DOGHERTY, GORICAN & DUMITRICA	Pl. 2 Figs. 8 and 9
Tetraditryma sp.	Pl. 2 Fig. 12

Thin lines are used for first and last appearance intervals. The samples are given with their geographic coordinates (WGS 84, °) (see also Fig. 2). The numbers of illustrations in this table correspond to those in Plate 2

Table 3 List of Middle-Late Jurassic and Early–Late Cretaceous radiolarian species of samples PR-SB07 and PR-SB08 from the Mariquita Chert Formation of the Bermeja Complex with ranges for the species considered important for the biostratigraphy (see Sect. 3 for detailed discussion)

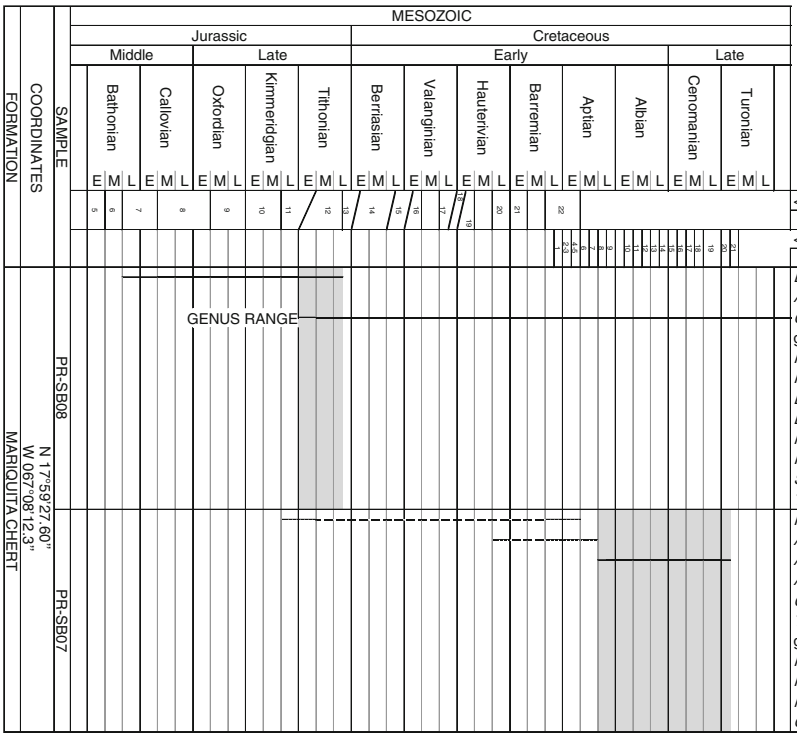

< Unitary Association Zones of BAUMGARTNER et al. 1995

< Unitary Association of O'DOGHERTY 1994

SPECIES	ILLUSTRATIONS
Loopus primitivus (MATSUOKA & YAO)	Pl. 3 Figs. 6 and 7
Archaeodictyomitra spp.	Pl. 3 Figs. 1-5
Cryptamphorella spp.	Pl. 3 Fig. 13-17
gen. et sp. indet.	Pl. 3 Fig. 20
Hiscocapsa campana (KIESSLING)	Pl. 3 Fig. 21
Hiscocapsa cf. *subcrassitestata* (AITA)	Pl. 3 Fig. 22
Loopus aff. *primitivus* (MATSUOKA & YAO)	Pl. 3 Figs. 8 and 9
Loopus sp.	Pl. 3 Fig. 10
Napora spp.	Pl. 3 Figs. 18 and 19
Praeconocaryomma sp.	Pl. 3 Fig. 24
Spinosicapsa (?) sp.	Pl. 3 Figs. 11 and 12
Triactoma sp.	Pl. 3 Fig. 23
Hiscocapsa cf. *uterculus* (PARONA)	Pl. 2 Fig. 27
Archaeodictyomitra cf. *chalilovi* (ALIEV)	Pl. 2 Fig. 13
Archaeodictyomitra montisserei (SQUINABOL)	Pl. 2 Fig. 15
Archaeodictyomitra sp.	Pl. 2 Fig. 14
Cryptamphorella spp.	Pl. 2 Figs. 20-23
Theocampe (?) sp.	Pl. 2 Figs. 16-18
gen. et sp. indet.	Pl. 2 Fig. 19
Hiscocapsa cf. *asseni* (TAN)	Pl. 2 Figs. 28, 30 and 31
Hiscocapsa pseudouterculus (AITA and OKADA)	Pl. 2 Figs. 24-26 and 29
Napora sp.	Pl. 2 Figs. 34 and 35
Obeliscoites (?) sp.	Pl. 2 Figs. 32 and 33

Thin lines are used for first and last appearance intervals and dashed lines for ranges of uncertain determination species ("cf."). The samples are given with their geographic coordinates (WGS 84, °) (see also Fig. 2). The numbers of illustrations in this table correspond to those in Plates 2 and 3

Table 4 List of Early Cretaceous radiolarian species of samples PR-SB11 and PR-SB12 from the Mariquita Chert Formation of the Bermeja Complex with ranges for the species considered important for the biostratigraphy (see Sect. 3 for detailed discussion)

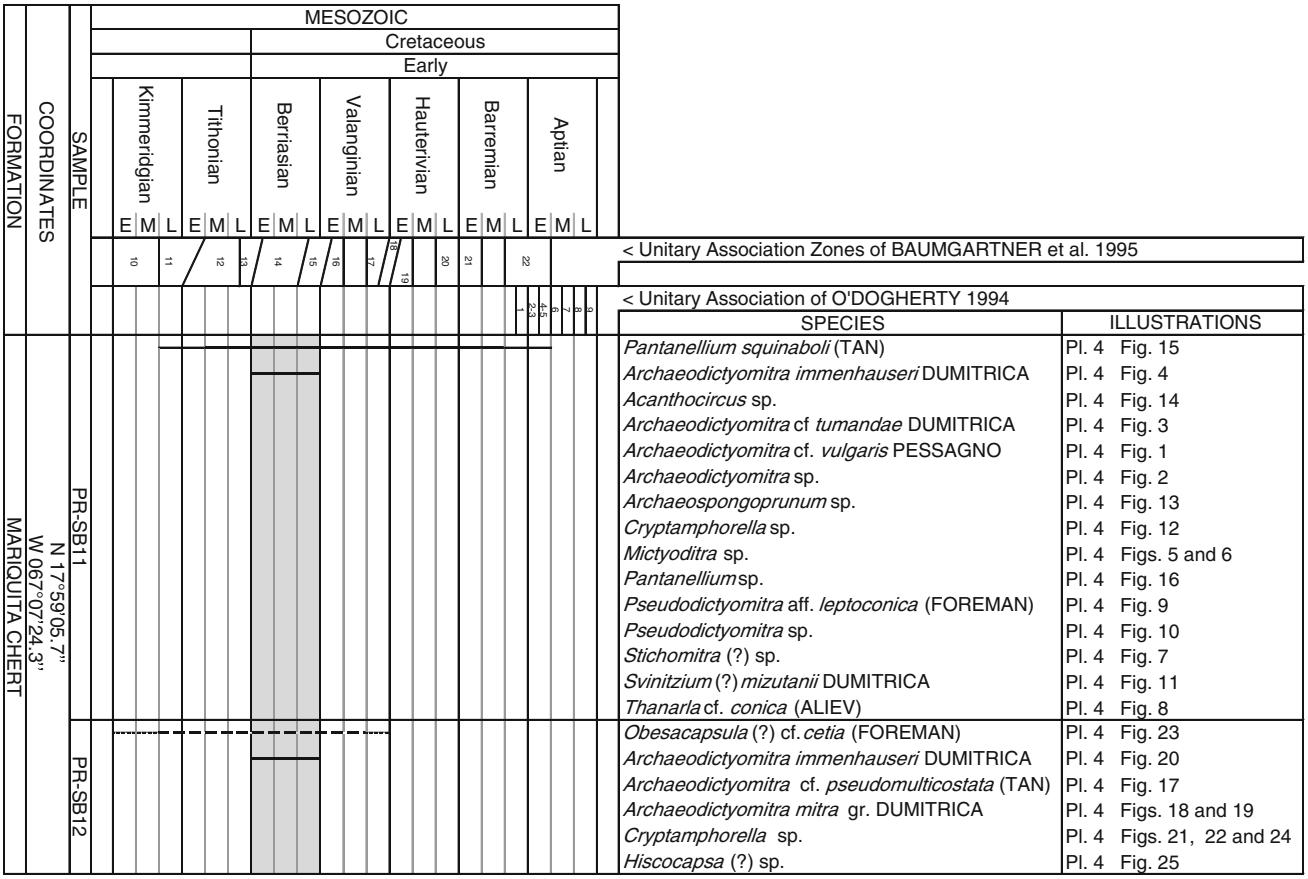

SPECIES	ILLUSTRATIONS
Pantanellium squinaboli (TAN)	Pl. 4 Fig. 15
Archaeodictyomitra immenhauseri DUMITRICA	Pl. 4 Fig. 4
Acanthocircus sp.	Pl. 4 Fig. 14
Archaeodictyomitra cf *tumandae* DUMITRICA	Pl. 4 Fig. 3
Archaeodictyomitra cf. *vulgaris* PESSAGNO	Pl. 4 Fig. 1
Archaeodictyomitra sp.	Pl. 4 Fig. 2
Archaeospongoprunum sp.	Pl. 4 Fig. 13
Cryptamphorella sp.	Pl. 4 Fig. 12
Mictyoditra sp.	Pl. 4 Figs. 5 and 6
Pantanellium sp.	Pl. 4 Fig. 16
Pseudodictyomitra aff. *leptoconica* (FOREMAN)	Pl. 4 Fig. 9
Pseudodictyomitra sp.	Pl. 4 Fig. 10
Stichomitra (?) sp.	Pl. 4 Fig. 7
Svinitzium (?) *mizutanii* DUMITRICA	Pl. 4 Fig. 11
Thanarla cf. *conica* (ALIEV)	Pl. 4 Fig. 8
Obesacapsula (?) cf. *cetia* (FOREMAN)	Pl. 4 Fig. 23
Archaeodictyomitra immenhauseri DUMITRICA	Pl. 4 Fig. 20
Archaeodictyomitra cf. *pseudomulticostata* (TAN)	Pl. 4 Fig. 17
Archaeodictyomitra mitra gr. DUMITRICA	Pl. 4 Figs. 18 and 19
Cryptamphorella sp.	Pl. 4 Figs. 21, 22 and 24
Hiscocapsa (?) sp.	Pl. 4 Fig. 25

Thin lines are used for first and last appearance intervals and dashed lines for ranges of uncertain determination species ("cf."). The samples are given with their geographic coordinates (WGS 84, °) (see also Fig. 2). The numbers of illustrations in this table correspond to those in Plate 4

3.2 Sample PR-SB05 (Table 2; Plate 2)

In this assemblage 4 species included in the zonation of Baumgartner et al. (1995) were found. The species *Williriedellum tetragona* (MATSUOKA) allows to assign the assemblage to the UAZ 5, latest Bajocian to early Bathonian.

3.3 Samples PR-SB07 and PR-SB08

Both radiolarite samples come from two blocks of chert of about 2 m long and 1 m high.

3.3.1 PR-SB07 (Table 3; Plate 2)

The species *Archaeodictyomitra montisserei* (SQUINABOL) is present in the Mid-Cretaceous zonation of O'Dogherty (1994) and corresponds to UA 8 to 20 of early late Aptian to early Turonian age. However, Danelian (2008) have also observed this species in the late Aptian–early Albian sequence of the Sopoti section (southern Albania). This poorly constrained age is also the youngest radiolarian age of the Bermeja Complex, but since this age is mainly based on the occurrence of only one species, which range is not very well constrained, it remains clearly disputable.

3.3.2 PR-SB08 (Table 3; Plate 3)

According to Baumgartner et al. (1995), the presence of *Loopus primitivus* (MATSUOKA & YAO) corresponds to UAZ 7–12 of late Bathonian–early Callovian to early Tithonian–early late Tithonian. Moreover, the presence of genus *Cryptamphorella*, which according to O'Dogherty et al. (2009a) has a range that extended between the early Tithonian and the late Maastrichtian, restricts this interval from early Tithonian to early late Tithonian.

Table 5 List of Middle to Late Jurassic radiolarian species of samples PR-SB14 and PR-SB17 from the Mariquita Chert Formation of the Bermeja Complex with ranges for the species considered important for the biostratigraphy (see Sect. 3 for detailed discussion)

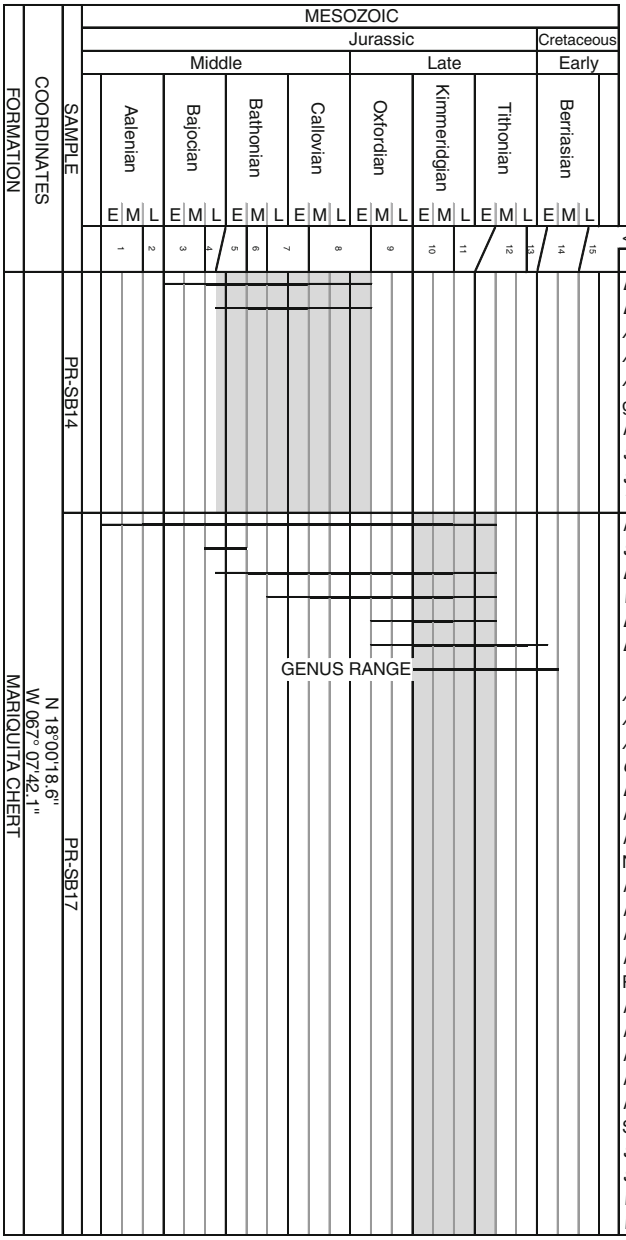

< Unitary Association Zones of BAUMGARTNER et al. 1995	
SPECIES	ILLUSTRATIONS
Eucyrtidiellum unumaense s.l. (YAO)	Pl. 4 Figs. 30 and 31
Eucyrtidiellum unumaense pustulatum BAUMGARTNER	Pl. 4 Fig. 32
Alievium cf. *longispineum* YANG and WANG	Pl. 4 Fig. 37
Archaeodictyomitra prisca KOZUR and MOSTLER	Pl. 4 Fig. 27
Archaeodictyomitra sp.	Pl. 4 Fig. 26
gen. et sp. indet.	Pl. 4 Fig. 29
Homeoparonaella sp.	Pl. 4 Figs. 35 and 36
Spinosicapsa (?) sp.	Pl. 4 Fig. 33
Striatojaponocapsa (?) sp.	Pl. 4 Fig. 34
Transhsuum sp.	Pl. 4 Fig. 28
Praewilliriedellum convexum (YAO)	Pl. 5 Fig. 22
Striatojaponocapsa plicarum (YAO)	Pl. 5 Fig. 20
Eucyrtidiellum ptyctum (RIEDEL and SANFILIPPO)	Pl. 5 Fig. 16
Williriedellum carpathicum DUMITRICA	Pl. 5 Figs. 24 and 25
Emiluvia ordinaria OZVOLDOVA	Pl. 5 Fig. 32
Deviatus diamphidius hipposidericus (FOREMAN)	Pl. 5 Fig. 35
Vallupus hopsoni PESSAGNO and BLOME	Pl. 5 Fig. 17
Archaeodictyomitra patricki KOCHER	Pl. 5 Fig. 1
Archaeodictyomitra spp.	Pl. 5 Figs. 2 and 3
Archaeospongoprunum elegans WU	Pl. 5 Fig. 41
Cryptamphorella sp.	Pl. 5 Fig. 29
Emiluvia (?) sp.	Pl. 5 Fig. 33
Hiscocapsa (?) sp.	Pl. 5 Fig. 23
Napora sp.	Pl. 5 Figs. 18 and 19
Nassellaria gen. et sp. indet.	Pl. 5 Figs. 30 and 31
Pantanellium sp.	Pl. 5 Fig. 37
Pantanellium karinae BANDINI n. sp.	Pl. 5 Figs. 38-40
Pantanellium ranchitoense PESSAGNO and MACLEOD	Pl. 5 Fig. 36
Parvicingula vera PESSAGNO and WHALEN	Pl. 5 Fig. 10
Parvicingulidae PESSAGNO gen. et sp. indet.	Pl. 5 Fig. 8, 9 and 11
Praeconocaryomma sp.	Pl. 5 Fig. 34
Praewilliriellum sp. aff. *robustum* (MATSUOKA)	Pl. 5 Fig. 21
Pseudodictyomitra (?) sp.	Pl. 5 Fig. 12
Pseudodictyomitra sp.	Pl. 5 Fig. 13
Pseudodictyomitrella (?) sp.	Pl. 5 Fig. 4
Spumellaria gen. et sp. indet.	Pl. 5 Fig. 42
Stichomitra (?) *doliolum* AITA gr.	Pl. 5 Figs.14 and 15
Stichomitra (?) spp.	Pl. 5 Figs. 5-7
Williriedellum formosum (CHIARI, MARCUCCI and PRELA)	Pl. 5 Figs. 27 and 28
Williriedellum sp.	Pl. 5 Fig. 26

Thin lines are used for first and last appearance intervals. The samples are given with their geographic coordinates (WGS 84, °) (see also Fig. 2). The numbers of illustrations in this table correspond to those in Plates 4 and 5

3.4 Samples PR-SB11 and PR-SB12

We sampled 3 metric greenish-white radiolarite blocks that weather dark grey and crop out on the slope of the hill, of which two yielded identifiable radiolarians. These blocks are embedded in a massive and brecciated greenish-grey siliceous rock that weathers reddish.

3.4.1 PR-SB11 (Table 4; Plate 4)

The occurrence of *Pantanellium squinaboli* (TAN) also present in the zonation of Baumgartner et al. (1995) indicates a late Kimmeridgian–early Tithonian to late Barremian–early Aptian (UAZ 11–22) age without further precision. This fauna is comparable with the late

Table 6 List of Middle Jurassic radiolarian species of samples PR-SB21 and PR-SB23 from the Mariquita Chert Formation of the Bermeja Complex with ranges for the species considered important for the biostratigraphy (see Sect. 3 for detailed discussion)

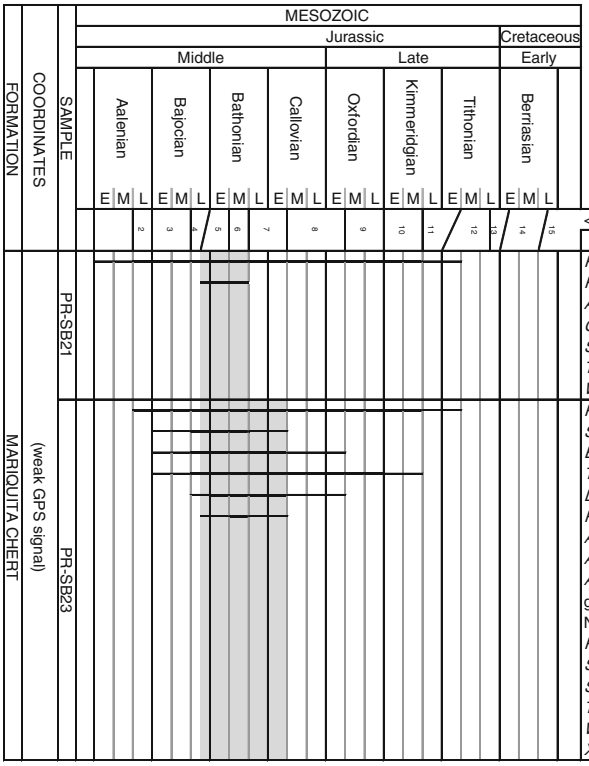

< Unitary Association Zones of BAUMGARTNER et al. 1995

SPECIES	ILLUSTRATIONS
Praewilliriedellum convexum (YAO)	Pl. 6 Fig. 5
Ristola turpicula PESSAGNO and WHALEN	Pl. 6 Fig. 4
Archaeodictyomitra aff. *rigida* PESSAGNO	Pl. 6 Fig. 1
Canoptum (?) sp.	Pl. 6 Fig. 3
Striatojaponocapsa synconexa O'DOGHERTY, GORICAN and DUMITRICA	Pl. 6 Figs. 6 and 7
Transhsuum sp.	Pl. 6 Fig. 2
Williriedellum yaoi (KOZUR)	Pl. 6 Fig. 8
Praewilliriedellum convexum (YAO)	Pl. 6 Figs. 18 and 19
Svinitzium kamoense (MIZUTANI and KIDO)	Pl. 6 Fig. 15
Eucyrtidiellum unumaense s.l. (YAO)	Pl. 6 Fig. 25
Transhsuum maxwelli gr. (PESSAGNO)	Pl. 6 Figs. 11 and 12
Levileugeo ordinarius YANG and WANG	Pl. 6 Fig. 29
Praewilliriedellum robustum (MATSUOKA)	Pl. 6 Fig. 20
Angulobracchia sp.	Pl. 6 Fig. 30
Archaeodictyomitra aff. *rigida* PESSAGNO	Pl. 6 Fig. 9
Archaeodictyomitra patricki KOCHER	Pl. 6 Fig. 10
gen. et sp. indet.	Pl. 6 Figs. 27 and 28
Nassellaria gen. et sp. indet. B	Pl. 6 Fig. 26
Parahsuum sp.	Pl. 6 Fig. 16
Stichomitra (?) sp.	Pl. 6 Fig. 13
*Striatojaponocapsa synconexa*O'DOGHERTY, GORICAN and DUMITRICA	Pl. 6 Figs. 23 and 24
Triversus (?) sp.	Pl. 6 Fig. 14
Williriedellum yaoi (KOZUR)	Pl. 6 Figs. 21 and 22
Xitus sp.	Pl. 6 Fig. 17

Thin lines are used for first and last appearance intervals. The numbers of illustrations in this table correspond to those in Plate 6

Table 7 List of Middle Jurassic radiolarian species of sample PR-SB24 from the Mariquita Chert Formation of the Bermeja Complex with ranges for the species considered important for the biostratigraphy (see Sect. 3 for detailed discussion)

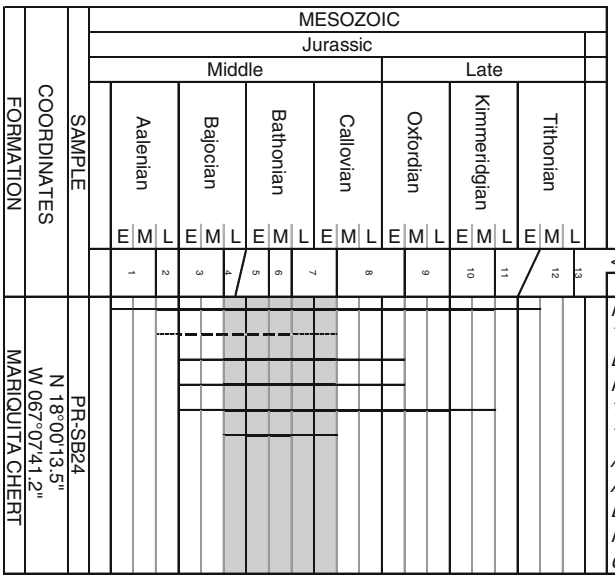

< Unitary Association Zones of BAUMGARTNER et al. 1995

SPECIES	ILLUSTRATIONS
Praewilliriedellum convexum (YAO)	Pl. 6 Fig. 37
Transhsuum cf. *hisuikyoense* (ISOZAKI and MATSUDA)	Pl. 6 Fig. 34
Eucyrtidiellum unumaense (YAO)	Pl. 6 Figs. 41 and 42
Praewilliriedellum japonicum (YAO)	Pl. 6 Fig. 36
Transhsuum cf. *maxwelli* gr. (PESSAGNO)	Pl. 6 Fig. 35
Triactoma parablakei YANG and WANG	Pl. 6 Fig. 39
Archaeodictyomitra aff. *rigida* PESSAGNO	Pl. 6 Fig. 31
Archaeodictyomitra sp.	Pl. 6 Fig. 32
Emiluvia sp.	Pl. 6 Fig. 40
Parahsuum sp.	Pl. 6 Fig. 33
Canoptum (?) sp.	Pl. 6 Fig. 38

Thin lines are used for first and last appearance intervals and dashed lines for ranges of uncertain determination species ("cf."). The samples are given with their geographic coordinates (WGS 84, °) (see also Fig. 2). The numbers of illustrations in this table correspond to those in Plate 6

Table 8 List of Early to Late Cretaceous radiolarian species of samples PR-SB26, PR-SB27 and PR-SB28 from the Mariquita Chert Formation of the Bermeja Complex with ranges for the species considered important for the biostratigraphy (see Sect. 3 for detailed discussion)

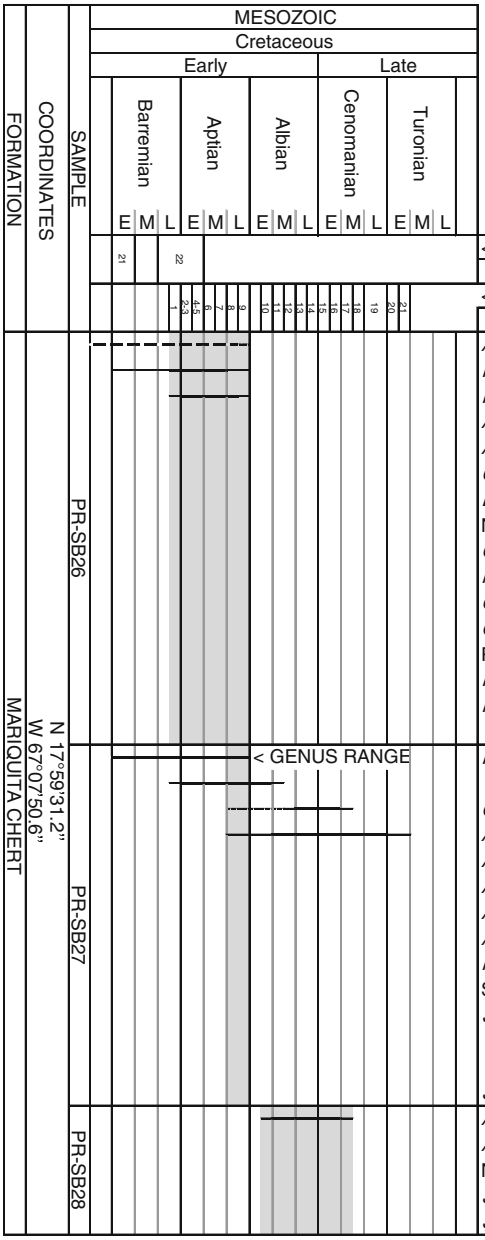

< Unitary Association Zones of BAUMGARTNER et al. 1995	
< Unitary Association of O'DOGHERTY 1994	
SPECIES	ILLUSTRATIONS
Acaeniotyle cf. *umbilicata* (RÜST)	Pl. 7 Fig. 12
Pseudoeucyrtis corpulentus DUMITRICA	Pl. 7 Fig. 5
Pseudoeucyrtis hanni (TAN)	Pl. 7 Fig. 7
Acanthocircus sp.	Pl. 7 Fig. 14
Archaeodictyomitra spp.	Pl. 7 Figs.1 and 2
Crucella sp.	Pl. 7 Fig. 15
Emiluvia sp.	Pl. 7 Fig. 13
Nassellaria gen. et sp. indet.	Pl. 7 Figs. 9 and 11
Crucella sp. (with five rays)	Pl. 7 Fig. 17
Napora sp.	Pl. 7 Fig. 10
Obeliscoites cf. *vinassai* (SQUINABOL)	Pl. 7 Fig. 8
Obesacapsula sp.	Pl. 7 Fig. 6
Pantanelliidae gen. et sp. indet.	Pl. 7 Fig. 16
Parvicingula sp.	Pl. 7 Fig. 4
Praeconocaryomma sp.	Pl. 7 Fig. 18
Thanarla sp.	Pl. 7 Fig. 3
Pantanellium sp.	Pl. 8 Figs. 19 and 20
Thanarla brouweri (TAN)	Pl. 8 Fig. 11
Quadrigastrum lapideum O'DOGHERTY	Pl. 8 Fig. 21
Archaeodictyomitra montisserei (SQUINABOL)	Pl. 8 Figs. 4 and 5
Archaeodictyomitra cf. *gracilis* (SQUINABOL)	Pl. 8 Fig. 3
Archaeodictyomitra cf. *immenhauseri* DUMITRICA	Pl. 8 Figs. 1 and 2
Archaeodictyomitra spp.	Pl. 8 Figs. 6 and 7
Archaeospongoprunum sp.	Pl. 8 Figs. 13-15
Halesium (?) cf. *palmatum* DUMITRICA	Pl. 8 Fig. 18
Spumellaria gen. et sp. indet.	Pl. 8 Fig. 22
Stichomitra (?) spp.	Pl. 8 Figs. 8 and 9
Thanarla aff. *veneta* (SQUINABOL)	Pl. 8 Fig. 10
Thanarla sp.	Pl. 8 Fig. 12
Stylosphaera spp.	Pl. 8 Figs. 16 and 17
Archaeodictyomitra gracilis (SQUINABOL) gr.	Pl. 9 Figs. 1 and 2
Archaeodictyomitra sp.	Pl. 9 Fig. 3
Neosciadiocapsidae PESSAGNO gen. et sp. Indet.	Pl. 9 Fig. 6
Squinabollum aff. *fossile* (SQUINABOL)	Pl. 9 Fig. 5
Stichomitra (?) sp.	Pl. 9 Fig. 4

Thin lines are used for first and last appearance intervals and dashed lines for ranges of uncertain determination species ("cf."). The samples are given with their geographic coordinates (WGS 84, °) (see also Fig. 2). The numbers of illustrations in this table correspond to those in Plates 7, 8 and 9

Tithonian–Berriasian assemblage 657 described by Dumitrica et al. (1997, Maghilah Unit, Oman). Moreover, the absence of *Ristola altissima altissima* (RÜST) and the presence of *Archaeodictyomitra immenhauseri* DUMITRICA in our fauna both suggest a Berriasian age for sample PR-SB11.

3.4.2 PR-SB12 (Table 4; Plate 4)

Despite the low diversity of this assemblage, a Berriasian age can be stated based on the presence of *Archaeodictyomitra immenhauseri* DUMITRICA, which has not been cited neither from earlier nor later than Berriasian. Moreover,

Table 9 List of Early Cretaceous radiolarian species of sample PR-SB30 from the Mariquita Chert Formation of the Bermeja Complex with ranges for the species considered important for the biostratigraphy (see Sect. 3 for detailed discussion)

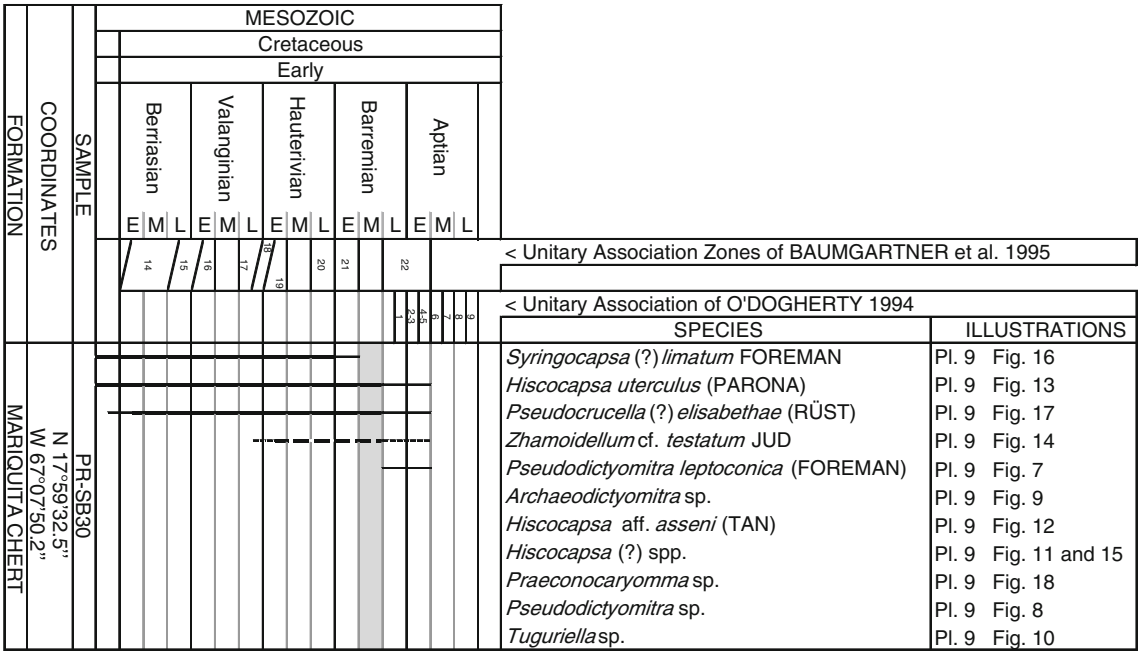

SPECIES	ILLUSTRATIONS
Syringocapsa (?) *limatum* FOREMAN	Pl. 9 Fig. 16
Hiscocapsa uterculus (PARONA)	Pl. 9 Fig. 13
Pseudocrucella (?) *elisabethae* (RÜST)	Pl. 9 Fig. 17
Zhamoidellum cf. *testatum* JUD	Pl. 9 Fig. 14
Pseudodictyomitra leptoconica (FOREMAN)	Pl. 9 Fig. 7
Archaeodictyomitra sp.	Pl. 9 Fig. 9
Hiscocapsa aff. *asseni* (TAN)	Pl. 9 Fig. 12
Hiscocapsa (?) spp.	Pl. 9 Fig. 11 and 15
Praeconocaryomma sp.	Pl. 9 Fig. 18
Pseudodictyomitra sp.	Pl. 9 Fig. 8
Tuguriella sp.	Pl. 9 Fig. 10

Thin lines are used for first and last appearance intervals and dashed lines for ranges of uncertain determination species ("cf."). The samples are given with their geographic coordinates (WGS 84, °) (see also Fig. 2). The numbers of illustrations in this table correspond to those in Plate 9

this age is consistent with the age of sample PR-SB11 (see above), which was collected near PR-SB12.

3.5 Samples PR-SB14 and PR-SB17

Four samples were collected from a very tectonized metric greenish-brown radiolarite block, which lies in an area adjacent to basalts. The location of this outcrop seems to correspond to this of the Early Jurassic sample PR92.1B from Montgomery et al. (1994b). Two out of 4 samples from this block yielded relatively well-preserved radiolarians.

3.5.1 PR-SB14 (Table 5; Plate 4)

Both species *Eucyrtidiellum unumaense* s.l. (YAO) and *E. unumaense pustulatum* BAUMGARTNER are present in the zonation proposed by Baumgartner et al. (1995) and give a latest Bajocian–early Bathonian to middle Callovian–early Oxfordian age (UAZ 5–8).

3.5.2 PR-SB17 (Table 5; Plate 5)

According to the zonation of Baumgartner et al. (1995), the occurrence of *Praewilliriedellum convexum* (YAO), *Eucyrtidiellum ptyctum* (RIEDEL & SANFILIPPO), *Williriedellum carpathicum* DUMITRICA, *Emiluvia ordinaria* OZVOLDOVA, and *Deviatus diamphidius hipposidericus* (FOREMAN) corresponds to UAZ 9–11 of middle–late Oxfordian to early Tithonian. Moreover, the presence of genus *Vallupus*, which according to O'Dogherty et al. (2009a) has a range that extended between the early Kimmeridgian and early Berriasian, restricts this interval from early Kimmeridgian to early Tithonian. Two characteristic species of Middle Jurassic are also present in the studied assemblage: *Striatojaponocapsa plicarum* (YAO) and *Williriedellum formosum* (CHIARI, MARCUCCI & PRELA) that may most probably be reworked into the younger material.

3.6 Samples PR-SB21 and PR-SB23

The radiolarite sequence is 1 m high and 3 m wide and appears as centimeter bedded greenish-orange radiolarian chert alternating with millimeter shale beds (Fig. 5).

3.6.1 PR-SB21 (Table 6; Plate 6)

According to Baumgartner et al. (1995), the presence of *Ristola turpicula* PESSAGNO & WHALEN corresponds to UAZ 5–6 of latest Bajocian–early Bathonian to middle Bathonian age.

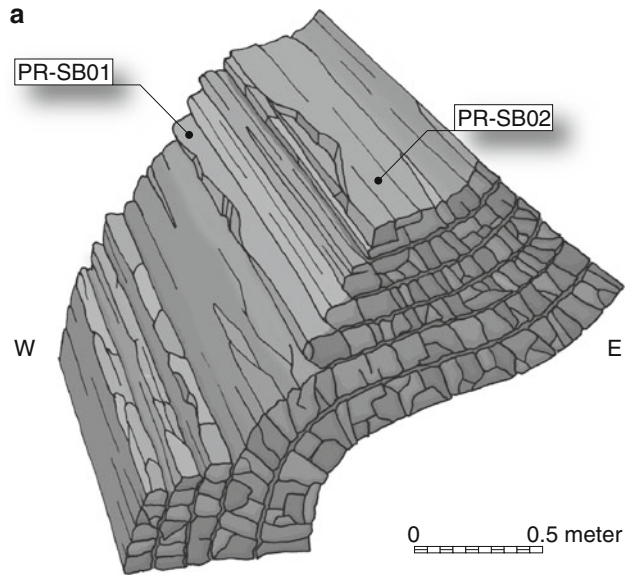

Fig. 3 **a** Sketch and **b** photograph of latest Jurassic–Early Cretaceous radiolarite outcrop showing the position of sample PR-SB01 and PR-SB02

Fig. 4 Photograph of the massive and intensely brecciated red or greenish-gray siliceous rock that weathers reddish and composes most of the Sierra Bermeja

3.6.2 PR-SB23 (Table 6; Plate 6)

This assemblage contain morphotypes present in the Tethys zonation of Baumgartner et al. (1995) and corresponds to UAZ 5–7 of latest Bajocian–early Bathonian to late Bathonian–early Callovian age.

3.7 Sample PR-SB24 (Table 7; Plate 6)

The radiolarite crops out in a 2 m sequence of centimeter bedded red radiolarian cherts alternating with millimeter shale beds (Fig. 6).

In this assemblage five species included in the zonation of Baumgartner et al. (1995) were found. The species *Triactoma parablakei* Yang & Wang allow to assign the assemblage to the UAZ 4–7. The corresponding time interval ranges from late Bajocian to late Bathonian–early Callovian.

3.8 Samples PR-SB26, PR-SB27 and PR-SB28

The radiolarite crops out in 2–15 cm boudinaged layers of dark green to black radiolarian cherts rich in organic matter that weather orange and interlayered with volcanic tuffs and may correspond to outcrop 7919-5B from Mattson and Pessagno (1979). The three samples PR-SB26, PR-SB27 and PR-SB28 come from the same section, respectively, 0, 40 and 240 cm from its base (Fig. 7).

Plate 1 Scanning electron microscope pictures of radiolarians from the Bermeja Complex, western Puerto Rico. Marker = 100 μm. Sample PR-SB01 (latest Tithonian–Late Valaginian). Fig. 1 ***Caneta* (?) sp.** Fig. 2 ***Archaeodictyomitra pseudomulticostata*** (Tan). Fig. 3 ***Archaeodictyomitra* cf. *tumandae*** Dumitrica. Figs. 4, 5 ***Archaeodictyomitra* spp.** Fig. 6 ***Cinguloturris* cf. *cylindra*** Kemkin & Rudenko. Fig. 7 ***Tethysetta boesii*** (Parona). Fig. 8 ***Svinitzium depressum*** (Baumgartner). Fig. 9 ***Pseudodictyomitra carpatica*** (Lozyniak). Fig. 10 ***Hiscocapsa* cf. *kaminogoensis*** (Aita). Fig. 11 ***Hiscocapsa* cf. *kitoi*** (Jud). Fig. 12 ***Cryptamphorella* sp.** Fig. 13 ***Emiluvia chica*** Foreman. Fig. 14 ***Emiluvia* cf. *ordinaria*** Ozvoldova. Fig. 15 ***Obesacapsula bullata*** Steiger. Fig. 16 ***Amuria* sp.** Fig. 17 ***Pantanellium squinaboli*** (Tan). Sample PR-SB02 (latest Tithonian–early Aptian). Fig. 18 ***Archaeodictyomitra* cf. *chalilovi*** (Aliev). Fig. 19 ***Archaeodictyomitra* cf. *tumandae*** Dumitrica. Fig. 20 ***Archaeodictyomitra mitra* gr.** Dumitrica. Fig. 21 ***Archaeodictyomitra* sp.** Fig. 22 ***Pseudodictyomitra* cf. *suyarii*** Dumitrica. Figs. 23–25 ***Cryptamphorella* spp.** Figs. 26, 27 ***Acanthocircus* sp.** Figs. 28–30 ***Pantanellium squinaboli*** (Tan). Fig. 31 ***Homoeoparonaella* cf. *irregularis*** (Squinabol) ▶

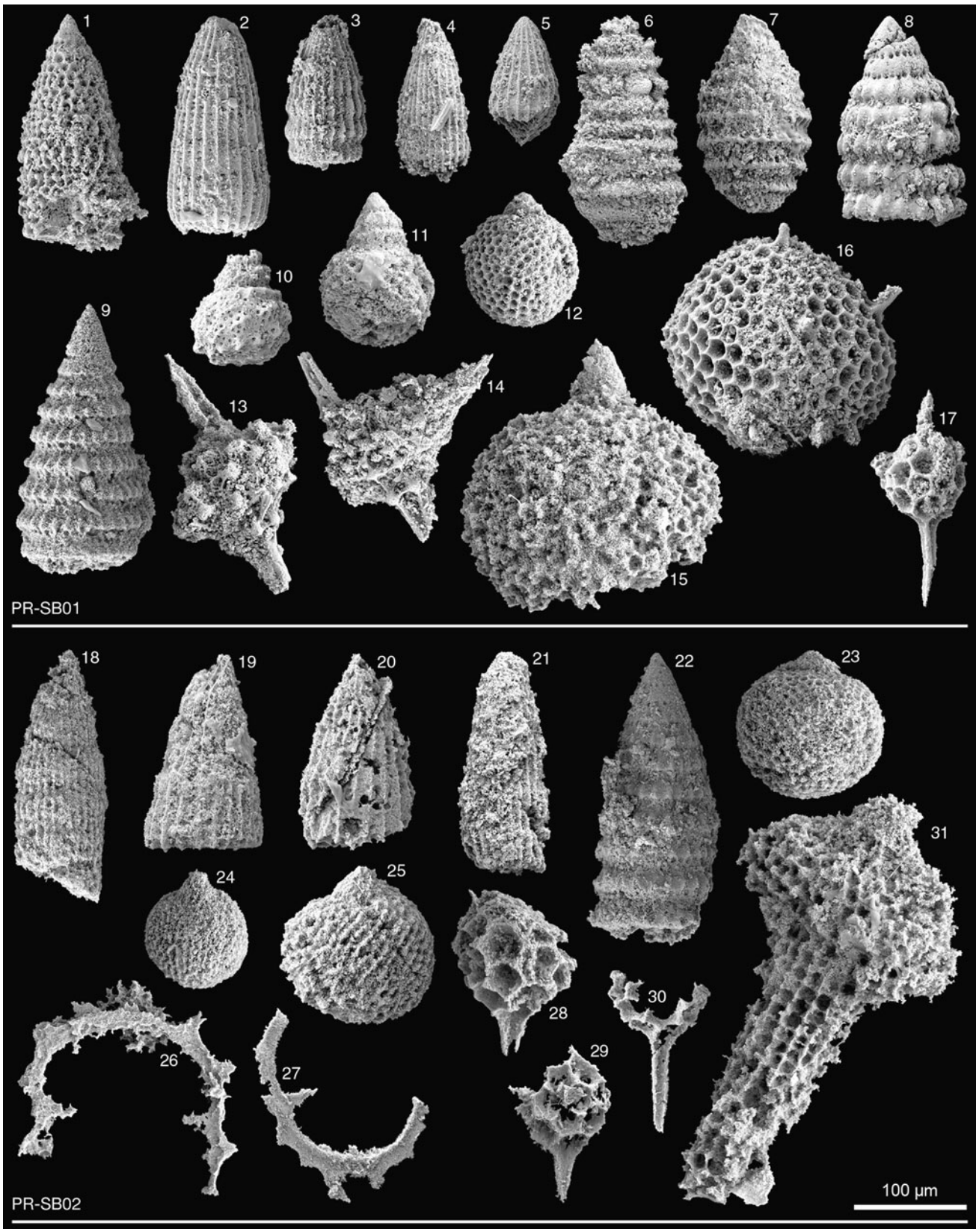
1
2
3
4
5
6
7
8
9
10
11
12
13
14
15
16
17
PR-SB01
18
19
20
21
22
23
24
25
26
27
28
29
30
31
PR-SB02
100 µm

3.8.1 PR-SB26 (Table 8; Plate 7)

The rare species *Pseudoeucyrtis corpulentus* Dumitrica has been recorded from the early–early late Barremian and late Aptian from Masirah Ophiolite in the Sultanate of Oman (Dumitrica et al. 1997). The species *Pseudoeucyrtis hanni* (Tan) is present in the zonation of O'Dogherty (1994) and corresponds to UA 1 to 9 of latest Barremian to latest Aptian age. The age of this assemblage could be constrained to latest Barremian to latest Aptian.

3.8.2 PR-SB27 (Table 8; Plate 8)

The species *Archaeodictyomitra montisserei* (Squinabol), *Quadrigastrum lapideum* O'Dogherty and *Thanarla brouweri* (Tan) are present in the middle Cretaceous zonation proposed by O'Dogherty (1994) The co-occurrence of *Archaeodictyomitra montisserei* (Squinabol) and *Thanarla brouweri* (Tan) allow to assign this assemblage to the late Aptian to early middle Albian (UA 8 to 11 of O'Dogherty 1994). Moreover, the genus *Pantanellium* Pessagno ranges from middle Carnian to late Aptian (O'Dogherty et al. 2009a, b), and indicates a late Aptian age for this assemblage. The first appearance of the species *Quadrigastrum lapideum* O'Dogherty, which is also present in the zonation proposed by O'Dogherty (1994), could therefore be at least in the latest Aptian (probably UA 9 instead of UA 12).

3.8.3 PR-SB28 (Table 8; Plate 9)

The species *Archaeodictyomitra gracilis* (Squinabol) gr. is present in the middle Cretaceous zonation proposed by O'Dogherty (1994, =*Dictyomitra gracilis*) and ranges from UA 10 (late early Albian) to 17 (middle Cenomanian).

3.9 PR-SB30 (Table 9; Plate 9)

The radiolarite crops out in 2–15 cm boudinaged layers of dark green to black radiolarian cherts that weather orange and interlayered with volcanic tuffs.

In this assemblage four species included in the zonation of Baumgartner et al. (1995) were found. The species *Syringocapsa* (?) *limatum* Foreman is present in UAZ 21 (early Barremian) but is absent in UAZ 22 (late Barremian–early Aptian). *Pseudodictyomitra leptoconica* (Foreman) is the only characteristic species in UAZ 22 but is absent in UAZ 21. The illustrated assemblage could correspond to an interval between UAZ 21 and 22 of middle Barremian age.

Plate 2 Scanning electron microscope pictures of radiolarians from the Bermeja Complex, western Puerto Rico. Marker = 100 μm. Sample PR-SB05 (latest Bajocian–early Bathonian). Fig. 1 ***Svinitzium* cf. *kamoense*** (Mizutani & Kido). Fig. 2 ***Triversus* (?) sp.** Fig. 3 ***Parahsuum* sp.** Fig. 4 ***Hiscocapsa lugeoni*** O'Dogherty, Goričan & Dumitrica. Figs. 5, 7 ***Praewilliriedellum convexum*** (Yao). Fig. 6 ***Praewilliriedellum japonicum*** (Yao). Figs. 8, 9 ***Striatojaponocapsa synconexa*** O'Dogherty, Goričan & Dumitrica. Fig. 10 ***Willirieddellum tetragona*** (Matsuoka). Fig. 11 ***Hexasaturnalis nakasekoi*** Dumitrica & Dumitrica-Jud. Fig. 12 ***Tetraditryma* sp.** Sample PR-SB07 (late early Albian–early early Turonian). Fig. 13 ***Archaeodictyomitra* cf. *chalilovi*** (Aliev). Fig. 14 ***Archaeodictyomitra* sp.** Fig. 15 ***Archaeodictyomitra montisserei*** (Squinabol) Figs. 16–18 ***Theocampe* (?) sp.** Fig. 19 **gen. et sp. indet.** Figs. 20–23 ***Cryptamphorella* spp.** Figs. 24–26, 29 ***Hiscocapsa pseudouterculus*** (Aita & Okada). Fig. 27 ***Hiscocapsa* cf. *uterculus*** (Parona) Figs. 28, 30 and 31 ***Hiscocapsa* cf. *asseni*** (Tan). Figs. 32, 33 ***Obeliscoites* (?) sp.** Figs. 34, 35 ***Napora* sp.**

4 Age of the Bermeja Complex

The age of the Bermeja Complex is based on both radiolarian biostratigraphy and radiometric determinations. The oldest K–Ar age is of 126 ± 3 Ma on hornblende in the amphibolites of the northeastern Sierra Bermeja (Cox et al. 1977). This age could be interpreted as a metamorphic age (Schellekens et al. 1990). Another K–Ar age of 110 ± 3.3 Ma was determined by Mattson (1964). This age and two others K–Ar ages for the amphibolites of 86.3 ± 8.6 Ma and 84.9 ± 8.5 Ma (Tobisch 1968) were all considered to be reset, possibly by intrusions (Schellekens et al. 1990). Schellekens et al. (1990) interpreted the 112 ± 15 Ma K–Ar age of Cox et al. (1977) as a magmatic age.

The two previous radiolarian studies have given ages that range from Early Jurassic (Montgomery et al. 1994b) and Late Jurassic to Early Cretaceous (Mattson and Pessagno 1979) for the Mariquita Chert Formation of the Bermeja Complex. However, the Early Jurassic interpretation by Montgomery et al. (1994b) of their faunal assemblage is nowadays somewhat misleading owing to the fact that the bibliography on radiolarian biostratigraphy has been enriched since 1994. Indeed, the assemblage illustrated by Montgomery et al. (1994b) as diagnostic of an Early Jurassic age is now known to range into the Middle Jurassic as discussed herein. Moreover, our revision of several samples from the same locality indicates a late Bajocian–early Callovian maximum age.

The figured taxa for the Puertorican oldest sample PR92.1B described as late Pliensbachian in age by Montgomery et al. (1994b) include *Parasaturnalis* (?) sp. (Montgomery et al. 1994b, Fig. 5, no. 1 and 2), which the authors considered comparable with the Early Jurassic form *Parasaturnalis* (?) n. sp. from the Maude Formation of the Queen Charlotte Islands, British Columbia (Montgomery et al. 1994b, Fig. 5, no. 3). In our opinion, *Parasaturnalis* (?) n. sp. differs clearly from *Parasaturnalis* (?) sp. by

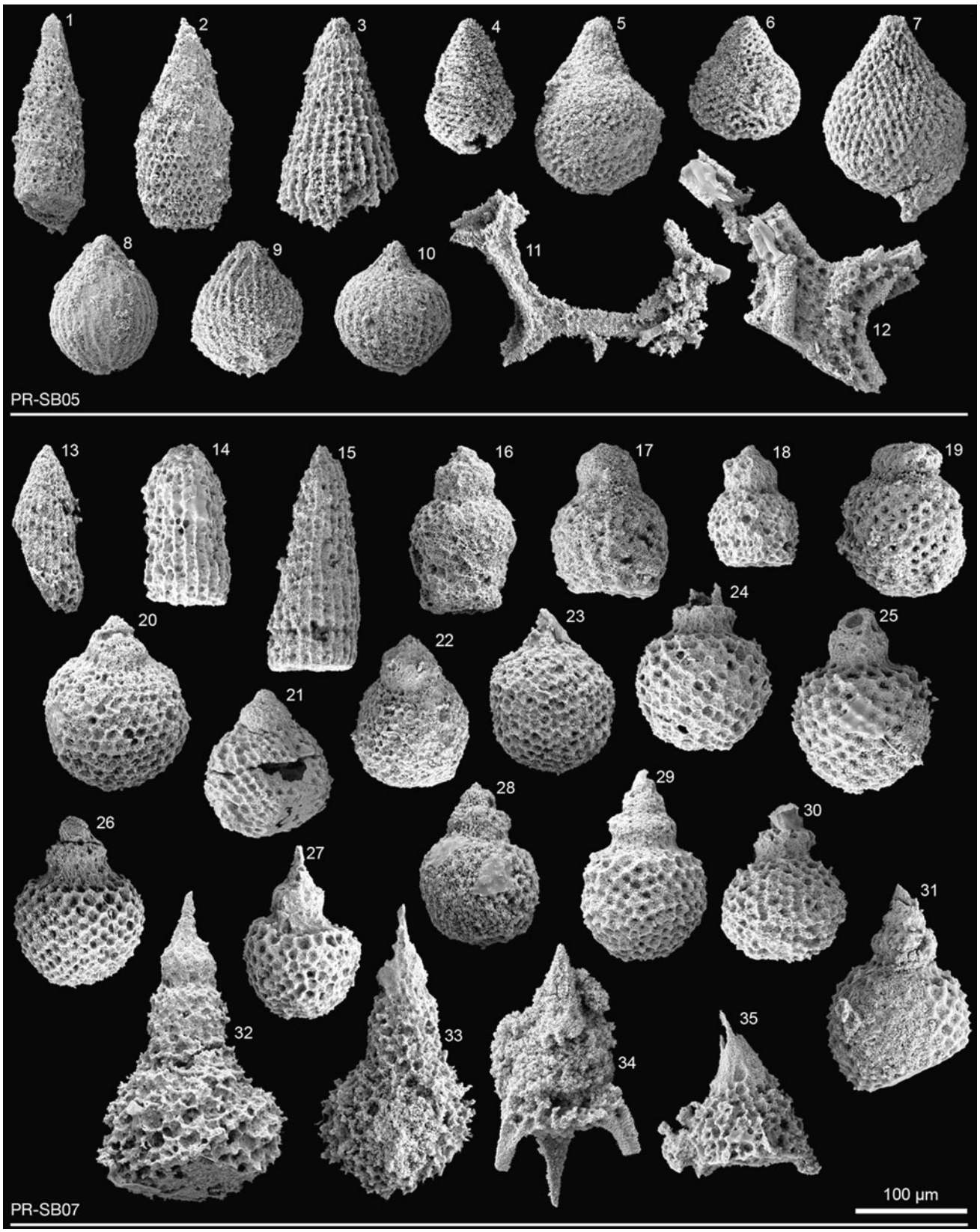
1
2
3
4
5
6
7
8
9
10
11
12
PR-SB05
13
14
15
16
17
18
19
20
21
22
23
24
25
26
27
28
29
30
31
32
33
34
35
100 µm
PR-SB07

having all the secondary spines aligned with primary spines rather than in staggered arrangement. We interpret the Figured specimens named *Parasaturnalis* (?) sp. by Montgomery et al. (1994b) as being *Parasaturnalis diplocyclis* (Yao), which is present in the zonation proposed by Baumgartner et al. (1995) and give an early–middle Aalenian to early–middle Bajocian age (UAZ 1–3). After Carter et al. (2010) the first appearance datum of *Parasaturnalis diplocyclis* (Yao) occurs in the early Pliensbachian. This assemblage illustrated by Montgomery et al. (1994b) also contains the species *Laxtorum* (?) *jurassicum* (Montgomery et al. 1994b, Fig. 5, no. 4), which presence corresponds to UAZ 2–3 of late Aalenian to early–middle Bajocian according to Baumgartner et al. (1995). The other figured species comprise *Acanthocircus hexagonus*, which is present in Baumgartner et al. (1995) zonation as *Hexasaturnalis hexagonus* (Yao) and correspond to UAZ 1–4 of early–middle Aalenian to late Bajocian. After Carter et al. (2010) the first appearance datum of *Hexasaturnalis hexagonus* (Yao) occurs in the middle–late Toarcian. This radiolarian assemblage also comprises the following genera *Ares*, *Bernoullius*, *Lupherium* and *Pantanellium*, which all have intervals of existence that include the Middle Jurassic (O'Dogherty et al. 2009a, b).

We conclude that the radiolarian age of sample PR92.1B described by Montgomery et al. (1994b) is restricted to Middle Jurassic (and not Early Jurassic) and ranges in age from late Aalenian to early–middle Bajocian by the presence of *Laxtorum* (?) *jurassicum* Isozaki & Matsuda. Moreover, the locality and description of the outcrop where Samples PR-SB14 and PR-SB17 of Middle Jurassic maximum age were collected, both correspond very closely to the locality and description of the outcrop PR92.1B of Montgomery et al. (1994b) (Fig. 8). However, this assemblage still establishes the Bermeja Complex as the oldest known island terrane on the Caribbean plate.

To summarize, the two previous radiolarian published works (Mattson and Pessagno 1979; Montgomery et al. 1994b) and our study on the blocks of Mariquita Chert Formation show that the Bermeja Complex ranges in age from Middle Jurassic to early Late Cretaceous (late Aalenian to early middle Cenomanian, Table 10). These studies also reveal a possible feature, which is the younging of radiolarian cherts from north to south (Fig. 8), suggesting an accretionary polarity. Five of the sixteen studied samples (Table 10) have biostratigraphic ranges comprising the Middle Jurassic, faunas of this age have never been illustrated by previous studies of the Bermeja Complex. This brings new and important information on the origin of the remnants of oceanic crust of the Bermeja Complex, more generally on the paleogeography of the Caribbean plate.

Plate 3 Scanning electron microscope pictures of radiolarians from the Bermeja Complex, western Puerto Rico. Marker = 100 μm. Sample PR-SB08 (late Bathonian–early late Tithonian). Figs. 1–5 ***Archaeodictyomitra* spp.** Figs. 6, 7 ***Loopus primitivus*** (Matsuoka & Yao). Figs. 8, 9 ***Loopus* aff. *primitivus*** (Matsuoka & Yao). Fig. 10 ***Loopus* sp.** Figs. 11, 12 ***Spinosicapsa* (?) sp.** Figs. 13–17 ***Cryptamphorella* spp.** Figs. 18, 19 ***Napora* spp.** Fig. 20 **gen. et sp. indet.** Fig. 21 ***Hiscocapsa* cf. *campana*** (Kiessling). Fig. 22 ***Hiscocapsa* cf. *subcrassitestata*** (Aita). Fig. 23 ***Triactoma* sp.** Fig. 24 ***Praeconocaryomma* sp.**

At first view, Montgomery et al. (1994b) presented a convincing argument for a Pacific origin of the radiolarites from the Bermeja Complex. They supposed the first Proto-Caribbean oceanic crust to have formed in Callovian times, and therefore, their Pliensbachian radiolarites (see Discussion above) could not have originated from the oceanic seaway between the Americas. At present, the oldest Proto-Caribbean crust is thought to have formed around 190 Ma (latest Sinemurian, according to Gradstein et al. 2004) based on $^{40}Ar/^{39}Ar$ ages on hornblende in the pegmatite and amphibole dikes of the oceanic Tinaquillo Complex from Venezuela (Sisson et al. 2005). Therefore, the age of the radiolarian faunas, either Pliensbachian or Aalenian is no longer an evidence for a Pacific origin of the radiolarite (Fig. 9).

Our argumentation for a Pacific origin of the oceanic remnants on the Caribbean plate (see list above) is based on the presence of the radiolarite facies *s.s.* in these units. Indeed, Middle Triassic to Early Cretaceous radiolarian ribbon cherts are widespread in Tethyan and circumpacific orogenic belts, but they are unknown from the Atlantic, the Gulf of Mexico, and the Venezuelan Mesozoic passive margin. Moreover, no radiolarites have been drilled in the Atlantic Ocean, Gulf of Mexico, and Caribbean sea.

5 Origins of radiolarites on the Caribbean plate

Paleogeographic models attempting to describe the Jurassic and Cretaceous history of the Caribbean tectonic plate can be divided into two main categories, an autochthonous (e.g., James 2009) and an allochthonous (e.g., Pindell and Kennan 2009) model. On the Caribbean plate, the radiolarites are often associated with remnants of Mesozoic oceanic crust and thus, is of great importance for paleogeographic reconstructions, like already suggested by previous authors (e.g., Cordey and Cornée 2009). In this debate, we think that the study of this facies is a key in seeking the origins of Mesozoic oceanic terranes of the Caribbean plate.

In this chapter, we define what we call radiolarites *s.s.* and give an actual exhaustive inventory of localities and

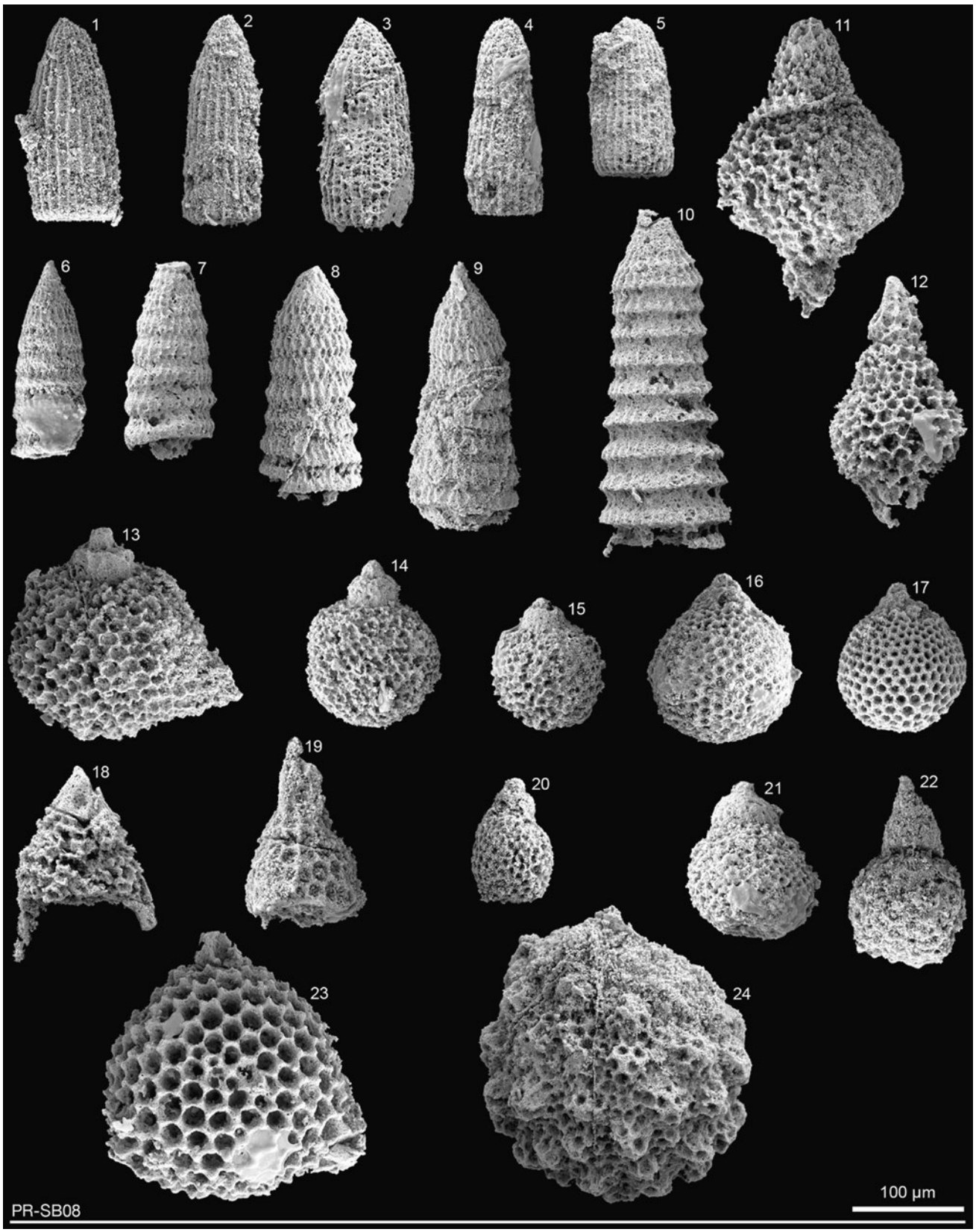
1
2
3
4
5
11
10
6
7
8
9
12
13
14
15
16
17
19
18
20
21
22
23
24
100 µm
PR-SB08

ages of this facies on the Caribbean plate. Then we discuss the Pacific origin of this facies based on paleoceanographic parameters that have influenced their deposition during the Mesozoic. This two-stage discussion focuses firstly on the paleoceanography of the radiolarite facies *s.s.* and its depositional settings, and secondly on the paleobiogeography of the radiolarian faunas to explain the presence of Northern (or Southern) Tethyan Province assemblages (22° to 30°N or S sensu Pessagno et al. 1987) in a low-latitude context.

5.1 Definition

Radiolarite s.l. is typically described as hard fine-grained chert of biogenic origin rich in radiolarian skeletons. The term radiolarite *s.s.* is herein restricted to the facies of centimeter ribbon-bedded radiolarian chert usually alternating with millimeter shale beds (Jenkyns and Winterer 1982, De Wever et al. 1994) and does not comprise other radiolarian-rich rocks (e.g. black shale and siliceous volcaniclastic limestone). Usually radiolarites are red—but also include a wide range of colors depending on inclusions and oxydes—and thus, could erroneously be compared to deep oceanic red clays.

5.2 Localities and ages

On the Caribbean plate, Late Triassic to early Late Cretaceous oceanic fragments associated with radiolarites *s.s.* (according to the definition above) are recognized along the western (Central America) and northeastern (Antilles) margin of the plate (Fig. 10). These are elements of the Nicoya Complex (Bajocian to late Coniacian–Santonian, Gursky 1994; Baumgartner and Denyer 2006) and the Santa Rosa Accretionary Complex of Costa Rica (Pliensbachian–Toarcian to Cenomanian, De Wever et al. 1985; Denyer and Baumgartner 2006), the El Castillo and Siuna Serpentinite Mélanges of Nicaragua (respectively, late Rhaetian and Bajocian–middle Bathonian to late Kimmeridgian–early Tithonian, Baumgartner et al. 2008), El Tambor Group Ophiolites of Guatemala (Oxfordian–Kimmeridgian, Chiari et al. 2006), the Duarte Complex of Hispaniola (Oxfordian–Tithonian, Montgomery et al. 1994a), the Bermeja Complex of Puerto Rico (late Aalenian to middle Cenomanian, Mattson and Pessagno 1979; Montgomery et al. 1994b; and this study) and the La Désirade Basement Complex of Guadeloupe, in the Lesser Antilles (Kimmeridgian–early late Tithonian, Montgomery et al. 1992; Mattinson et al. 2008; Cordey and Cornée 2009; Montgomery and Kerr 2009).

Plate 4 Scanning electron microscope pictures of radiolarians from the Bermeja Complex, western Puerto Rico. Marker = 100 μm. Sample PR-SB11 (Berriasian). Fig. 1 ***Archaeodictyomitra* cf. *vulgaris*** Pessagno. Fig. 2 ***Archaeodictyomitra* sp.** Fig. 3 ***Archaeodictyomitra* cf. *tumandae*** Dumitrica. Fig. 4 ***Archaeodictyomitra immenhauseri*** Dumitrica. Figs. 5, 6 ***Mictyoditra* sp.** Fig. 7 ***Stichomitra* (?) sp.** Fig. 8 ***Thanarla* cf. *conica*** (Aliev). Fig. 9 ***Pseudodictyomitra* aff. *leptoconica*** (Foreman). Fig. 10 ***Pseudodictyomitra* sp.** Fig. 11 ***Svinitzium* (?) *mizutanii*** Dumitrica. Fig. 12 ***Cryptamphorella* sp.** Fig. 13 ***Archaeospongoprunum* sp.** Fig. 14 ***Acanthocircus* sp.** Fig. 15 ***Pantanellium squinaboli*** (Tan) Fig. 16 ***Pantanellium* sp.** Sample PR-SB12 (Berriasian). Fig. 17 ***Archaeodictyomitra* cf. *pseudomulticostata*** (Tan). Figs. 18, 19 ***Archaeodictyomitra mitra* gr.** Dumitrica. Fig. 20 ***Archaeodictyomitra immenhauseri*** Dumitrica. Figs. 21, 22, 24 ***Cryptamphorella* sp.** Fig. 23 ***Obesacapsula* (?) cf. *cetia*** (Foreman). Fig. 25 ***Hiscocapsa* (?) sp.** Sample PR-SB14 (latest Bajocian–early Oxfordian). Fig. 26 ***Archaeodictyomitra* sp.** Fig. 27 ***Archaeodictyomitra prisca*** Kozur & Mostler. Fig. 28 ***Transhsuum* sp.** Fig. 29 **gen. et sp. indet.** Figs. 30, 31 ***Eucyrtidiellum unumaense* s.l.** (Yao). Fig. 32 ***Eucyrtidiellum unumaense pustulatum*** Baumgartner. Fig. 33 ***Spinosicapsa* (?) sp.** Fig. 34 ***Striatojaponocapsa* (?) sp.** Figs. 35, 36 ***Homeoparonaella* sp.** Fig. 37 ***Alievium* cf. *longispineum*** Yang & Wang

5.3 Paleoceanography of radiolarites

Our hypothesis presented herein for the radiolarian cherts deposition is an attempt to explain the absence of radiolarites *s.s.* in the Central Atlantic and Proto-Caribbean basins. It is mainly based on actualistic paradigms, which could be disputable (see Racki and Cordey 2000).

In the circum-Pacific regions, radiolarites *s.s.* are commonly found in Devonian to Cretaceous ophiolitic or suture belts (Racki and Cordey 2000). The Tethyan and Pacific realms were characterized by a number of internal subduction zones (Johnston and Borel 2007). These relatively large oceanic basins covering wide paleolatitude and paleolongitude ranges were most of the time fully connected with each other (Fig. 11). This oceanic connexion allowed the dispersal of pelagic faunas and the presence of sub-surface and deep-water circulation belts partly directed by the landmasses they encountered. The existence of a deep cold water circulation during this period may be hypothesized based on a relatively steep pole-to-equator temperature gradient, warm or warmer than today low-latitude regions, and glacial or cold polar conditions (Price 1999). The presence of deep cold water circulations, winds, and a combination of topographic features may have induced upwelling currents, and other phenomenons (*e.g.*, mesoscale eddies, circulation of the equatorial surface ocean, river inputs) resulting in the occurrence of high plankton productivity zones, which have produced paleoceanographic conditions for the sedimentation of the radiolarite facies *s.s.* (Baumgartner 1987). This change to siliceous sedimentation occurred for instance during the

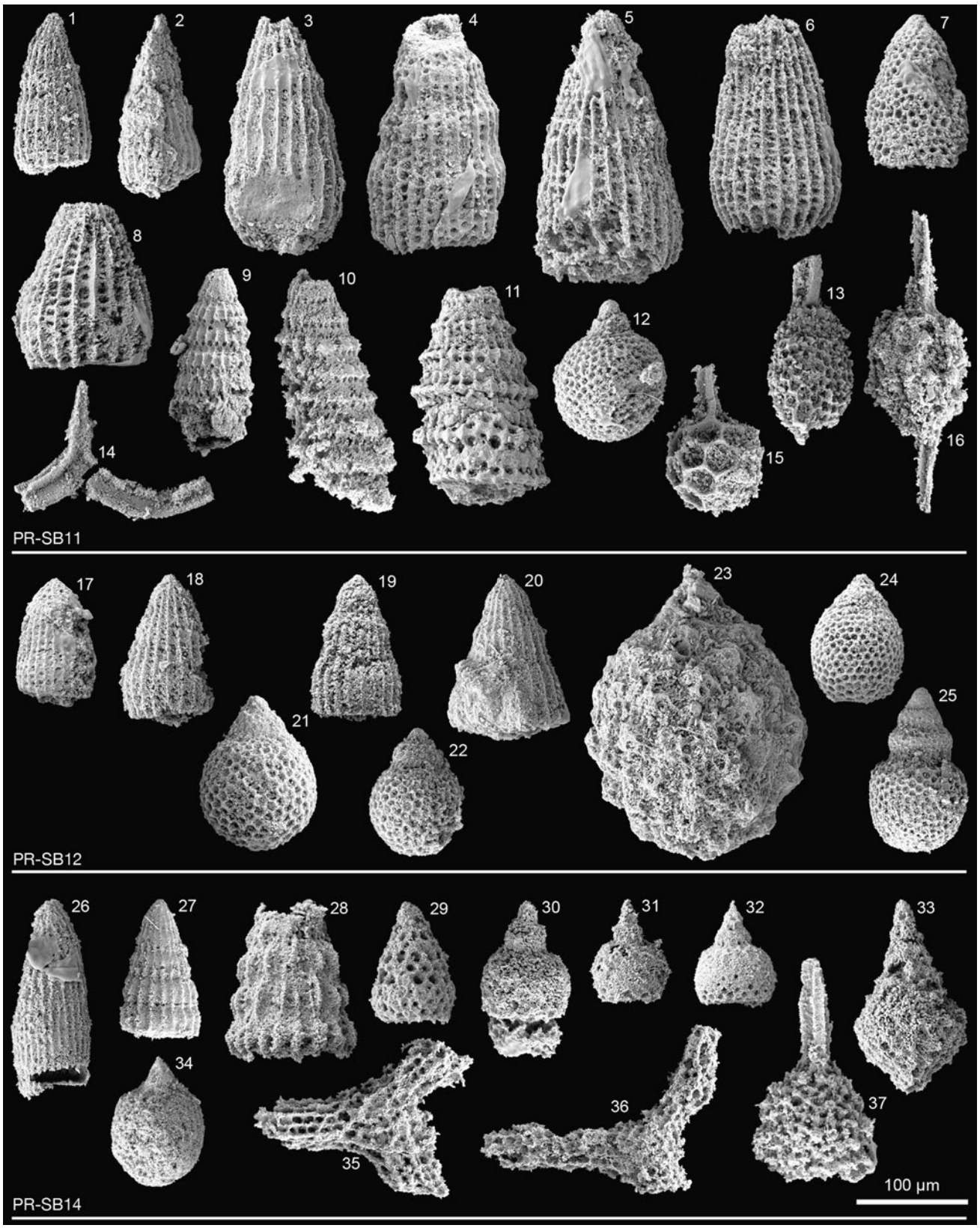
1
2
3
4
5
6
7
8
9
10
11
12
13
14
15
16
PR-SB11
17
18
19
20
21
22
23
24
25
PR-SB12
26
27
28
29
30
31
32
33
34
35
36
37
100 µm
PR-SB14

continental breakup and oceanic spreading of the Alpine Tethys between the continents of Laurasia and Gondwana, which caused a deep-water connection with the Central Tethys and extended this water circulation system to the west at least since the Bathonian (Bill et al. 2001), forming a Gulf of California-like restricted sea connected to the world ocean.

During the Middle Jurassic, two natural barriers bound the Pacific-Tethyan deep-water circulation system: to the west by the thin seaway between Iberia and Gondwana, and to the east by the western border of the American plates. The Central Atlantic and Proto-Caribbean oceanic basins formed a low-latitude restricted Mediterranean-like sea not connected to this deep-water circulation system. However, these two basins shared indirect surface-water connections with the world ocean (Iturralde-Vinent 2006). For the radiolarians, this is attested for example, by the faunal affinities of the Bathonian radiolarian assemblages from the Central Atlantic and the Alpine Tethys (Bill et al. 2001).

Lithologically, the Central Atlantic and Proto-Caribbean oceanic basins were rich in detritals along their margins, but of low surface productivity, resulting in clay-rich (below the CCD) and/or calcareous pelagic facies throughout (Baumgartner 1987). In the Central Atlantic and Caribbean area, Middle Jurassic sediments associated with oceanic crust remnants have been reported from several localities. These series do not contain any radiolarite *s.s.* (Fig. 9):

1. In the southern Caribbean region, the Siquisique Ophiolite Complex located in west-central Venezuela is interpreted as a remnant of an early Proto-Caribbean rift (Bartok et al. 1985). It exhibits Bajocian to possibly early Bathonian ammonite-bearing shale enveloped by mid oceanic ridge pillow basalts (MORB, Bartok et al. 1985).
2. In western Cuba, the Guaniguanico Terrane shows a passive margin sedimentary sequence of the Proto-Caribbean ocean (Pszczolkowski 1999; Pszczolkowski and Myczynski 2003). Belonging to this terrane, normal oceanic crust (N-MORB) has been reported from the Oxfordian–early Kimmeridgian El Sábalo Formation (Pszczolkowski 1999). The oldest sediment of this sequence is a black shale of the Early(?)-Middle to Late Jurassic San Cayetano Formation (Pszczolkowski 1978, 1999).
3. The oldest known sediments resting on basalts from the western-central Atlantic ocean, which are middle Bathonian in age, are found at the Blake Bahama Basin (Baumgartner and Matsuoka 1995). This sedimentary sequence includes claystone/shale, calcareous claystone, carbonate turbidites, and pelagic limestone with secondary silicifications.
4. In the eastern-central Atlantic, the oldest sediments lying on normal-mid oceanic ridge basalt (N-MORB) are found in the Mesozoic sequence of Fuerteventura (Canary Islands, Favre et al. 1991; Favre and Stampfli 1992). The age of the initiation of the uplift of the rift shoulders is based on the radiometric age of 184 ± 4 Ma (Huon et al. 1993, Pliensbachian according to the time scale of Gradstein et al. 2004). The overlaying sedimentary sequence, of which the oldest sediments are of at least late Toarcian–early Aalenian age (late Early Jurassic–early Middle Jurassic), includes dark, green and red claystone, and black shale (Steiner et al. 1998). According to the Middle Jurassic distribution of sediments associated with oceanic crust and associated paleoceanographic conditions, we believe the radiolarite facies *s.s.* was common in the Pacific-Tethys world ocean, but was absent in the restricted Central Atlantic-Proto-Caribbean sea. This is consistent with a Pacific origin of the radiolarite of the Caribbean plate and thus, of the associated Mesozoic oceanic terranes (see also Baumgartner et al. 2008).

Plate 5 Scanning electron microscope pictures of radiolarians from the Bermeja Complex, western Puerto Rico. Marker = 100 µm. Sample PR-SB17 (early Kimmeridgian–early Tithonian). Fig. 1 ***Archaeodictyomitra patricki*** Kocher. Figs. 2, 3 ***Archaeodictyomitra* spp.** Fig. 4 ***Pseudodictyomitrella* (?) sp.** Figs. 5–7 ***Stichomitra* (?) spp.** Figs. 8, 9, 11 **Parvicingulidae gen. et sp. indet.** Fig. 10 ***Parvicingula vera*** Pessagno & Whalen. Fig. 12 ***Pseudodictyomitra* (?) sp.** Fig. 13 ***Pseudodictyomitra* sp.** Figs. 14, 15 ***Stichomitra* (?) *doliolum*** Aita gr. Fig. 16 ***Eucyrtidiellum ptyctum*** (Riedel & Sanfilippo). Fig. 17 ***Vallupus hopsoni*** Pessagno & Blome. Figs. 18, 19 ***Napora* sp.** Fig. 20 ***Striatojaponocapsa plicarum*** (Yao). Fig. 21 ***Praewilliriedellum* sp. aff. *robustum*** (Matsuoka). Fig. 22 ***Praewilliriedellum convexum*** (Yao). Fig. 23 ***Hiscocapsa* (?) sp.** Figs. 24, 25 ***Williriedellum carpathicum*** Dumitrica. Fig. 26 ***Williriedellum* sp.** Figs. 27, 28 ***Williriedellum formosum*** (Chiari, Marcucci & Prela). Fig. 29 ***Cryptamphorella* sp.** Figs. 30, 31 **Nassellaria gen. et sp. indet.** Fig. 32 ***Emiluvia ordinaria*** Ozvoldova. Fig. 33 ***Emiluvia* (?) sp.** Fig. 34 ***Praeconocaryomma* sp.** Fig. 35 ***Deviatus diamphidius hipposidericus*** (Foreman). Fig. 36 ***Pantanellium ranchitoense*** Pessagno & Macleod. Fig. 37 ***Pantanellium* sp.** Figs. 38–40 ***Pantanellium karinae*** Bandini, n. sp. Fig. 41 ***Archaeospongoprunum elegans*** Wu. Fig. 42 **Spumellaria gen. et sp. indet**

5.4 Paleobiogeography of radiolarians

Montgomery et al. (1994a) presented an argument based on faunal observations for a Pacific origin of the radiolarites from the Bermeja Complex. They interpreted the radiolarian faunas associated with some of the Caribbean radiolarites (Bermeja Complex of Puerto Rico, Duarte

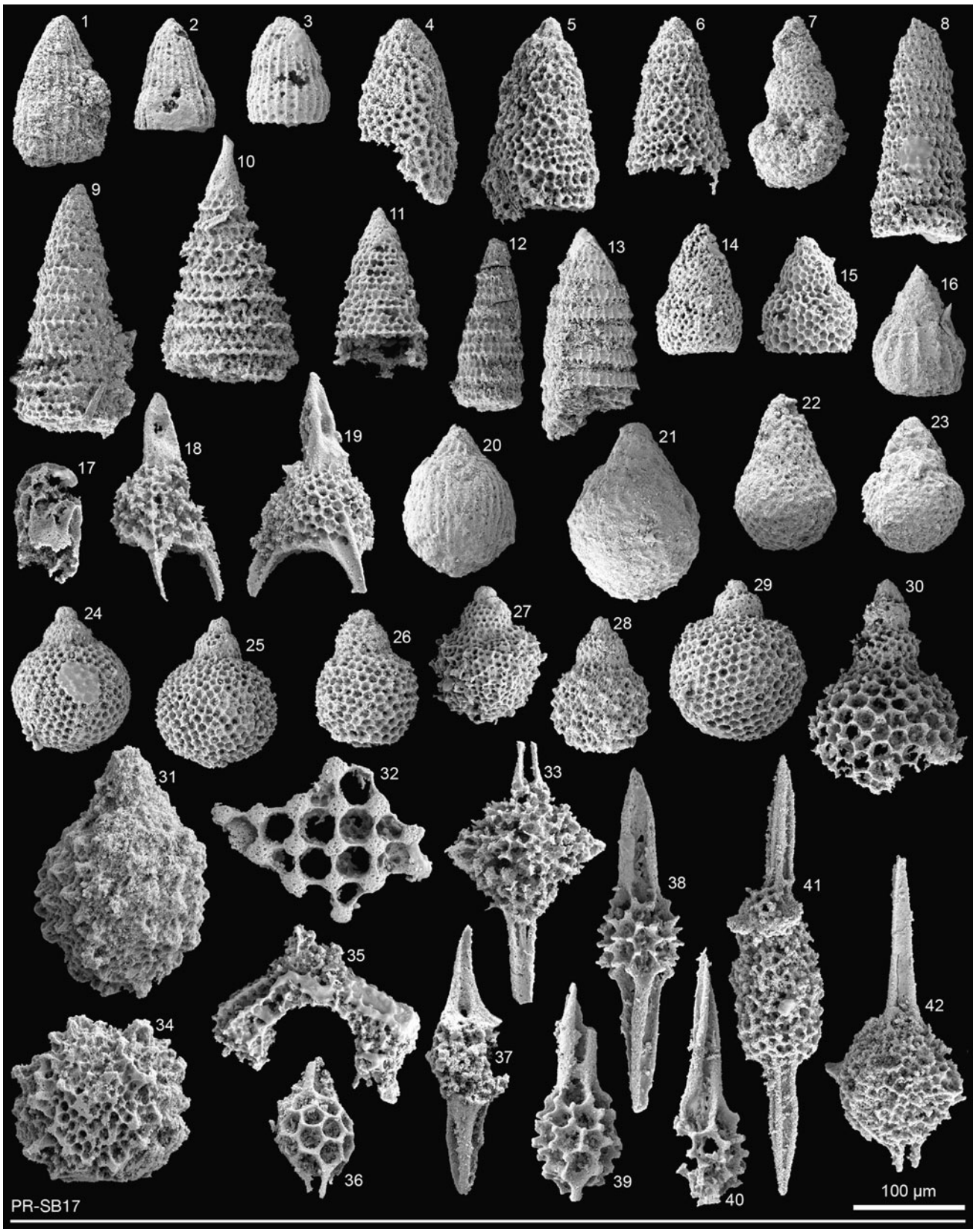
1
2
3
4
5
6
7
8
9
10
11
12
13
14
15
16
17
18
19
20
21
22
23
24
25
26
27
28
29
30
31
32
33
34
35
36
37
38
39
40
41
42
PR-SB17
100 µm

Complex of Hispaniola and La Désirade Basement Complex of Guadeloupe) like having Pacific faunal affinities based on the paleolatitudinal model for the radiolarian assemblages developed by Pessagno and Blome (1986) and modified later on by Pessagno et al. (1986, 1987, 1993). This model is based on Gordon's hypothesis (1974) that one of the most important factors of biogeographic distribution of the marine plankton is the decline of the mean ocean water temperature from the equator to the poles. Provinces and realms of this model were defined using multiple criteria (ammonites, *Buchia* spp., calpionellids and other well-studied fossil groups) and is mainly based on the relative abundance of *Parvicingula* and *Praeparvicingula* radiolarian genera versus *Pantanelliidae* radiolarian family (Pessagno et al. 1987). With the help of this model, it should be possible to determine the relative paleolatitudinal position of any given terrane from the study of the radiolarian assemblage. The inductive reasoning resulting from this model applied to the above-cited Caribbean terranes stated that no high latitudes fauna of Late Jurassic age would have been endemic in a low paleolatitude constrained Proto-Caribbean ocean between North and South America (Fig. 12). Therefore, all these radiolarites were originated from either the eastern Pacific or the "Mediterranean" region. The Pacific faunal affinities sensu Montgomery et al. (1994a) based on this paleolatitudinal argument was included in the literature in many occasions in order to consolidate certain paleogeographic hypotheses (e.g., Hoernle et al. 2002; Bosch et al. 2002; Bortolotti and Principi 2005).

Montgomery et al. (1994a) applied this model to the Jurassic radiolarian assemblages from the Bermeja Complex of Puerto Rico. Though, it is difficult to reproduce their results as the paleolatitudinal model presented above is based on planktonic relative abundances and no quantified data or complete faunal list from these assemblages have been made available to the readers. Their conclusions were a Central Tethyan (22°S–22°N) origin for most of the assemblages, with two exceptions, both of Late Jurassic age and from Northern (or Southern) Tethyan Province (22°–30°N or S) origin. We do not bring into question the paleolatitudinal endemism of certain characteristic faunas as presented by several previous authors (e.g., Empson-Morin 1984; Matsuoka 1995; Kiessling 1999), but is it really possible to make the difference among a radiolarian assemblage originating from a Central Tethyan Province (22°S–22°N) and another one originating from a Northern (or Southern) Tethyan Province (22°–30°N or S)?

Plate 6 Scanning electron microscope pictures of radiolarians from the Bermeja Complex, western Puerto Rico. Marker = 100 μm. Sample PR-SB21 (latest Bajocian–middle Bathonian). Fig. 1 ***Archaeodictyomitra* aff. *rigida*** Pessagno. Fig. 2 ***Transhsuum* sp.** Fig. 3 ***Canoptum* (?) sp.** Fig. 4 ***Ristola turpicula*** Pessagno & Whalen. Fig. 5 ***Praewilliriedellum convexum*** (Yao). Figs. 6, 7 ***Striatojaponocapsa synconexa*** O'Dogherty, Goričan & Dumitrica. Fig. 8 ***Williriedellum yaoi*** (Kozur). Sample PR-SB23 (latest Bajocian–early Callovian). Fig. 9 ***Archaeodictyomitra* aff. *rigida*** Pessagno. Fig. 10 ***Archaeodictyomitra patricki*** Kocher. Figs. 11, 12 ***Transhsuum maxwelli* gr.** (Pessagno). Fig. 13 ***Stichomitra* (?) sp.** Fig. 14 ***Triversus* (?) sp.** Fig. 15 ***Svinitzium kamoense*** (Mizutani & Kido). Fig. 16 ***Parahsuum* (?) sp.** Fig. 17 ***Xitus* sp.** Figs. 18, 19 ***Praewilliriedellum convexum*** (Yao). Fig. 20 ***Praewilliriedellum robustum*** (Matsuoka). Figs. 21, 22 ***Williriedellum yaoi*** (Kozur). Figs. 23, 24 ***Striatojaponocapsa synconexa*** O'Dogherty, Goričan & Dumitrica. Fig. 25 ***Eucyrtidiellum unumaense* s.l.** (Yao). Fig. 26 **Nassellaria gen. et sp. indet.** Figs. 27, 28 **gen. et sp. indet.** Fig. 29 ***Levileugeo ordinarius*** Yang & Wang. Fig. 30 ***Angulobracchia* sp.** Sample PR-SB24 (late Bajocian-early Callovian). Fig. 31 ***Archaeodictyomitra* aff. *rigida*** Pessagno. Fig. 32 ***Archaeodictyomitra* sp.** Fig. 33 ***Parahsuum* sp.** Fig. 34 ***Transhsuum* cf. *hisuikyoense*** (Isozaki & Matsuda). Fig. 35 ***Transhsuum* cf. *maxwelli* gr.** (Pessagno). Fig. 36 ***Praewilliriedellum japonicum*** (Yao). Fig. 37 ***Praewilliriedellum convexum*** (Yao). Fig. 38 ***Canoptum* (?) sp.** Fig. 39 ***Triactoma parablakei*** Yang & Wang. Fig. 40 ***Emiluvia* sp.** Figs. 41, 42 ***Eucyrtidiellum unumaense* s.l.** (Yao)

We believe these faunal changes could not only be a consequence of paleolatitude, but could result more generally from a significant switch of the paleoenvironmental conditions (Boltovskoy et al. 1996). A drop in water temperature, higher nutrients availability, and higher productivity levels, could represent an alternative hypothesis to explain these distinct radiolarian assemblages (e.g., Abelmann and Gowing 1997). Similar substitutions of paleoenvironmental conditions could be encountered near large landmasses as continents (Americas) or volcanic arcs associated with intra-oceanic subduction zones resulting in coastal upwelling (Molina-Cruz et al. 1999) or river inputs (Fig. 13). Moreover, the presence of Late Jurassic tuffaceous cherts reported by Montgomery et al. (1994a) would be consistent with this hypothesis.

Despite the work started by Pessagno et al. 1986, which underlined how radiolarian assemblages could be a powerful tool to solve complex paleogeographic problems, it seems that faunal compositions are linked to variation of paleoceanographic variables, rather than only paleolatitude. In the generally low-latitude context of the Proto-Caribbean and Central Pacific, we interpret "high-latitude" assemblages as "margin-related"—even though none assemblage of this kind have been illustrated from the Caribbean plate. They can be associated with intraoceanic subduction zones or active continental margins of the Americas, both acting as upwelling margins or providers of land nutrients inputs (Fig. 13).

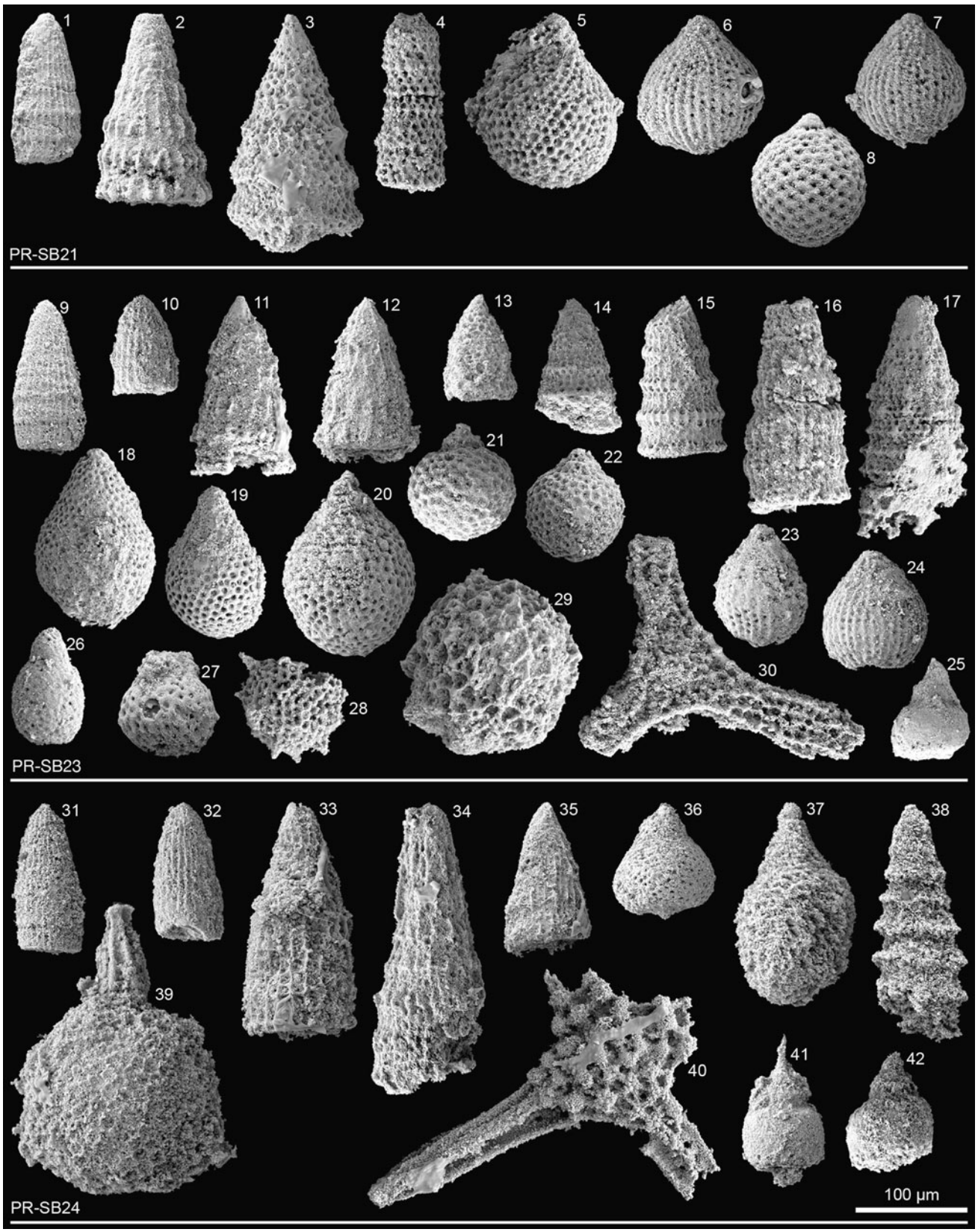
1
2
3
4
5
6
7
8
PR-SB21
9
10
11
12
13
14
15
16
17
18
19
20
21
22
23
24
25
26
27
28
29
30
PR-SB23
31
32
33
34
35
36
37
38
39
40
41
42
100 µm
PR-SB24

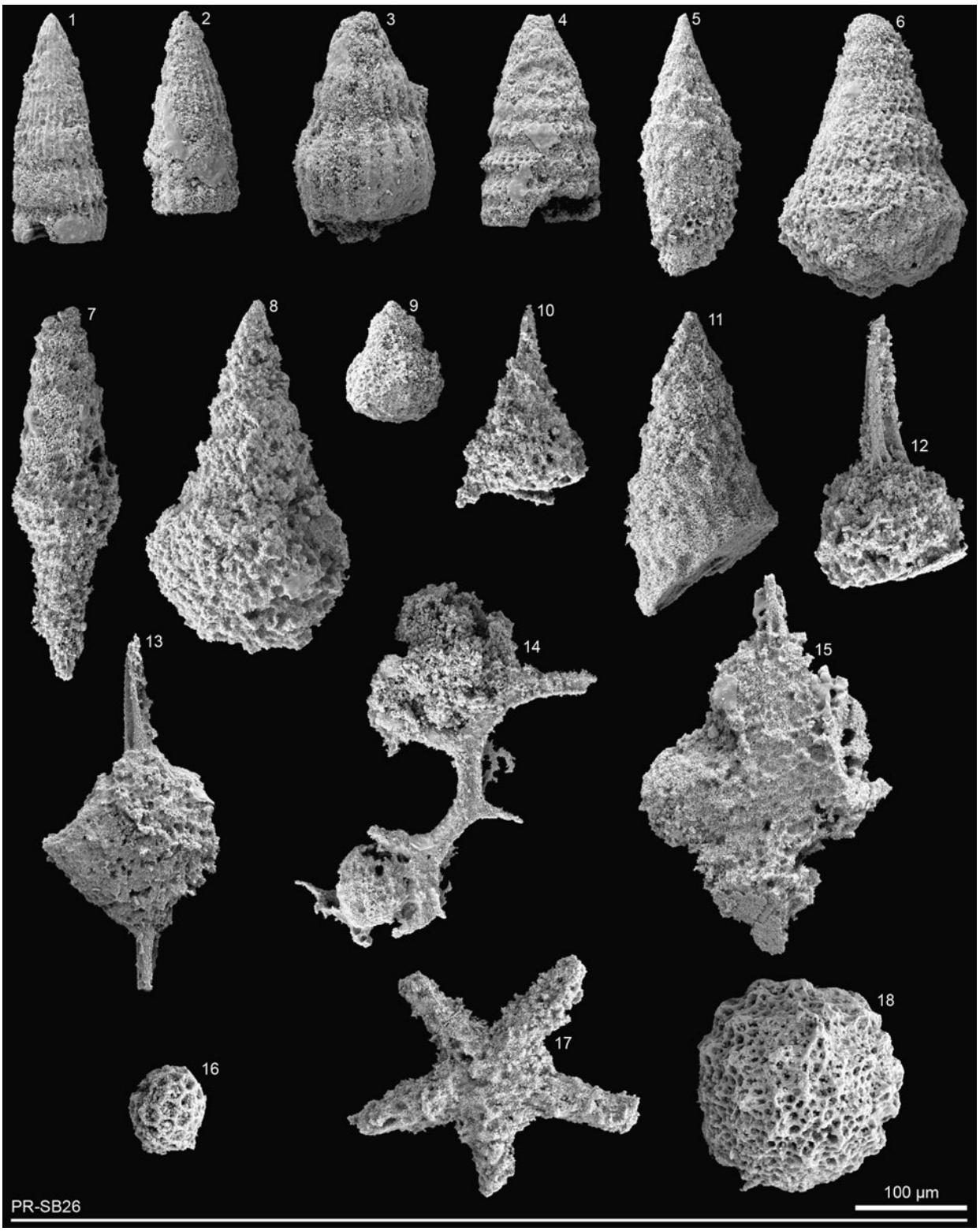

Plate 7 Scanning electron microscope pictures of radiolarians from the Bermeja Complex, western Puerto Rico. Marker = 100 µm. Sample PR-SB26 (latest Barremian–late Aptian) Figs. 1, 2 ***Archaeodictyomitra*** **spp.** Fig. 3 ***Thanarla*** **sp.** Fig. 4 ***Parvicingula*** **sp.** Fig. 5 ***Pseudoeucyrtis corpulentus*** DUMITRICA. Fig. 6 ***Obesacapsula*** **sp.** Fig. 7 ***Pseudoeucyrtis hanni*** (TAN). Fig. 8 ***Obeliscoites*** **cf.** ***vinassai*** (SQUINABOL). Fig. 9 **Nassellaria gen. et sp. indet.** Fig. 10 ***Napora*** **sp.** Fig. 11 **Nassellaria gen. et sp. indet.** Fig. 12 ***Acaeniotyle*** **cf.** ***umbilicata*** (RÜST). Fig. 13 ***Emiluvia*** **sp.** Fig. 14 ***Acanthocircus*** **sp.** Fig. 15 ***Crucella*** **sp.** Fig. 16 **Pantanelliidae gen. et sp. indet.** Fig. 17 ***Crucella*** **sp. (with five rays).** Fig. 18 ***Praeconocaryomma*** **sp.**

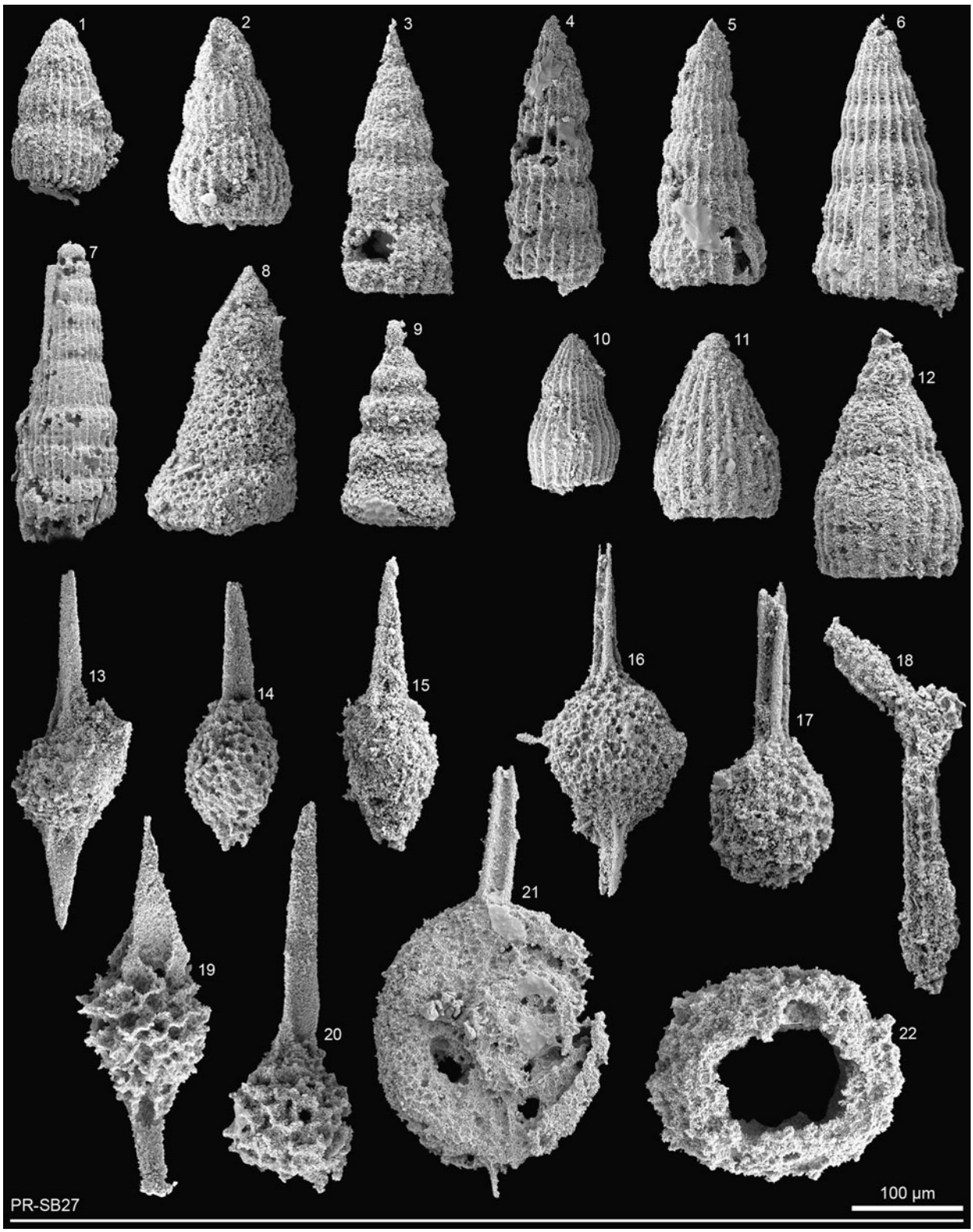

Plate 8 Scanning electron microscope pictures of radiolarians from the Bermeja Complex, western Puerto Rico. Marker = 100 µm. Sample PR-SB27 (late Aptian–middle Cenomanian). Figs. 1, 2 ***Archaeodictyomitra*** **cf.** ***immenhauseri*** DUMITRICA. Fig. 3 ***Archaeodictyomitra*** **cf.** ***gracilis*** (SQUINABOL). Figs. 4, 5 ***Archaeodictyomitra montisserei*** (SQUINABOL). Figs. 6, 7 ***Archaeodictyomitra*** **spp.** Figs. 8, 9 ***Stichomitra*** **(?) spp.** Fig. 10 ***Thanarla*** **aff.** ***veneta*** (SQUINABOL). Fig. 11 ***Thanarla brouweri*** (TAN). Fig. 12 ***Thanarla*** **sp.** Figs. 13–15 ***Archaeospongoprunum*** **sp.** Figs. 16, 17 ***Stylosphaera*** **spp.** Fig. 18 ***Halesium*** **(?) cf.** ***palmatum*** DUMITRICA. Figs. 19, 20 ***Pantanellium*** **sp**. Fig. 21 ***Quadrigastrum lapideum*** O'DOGHERTY. Fig. 22 **Spumellaria gen. et sp. indet**

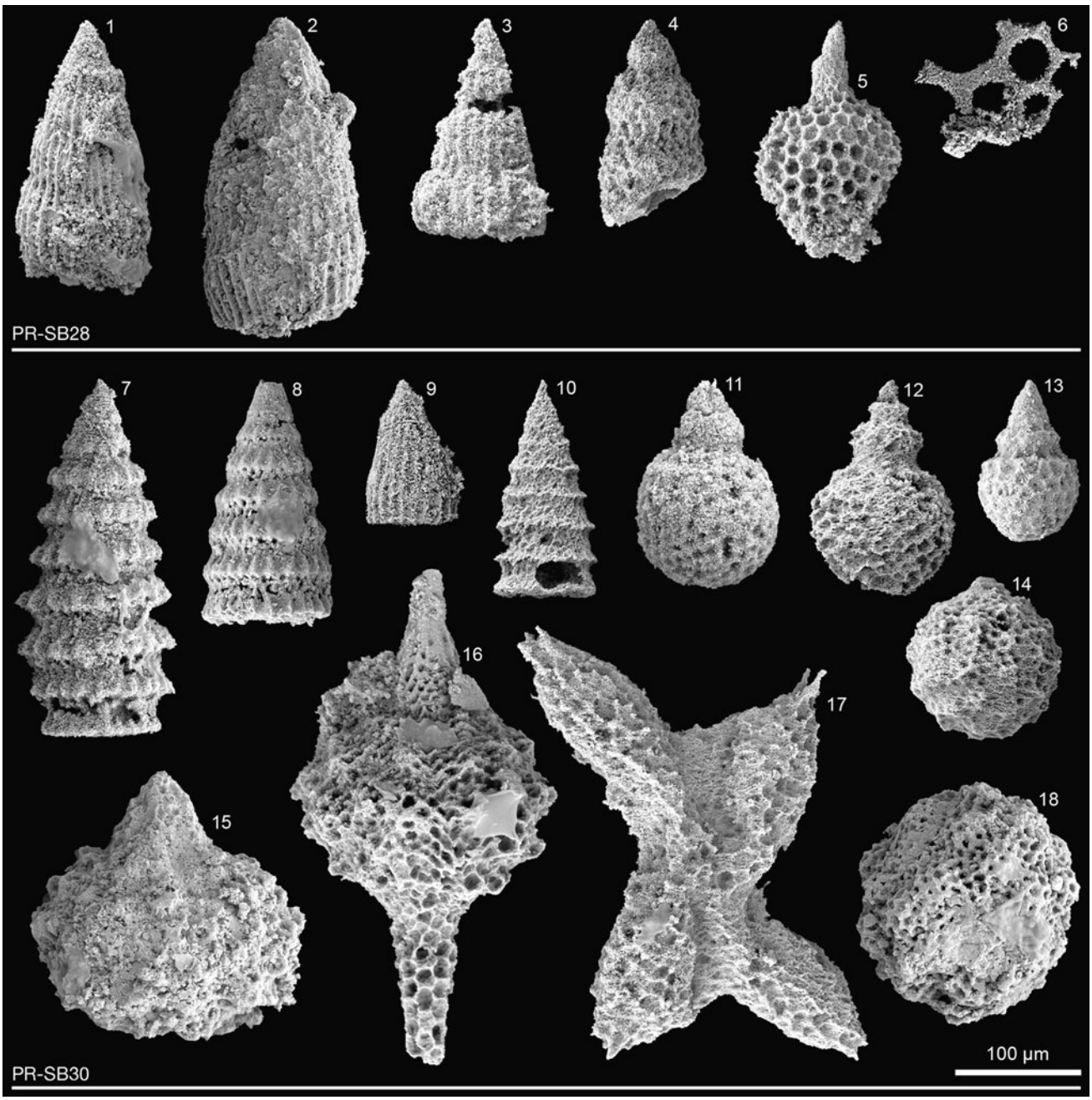

Plate 9 Scanning electron microscope pictures of radiolarians from the Bermeja Complex, western Puerto Rico. Marker = 100 µm. Sample PR-SB28 (late early Albian–middle Cenomanian). Figs 1, 2 ***Archaeodictyomitra gracilis*** (SQUINABOL) gr. Fig. 3 ***Archaeodictyomitra*** **sp.** Fig. 4 ***Stichomitra*** **(?) sp.** Fig. 5 ***Squinabollum*** **aff.** ***fossile*** (SQUINABOL). Fig. 6 **Neosciadiocapsidae** PESSAGNO **gen. et sp. indet.** Sample PR-SB30 (Barremian). Fig. 7 ***Pseudodictyomitra leptoconica*** (FOREMAN). Fig. 8 ***Pseudodictyomitra*** **sp.** Fig. 9 ***Archaeodictyomitra*** **sp.** Fig. 10 ***Tuguriella*** **sp.** Figs. 11, 15 ***Hiscocapsa*** **(?) spp.** Fig. 12 ***Hiscocapsa*** **aff.** ***asseni*** (TAN). Fig. 13 ***Hiscocapsa uterculus*** (PARONA). Fig. 14 ***Zhamoidellum*** **cf.** ***testatum*** JUD. Fig. 16 ***Syringocapsa*** **(?)** ***limatum*** FOREMAN. Fig. 17 ***Pseudocrucella*** **(?)** ***elisabethae*** (RÜST). Fig. 18 ***Praeconocaryomma*** **sp.**

Fig. 5 Photograph of the Middle Jurassic 1 m high and 3 m wide radiolarite sequence appearing as centimeter bedded greenish-orange radiolarian chert alternating with millimeter shale beds (sample PR-SB21 and PR-SB23)

Fig. 6 Photograph of the Middle Jurassic 2 m sequence of centimeter bedded red radiolarian cherts alternating with millimeter shale beds (sample PR-SB24)

Fig. 7 Photograph of the Early Cretaceous radiolarite, which crops out in 2–15 cm boudinaged layers of dark green to black radiolarian cherts rich in organic matter that weather orange (samples PR-SB26, PR-SB27, and PR-SB28)

6 Geodynamic models

Our plate tectonic model for the Middle Jurassic to Early Cretaceous western Pacific and Caribbean region, constrained by dynamic plate boundaries, plate buoyancy factors, oceanic spreading rates, subsidence patterns, stratigraphy and paleobiogeographic data, as well as the major tectonic and magmatic events, is an alternative explanation for the genesis and accretion of Pacific radiolarites (Fig. 14a–c). The reconstructions presented herein are part of a study developed at the Université de Lausanne (Stampfli and Borel 2002, Ferrari et al. 2008; Hochard 2008; Stampfli and Hochard 2009; Flores 2009), which describes the geodynamic history of several regions of the world.

6.1 165 Ma (Bathonian)

Several internal subduction zones characterized the Panthalassa (or Pacific) superocean as shown by Johnston and Borel (2007). One of these intra-oceanic subduction zones did develop immediately adjacent to the western margin of North America (Fig. 14a). The herein called Mezcalera ocean subducted northwest beneath the Mackinley ocean and leaded to the formation of the Guerrero-Phoenix island arcs system and the opening of the Guerrero back-arc ocean. The Triassic to Jurassic magmatic belt from British Columbia to Peru testify to a west-facing arc system on the western margin of the American plates (e.g., Pindell et al. 2005). This arc system resulted from the east-dipping subduction of the Mezcalera ocean. The

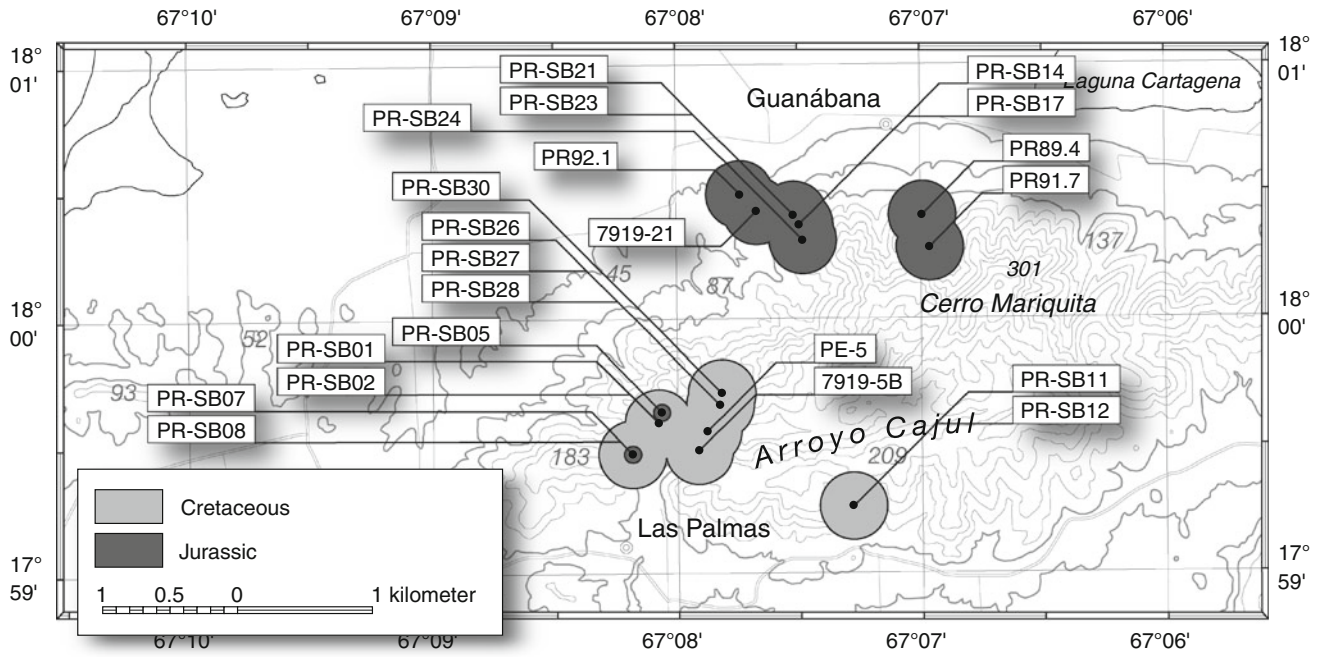

Fig. 8 Radiolarite outcrop map of Sierra Bermeja Complex showing the younging of radiolarian cherts from north to south, evoking a polarity of accretion. Outcrops 7919-5B, 7919-21, and PE-5 were sampled by Mattson and Pessagno (1979). Outcrops PR89.4, PR91.7, and PR92.1B were sampled by Montgomery et al. (1994a)

Proto-Caribbean ocean opening, separating the North American plate from the South American plate, is weakly constrained. However, $^{40}Ar/^{39}Ar$ ages of 190 to 154 Ma on hornblende in both the pegmatite and amphibole dikes of the oceanic Tinaquillo Complex from Venezuela (Sisson et al. 2005) attest to the presence of a pre-Pliensbachian active oceanic ridge between the Americas. Whereas, the oldest sea-floor magnetic anomaly in the Central Atlantic is of Toarcian age (175–183 Ma, Steiner et al. 1998).

During the Middle Jurassic, the oldest radiolarites of the Bermeja Complex (sample PR92.1B of Montgomery et al. 1994b, and samples PR-SB05, PR-SB14, PR-SB21, PR-SB23, and PR-SB24 of this study, see Table 10) could have been deposited in the southeastern Mackinley ocean or in the young Guerrero back-arc ocean, close to their spreading ridge, but a Mezcalera origin seems more probable. This oceanic complex comprises a very tectonized Late Jurassic radiolarite (sample PR-SB17), which yielded reworked radiolarian specimens of Middle Jurassic age. Moreover, this Late Jurassic outcrop is surrounded by scattered Middle Jurassic cherts. This could be a convincing indication for a Late Jurassic deposition of this sediment near an accretionary prism enclosing Middle Jurassic accreted material. Furthermore, Montgomery et al. (1994a) reported the presence of Late Jurassic (Kimmeridgian–Tithonian) tuffaceous cherts, which deposition would be consistent with a subduction context. These observations may indicate that these rocks would have undergone a Kimmeridgian–Tithonian accretionary event. This tectonic situation could have been encountered south of the Guerrero-Phoenix arc. In the case of this hypothesis is accepted, most probably all the Middle Jurassic sediments of the Bermeja Complex would have been deposited in the Mezcalera ocean.

6.2 142 Ma (Berriasian)

During the Late Jurassic, the Mesquito Terrane collided with and accreted to the North American plate (Fig. 14b). The old oceanic crust of the Mezcalera ocean continued its north-west-dipping subduction beneath the Guerrero ocean displacing the Guerrero-Phoenix Island arc southward. Rifting of the Gulf of Mexico began during the late Middle Jurassic (Pindell and Kennan 2007) and was synchronous with the opening of the Arpero oceanic basin. This basin was extended to the south with the opening of the Quebrada Grande oceanic basin during the early Early Cretaceous.

The Late Jurassic radiolarian cherts of the Bermeja Complex (samples PR-SB08 and PR-SB17, see also discussion above concerning sample PR-SB17) could have been deposited in the Mezcalera ocean.

Table 10 Synopsis of the biochronologic ages determined from outcrops of the Mariquita Chert Formation of the Bermeja Complex

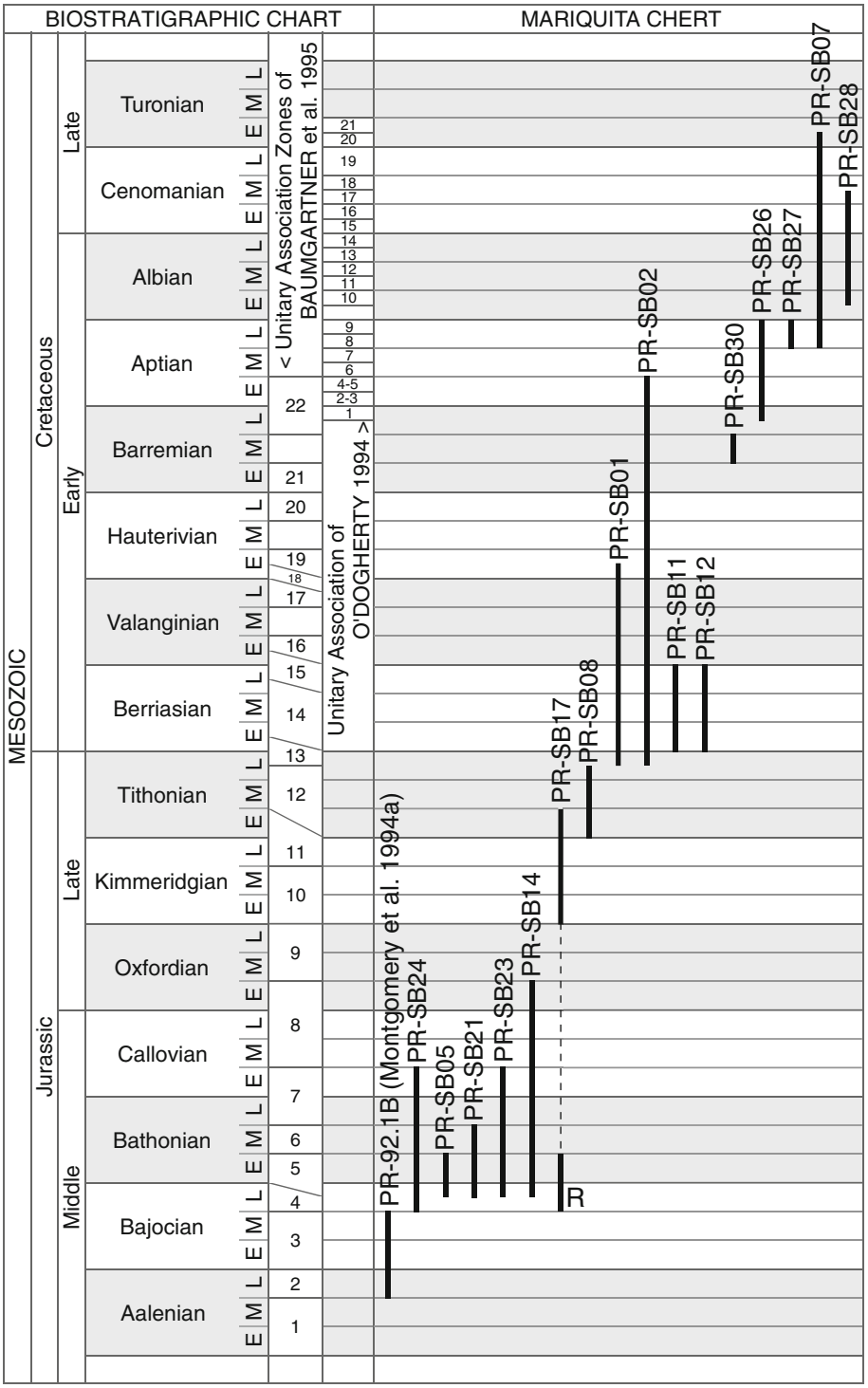

R reworked specimens

6.3 112 Ma (Aptian–Albian)

The Mezcalera ocean was completely consumed in subduction zones during the Early Cretaceous and was replaced by the Guerrero ocean in its former equatorial position dragging the Farallon oceanic plate eastward (Fig. 14c). During the Early Cretaceous, the Farallon plate was subducting beneath the North American plate. Closure

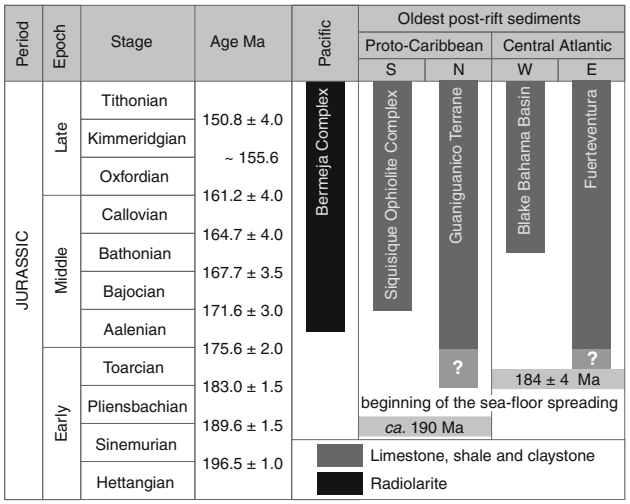

Fig. 9 Comparison of the age of the Mariquita Formation and the ages of the oldest known post-rift sediments of the Proto-Caribbean and the Central Atlantic. The age of the radiolarian faunas is no longer an evidence for a Pacific origin of the Bermeja Complex. Whereas, the presence of the radiolarite facies in Mesozoic oceanic terranes of the Caribbean plate is a good indication for a Pacific origin, because this facies has never been observed in neither the sediments of the Proto-Caribbean and the Central Atlantic. Initiation of the sea-floor spreading for the Proto-Caribbean after Sisson et al. (Tinaquillo Complex, 2005) and for the central Atlantic (Fuerteventura, Canary Islands) after Huon et al. (1993) and Steiner et al. (1998). Geological time scale after Gradstein et al. (2004)

of the Arpero oceanic basin and the collision of the Chortis block with the North American plate also occurred during this period.

The Early Cretaceous radiolarites of the Bermeja Complex (samples PR-SB01, PR-SB02, PR-SB11, and PR-SB12, see Table 10) were probably deposited in the Mezcalera ocean out of range from any continental or volcanic arc influence (Fig. 14b). Whereas, the late Early Cretaceous cherts rich in organic matter and interbedded with tuffs (samples PR-SB26, PR-SB27, PR-SB28, and PR-SB30, see Table 10) were probably sedimented in the Guerrero ocean closer to the Taino arc formed by the east-dipping subduction of this ocean beneath the Proto-Caribbean realm (Fig. 14c).

7 Conclusions

Sixteen radiolarian samples directly date the Mariquita Chert Formation, ranging in age from early Middle Jurassic to early Late Cretaceous (late Bajocian–early Callovian to late early Albian–early middle Cenomanian). The radiolarian ages presented in this study, the review of previous radiolarian studies, and published radiometric ages show that the Bermeja Complex ranges in age from Middle Jurassic to early Late Cretaceous (late Aalenian to middle

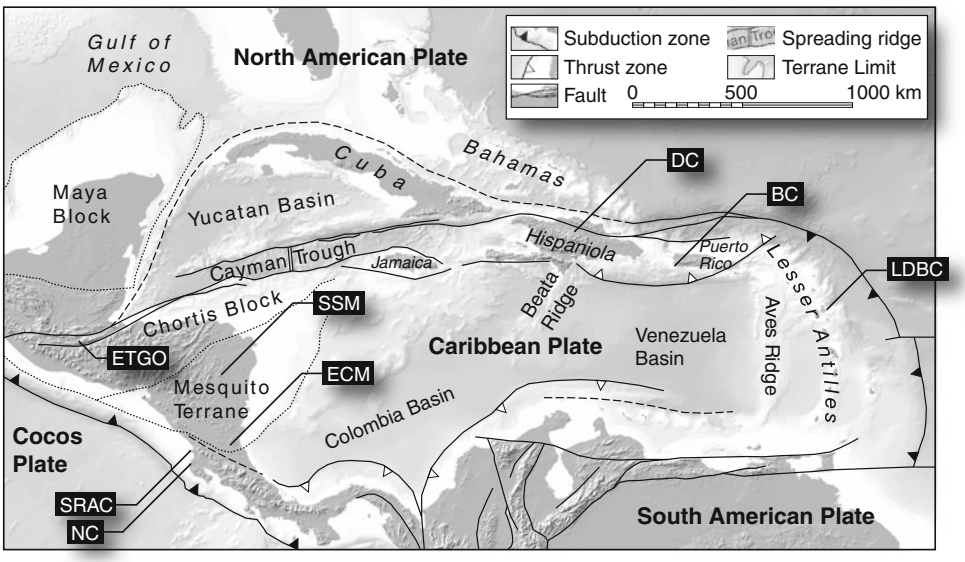

Fig. 10 Circum-Caribbean region map modified from Baumgartner et al. (2008), and Pindell and Kennan (2009) with plate-boundaries and bathymetry, showing important tectonic features and radiolarite localities discussed in the text. From west to east, *ETGO* El Tambor Group Ophiolites, *SRAC* Santa Rosa Accretionary Complex, *NC* Nicoya Complex, *SSM* Siuna Serpentinite Mélange, *ECM* El Castillo Mélange, *DC* Duarte Complex, *BC* Bermeja Complex, and *LDBC* La Désirade Basement Complex of Guadeloupe

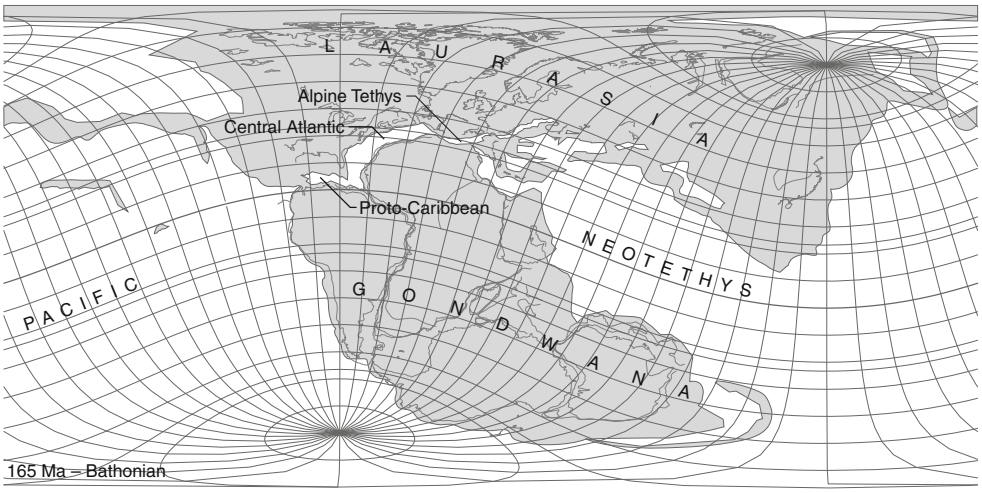

Fig. 11 Paleogeographic map for 165 Ma (Bathonian, according to Gradstein et al. 2004) showing the oceanic basins discussed in the text, with continental crust in *grey* and oceanic crust in *white*. The Neotethys and the Pacific oceans were covering wide paleolatitude and paleolongitude ranges and were most of the time fully connected with each other. Whereas, the Central Atlantic and the Proto-Caribbean oceanic basins formed a low-latitude restricted Mediterranean-like sea with indirect surface-water connections with the world ocean

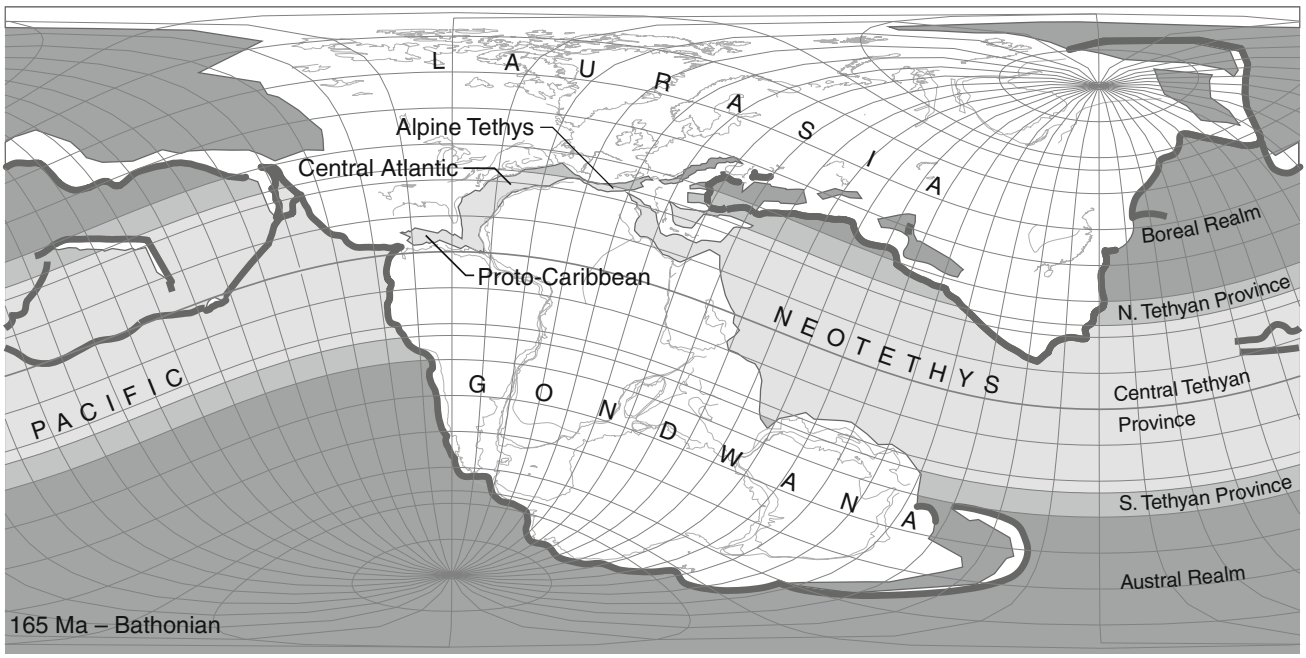

Fig. 12 Paleogeographic map for 165 Ma (Bathonian, according to Gradstein et al. 2004) showing the oceanic basins discussed in the text, with continental crust in *white*, the different provinces of the paleolatitudinal model of Pessagno et al. (1993) in *grey*, and active margins in *dark grey*. The model of Pessagno et al. (1993) does not take in account the paleogeography and the oceanic currents

Cenomanian). Moreover, the study of radiolarian ages of the Bermeja Complex reveals a possible feature, which is the younging of the cherts to the south. This could suggest an accretionary mechanism along an active margin. However, this hypothesis still remains debatable, as it needs a more systematic study to be validated.

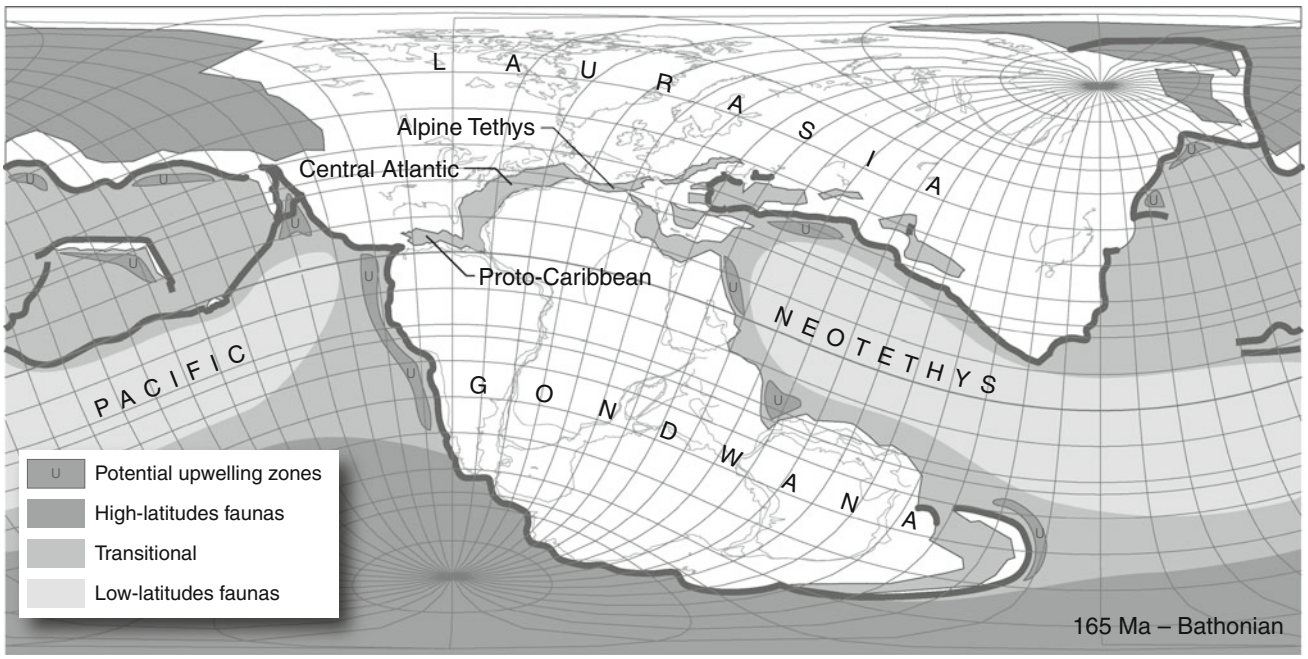

Fig. 13 Paleogeographic map for 165 Ma (Bathonian, according to Gradstein et al. 2004) showing the oceanic basins discussed in the text, with continental crust in *white* and active margins in *dark grey*. This map represents an attempt to show the distribution of radiolarian assemblages taking in account the paleogeography and potential water currents. In the generally low-latitude context of the Proto-Caribbean and Central Pacific, "high-latitude-faunas" can be associated with intraoceanic subduction zones or active continental margins of the Americas, both acting as upwelling margins or providers of land nutrients inputs

We think that the deep oceanic water currents, have played a major role in the deposition of radiolarian cherts. During the Jurassic, these currents, driven by density and temperature gradients, could not be normally generated in the low-latitude restricted Proto-Caribbean and Central Atlantic basins. Based on this paleoceanographic argument and on the global distribution of Middle Jurassic sediments associated with oceanic crust, we come to the conclusion that the radiolarite facies *s.s.* and the associated Mesozoic oceanic terranes of the Caribbean plate, i.e. the Nicoya Complex and the Santa Rosa Accretionary Complex of Costa Rica, the El Castillo and Siuna Serpentinite Mélanges of Nicaragua, the El Tambor Group Ophiolites of Guatemala, the Duarte Complex of Hispaniola, the Bermeja Complex of Puerto Rico, and the La Désirade Basement Complex of Guadeloupe are of Pacific origin. The previous argument for a Pacific origin of the Bermeja Complex presented by Montgomery et al. (1994b), based on their radiolarian age and their estimation of the oldest Proto-Caribbean oceanic crust, is nowadays seriously questionable, owing to the recent progresses in radiolarian biostratigraphy and new discoveries on the age of the first oceanic crust spreading between the Americas.

The observed changes in radiolarian faunal composition suggest a variation of the paleoceanographic conditions, rather than an indication on the paleolatitude of deposition, as firstly stated by Pessagno and Blome (1986). In the low-latitudinal Caribbean context, *Parvicingulidae*-rich assemblages could indicate the proximity of important landmasses acting as upwelling margins or land nutrients inputs, instead of higher paleolatitudinal deposition.

According to this radiolarian study and our plate tectonic model, the Middle Jurassic to Early Cretaceous radiolarian ribbon chert of the Bermeja Complex are remnants of the Mezcalera ocean and may have undergone at least one accretionary and one collisional events. The first one during the northwest dipping intra-oceanic subduction of the Mescalera ocean beneath the Mackinley ocean (and later the Guerrero ocean). The second one during the late Early Cretaceous collision of the Guerrero-Phoenix arc with the Chortis block. Finally, we interpret the middle Cretaceous radiolarites as remnants of the Guerrero ocean sedimented close to the Taino Arc.

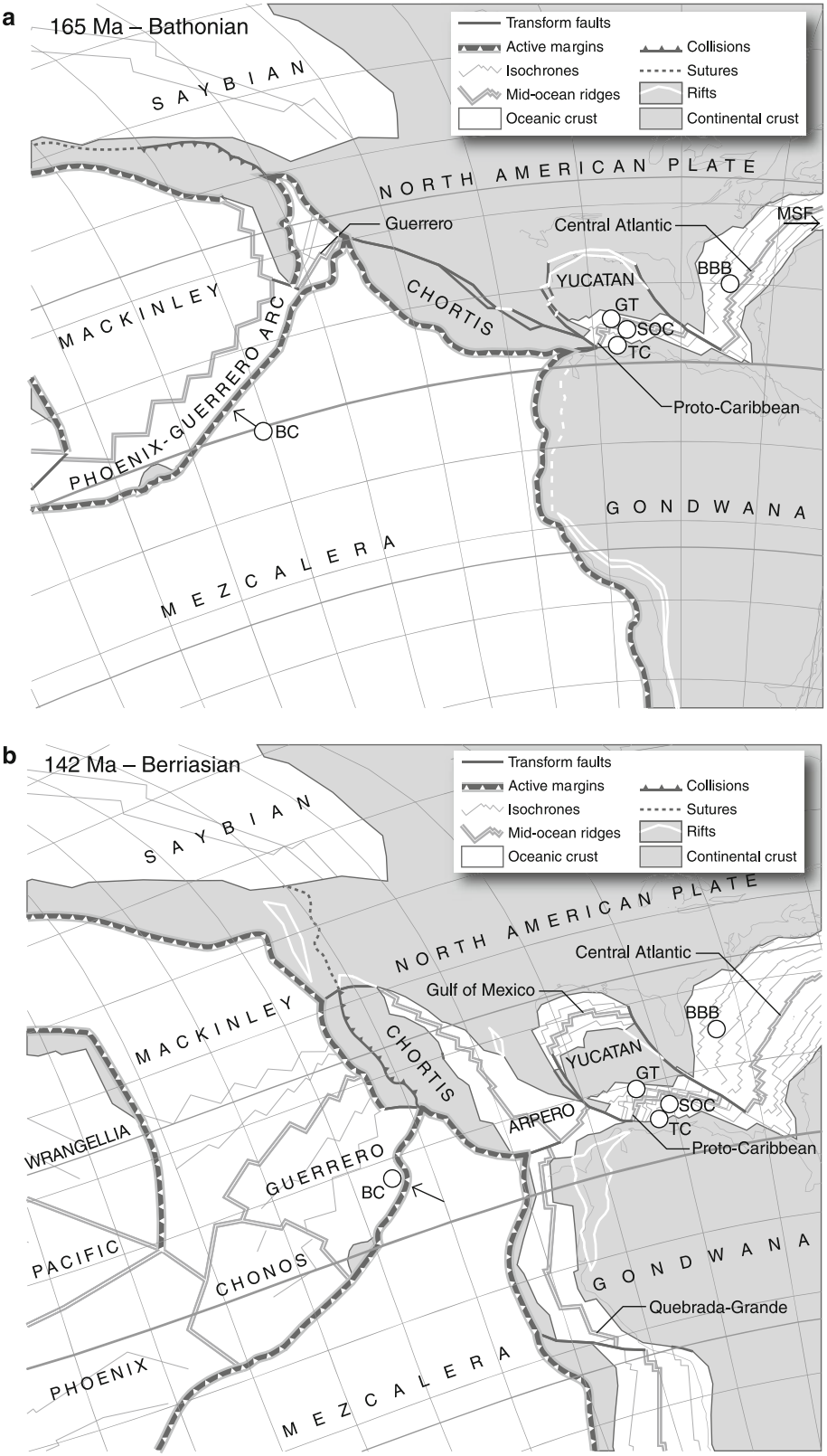

Fig. 14 Paleogeographic map for **a** 165 Ma (Bathonian, according to Gradstein et al. 2004), **b** 142 Ma (Berriasian, according to Gradstein et al. 2004), and **c** 112 Ma (Aptian–Albian, according to Gradstein et al. 2004) showing the main geodynamic units discussed in the text, potential position of the rocks composing the Bermeja Complex of Puerto Rico (BC) and position of the Taino Arc (TAI), the Guaniguanico Terrane of Cuba (GT), the Tinaquillo Complex (TC) and the Siquisique Ophiolite Complex (SOC) of Venezuela, the Blake Bahama Basin (BBB) in the western central Atlantic, and the Mesozoic sequence of Fuerteventura (MSF) in the eastern central Atlantic

Fig. 14 continued

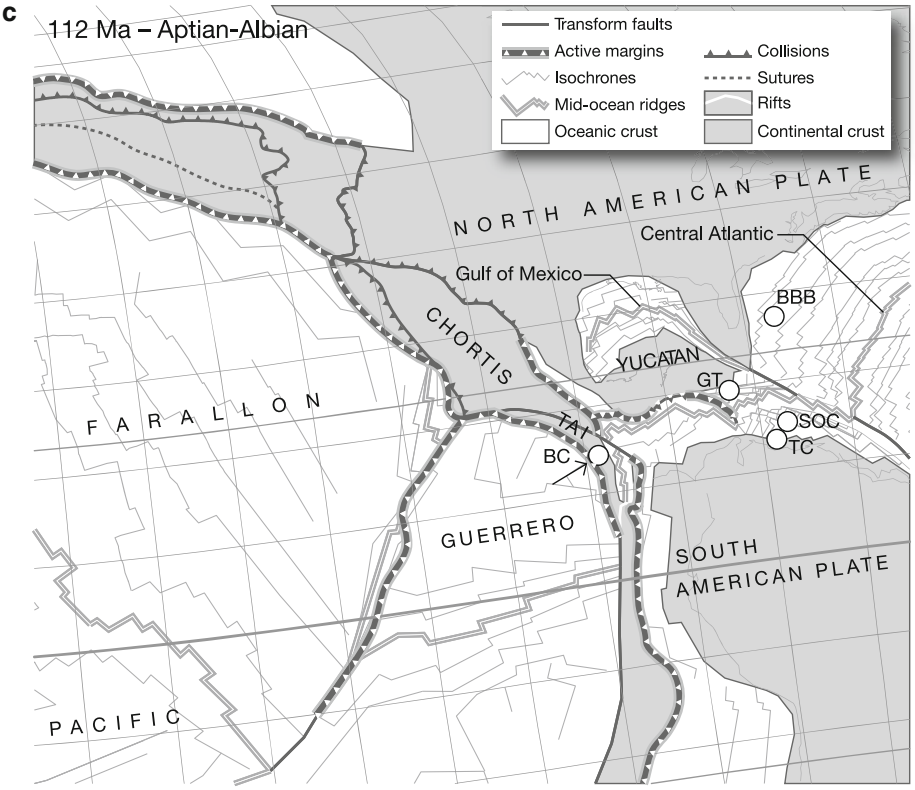

Acknowledgments The authors are grateful to Spela Gorican, Paleontoloski Institut Ivana Rakova (Ljubljana, Slovenia), and Luis O'Dogherty, Universidad de Cádiz (Spain) for their invaluable comments. A cordial thanks for their very useful commentaries to Marco Chiari, Istituto di Geoscienze e Georisorse (Florence, Italy), and Fabrice Cordey, Université Lyon 1 (France), who have kindly accepted to review this study.We are thankful to Patrice Moix and Laurent Thum, Université de Lausanne (Switzerland), for their considerable contribution to the geodynamic part of this work. We also express our gratitude to Marc-Olivier Diserens, Pascal Tschudin, and Mélanie Barboni, Université de Lausanne (Switzerland), for their assistance during the SEM and laboratory work. We thank Johannes H. Schellekens, Universidad de Mayagüez (Puerto Rico), for supplying us with topographic maps of the Sierra Bermeja and unobtainable literature. This work has been supported by the Swiss National Foundation (Grants no. 200020-116667 and 125130), by the Société Académique Vaudoise (Bourse Félix Bonjour) and by *the Swiss Palaeontological Society*.

Appendix A: Systematic paleontology

Three new radiolarian taxa are described herein. Although these new species have been described on the basis of three or even of a single specimen, they present well-individualized morphological characters.

Holotypes and paratypes are stored in the collection of the Musée de Géologie de Lausanne, Université de Lausanne, Switzerland (MGL no. 97012 and 97016).

Subclass **RADIOLARIA**

Order **POLYCYSTINA**

Suborder **SPUMELLARIA**

Family **PANTANELLIIDAE** Pessagno

Genus ***Pantanellium*** Pessagno

Type species *Pantanellium riedeli* Pessagno

Pantanellium karinae Bandini, n. sp.

Plate 5, Figs. 38–40

Description Cortical shell small, subspherical to ellipsoid and relatively thick-walled with four to five massive hexagonal and pentagonal pore frames on half the circumference with relatively high nodes at vertices. In the equatorial zone, nodes with short and conical secondary spines circular in cross-section. Cortical shell with triradiate bipolar primary spines, massive, relatively long, and subequal having three wide ridges alternating with three wide grooves. Diameter of cortical shell about half-length of primary spines. Diameter of primary spines at their base about two-third that of cortical shell.

Dimensions (based on one complete and two partial specimens) Diameter of the cortical shell 60–80 μm, length of primary spines 110–130 μm.

Holotype Plate 5, Fig. 38, MGL no. 97016, Musée de Géologie de Lausanne, Université de Lausanne, Switzerland.

Remarks Pantanellium karinae n. sp. differs from *P. riedeli* Pessagno by having secondary spines in the equatorial zone, wider bipolar primary spines, and a more elongated cortical shell. *P. karinae* n. sp. differs from

P. coronense Cheng by having a subspherical to ellipsoid cortical shell with maximum width along the bipolar primary spines axis, and primary spines subequal in length. *P. karinae* n. sp. differs from *P. philippinense* Cheng by having bipolar primary spines subequal in length and width.

Etymology This species is named for the London-based architect and contemporary art curator Karine Teyssier.

Occurrence and possible range Rare in the early Kimmeridgian to early Tithonian sample PR-SB17 (however, some reworked characteristic species of Middle Jurassic are also present in this sample). This species was also found in the late Kimmeridgian–Tithonian of Romania (Dumitrica unpublished data).

Appendix B: Locality description

Samples PR-SB01 and PR-SB02

This outcrop is approximately located 1 km north of the small village of Las Palmas (Fig. 2). To reach this outcrop (Fig. 3) from Las Palmas leave road 303 and follow the track called "Camino El Zapato" going northward and crossing the Bermeja mountain range. About 1.5 km further, take a small road going westward and up the hill to an antenna (coordinates N17°59′33.10″ W067°08′05.70″). Following this small road, one crosses two small valleys (approximately 150 and 300 m after the crossing), the outcrop is located in the second valley a few meters above the road (coordinates N17°59′28.40″ W067°08′03.00″).

PR-SB01 (Table 1; Plate 1)

This sample yielded a radiolarian association comprising: *Amuria* sp., *Archaeodictyomitra* cf. *tumandae* Dumitrica, *Archaeodictyomitra pseudomulticostata* (Tan), *Archaeodictyomitra* spp., *Caneta* (?) sp., *Cinguloturris* cf. *cylindra* Kemkin & Rudenko, *Cryptamphorella* sp., *Emiluvia* cf. *ordinaria* Ozvoldova, *Emiluvia chica* Foreman, *Hiscocapsa* cf. *kitoi* (Jud), *Hiscocapsa* cf. *kaminogoensis* (Aita), *Obesacapsula bullata* Steiger, *Pantanellium squinaboli* (Tan), *Pseudodictyomitra carpatica* (Lozyniak), *Svinitzium depressum* (Baumgartner), *Tethysetta boesii* (Parona).

PR-SB02 (Table 1; Plate 1)

This sample yielded a radiolarian association comprising: *Acanthocircus* sp., *Archaeodictyomitra* cf. *chalilovi* (Aliev), *Archaeodictyomitra* cf. *tumandae* Dumitrica, *Archaeodictyomitra mitra* gr. Dumitrica, *Archaeodictyomitra* sp., *Cryptamphorella* spp., *Homoeoparonaella* cf. *irregularis* (Squinabol), *Pantanellium squinaboli* (Tan), *Pseudodictyomitra* cf. *suyarii* Dumitrica.

Sample PR-SB05 (Table 2; Plate 2)

The outcrop is located approximately 20 m in elevation above outcrop PR-SB01 in the same valley (Fig. 2). The radiolarite crops out in a block of about 2 m long and 1 m high. The greenish-grey radiolarite block is embedded in a massive and brecciated greenish-grey siliceous rock that weathers reddish and compose most of the Sierra Bermeja (Fig. 4).

This sample yielded a radiolarian association comprising: *Hexasaturnalis nakasekoi* Dumitrica & Dumitrica-Jud, *Hiscocapsa lugeoni* O'Dogherty, Goričan & Dumitrica, *Parahsuum* sp., *Praewilliriedellum convexum* (Yao), *Praewilliriedellum japonicum* (Yao), *Striatojaponocapsa synconexa* O'Dogherty, Goričan & Dumitrica, *Tetraditryma* sp., *Svinitzium* cf. *kamoense* (Mizutani & Kido), *Triversus* (?) sp., *Williriedellum tetragona* (Matsuoka).

Samples PR-SB07 and PR-SB08

This outcrop (coordinates N17°59′27.60″ W067°08′12.3″) situated on top of a crest is located 300 m southwest of the antenna (coordinates N17°59′33.10″ W067°08′05.70″, see above PR-SB01 and PR-SB02 for the pathway to reach the antenna, see also Fig. 2).

PR-SB07 (Table 3; Plate 2)

This sample yielded a radiolarian association comprising: *Archaeodictyomitra* cf. *chalilovi* (Aliev), *Archaeodictyomitra montisserei* (Squinabol), *Archaeodictyomitra* sp., *Cryptamphorella* spp., gen. et sp. indet., *Hiscocapsa* cf. *asseni* (Tan), *Napora* sp., *Obeliscoites* (?) sp., *Hiscocapsa pseudouterculus* (Aita & Okada), *Hiscocapsa* cf. *uterculus* (Parona), *Theocampe* (?) sp.

PR-SB08 (Table 3; Plate 3)

This sample includes the following radiolarian association: *Archaeodictyomitra* spp., *Cryptamphorella* spp., gen. et sp. indet., *Hiscocapsa* cf. *campana* (Kiessling), *Hiscocapsa* cf. *subcrassitestata* Aita, *Loopus* aff. *primitivus* (Matsuoka & Yao), *Loopus* sp., *Loopus primitivus* (Matsuoka & Yao), *Napora* spp., *Praeconocaryomma* sp., *Spinosicapsa* (?) sp., *Triactoma* sp.

Samples PR-SB11 and PR-SB12

The outcrops (coordinates N17°59′05.7″ W67°07′24.3″) are located approximately 1.5 km east of the small town of Las Palmas (Fig. 2). To reach these outcrops follow road 303 to the east for 2 km from Las Palmas. The outcrops are situated on the hill to the north of the road.

PR-SB11 (Table 4; Plate 4)

This sample yielded a radiolarian association comprising: *Acanthocircus* sp., *Archaeodictyomitra* cf. *vulgaris* Pessagno, *Archaeodictyomitra immenhauseri* Dumitrica, *Archaeodictyomitra* cf. *tumandae* Dumitrica, *Archaeodictyomitra* sp., *Archaeospongoprunum* sp., *Cryptamphorella* sp., *Mictyoditra* sp., *Pantanellium squinaboli* (Tan), *Pantanellium* sp., *Pseudodictyomitra* aff. *leptoconica* (Foreman), *Pseudodictyomitra* sp., *Svinitzium* (?) *mizutanii* Dumitrica, *Thanarla* cf. *conica* (Aliev), *Stichomitra* (?) sp.

PR-SB12 (Table 4; Plate 4)

This sample includes the following radiolarian association: *Archaeodictyomitra* cf. *pseudomulticostata* (Tan), *Archaeodictyomitra immenhauseri* Dumitrica, *Archaeodictyomitra mitra* gr. Dumitrica, *Hiscocapsa* (?) sp., *Obesacapsula* (?) cf. *cetia* (Foreman), *Cryptamphorella* sp.

Samples PR-SB14 and PR-SB17

The outcrop (coordinates N18°00′18.6″ W67°07′42.1″) is located along the northwestern margin of Sierra Bermeja (Fig. 2). To reach this outcrops from Las Palmas leave road 303 and follows the track called "Camino El Zapato" going north–north-east and crossing the Bermeja mountain range. About 3 km further, a very tectonized metric green–brown radiolarite block crops out where the path crosses a stream gully in an area adjacent to basalts. The location of this outcrop seems to correspond to this of the Early Jurassic sample PR92.1B from Montgomery et al. (1994b).

PR-SB14 (Table 5; Plate 4)

This sample includes the following radiolarian association: *Alievium* cf. *longispineum* Yang & Wang, *Archaeodictyomitra prisca* Kozur & Mostler, *Archaeodictyomitra* sp., *Eucyrtidiellum unumaense* s.l. (Yao), *Eucyrtidiellum unumaense pustulatum* Baumgartner, gen et sp. indet., *Homeoparonaella* sp., *Spinosicapsa* (?) sp., *Striatojaponocapsa* (?) sp., *Transhsuum* sp.

PR-SB17 (Table 5; Plate 5)

This sample contains by far the richest radiolarian assemblage of this study: *Archaeodictyomitra patricki* Kocher, *Archaeodictyomitra* spp., *Archaeospongoprunum elegans* Wu, *Cryptamphorella* sp., *Deviatus diamphidius hipposidericus* (Foreman), *Emiluvia ordinaria* Ozvoldova, *Emiluvia* (?) sp., *Eucyrtidiellum ptyctum* (Riedel & Sanfilippo), *Hiscocapsa* (?) sp., *Napora* sp., Nassellaria gen. et sp. indet., *Pantanellium karinae* Bandini n. sp., *Pantanellium ranchitoense* Pessagno & Macleod, *Pantanellium* sp., *Parvicingula vera* Pessagno & Whalen, Parvicingulidae gen. et sp. indet., *Praeconocaryomma* sp., *Praewilliriedellum convexum* (Yao), *Praewilliriellum* sp. aff. *robustum* (Matsuoka), *Pseudodictyomitra* (?) sp., *Pseudodictyomitra* sp., *Pseudodictyomitrella* (?) sp., Spumellaria gen. et sp. indet., *Stichomitra* (?) *doliolum* Aita gr., *Stichomitra* (?) spp., *Striatojaponocapsa plicarum* (Yao), *Vallupus hopsoni* Pessagno & Blome, *Williriedellum carpathicum* Dumitrica, *Williriedellum formosum* (Chiari, Marcucci & Prela), *Williriedellum* sp..

Samples PR-SB21 and PR-SB23

This outcrop (no coordinates, because GPS signal was too weak) is located 20 m upstream from outcrop PR-SB14 and PR-SB17 (Fig. 2). The radiolarite sequence is 1 m high and 3 m wide and appears as centimeter bedded green-orange radiolarian chert alternating with millimeter shale beds (Figs. 5, 6). Sample PR-SB21 comes from the east side of the stream gully and sample PR-SB23 from the west side of the stream gully.

PR-SB21 (Table 6; Plate 6)

This sample yielded a radiolarian association comprising: *Archaeodictyomitra* aff. *rigida* Pessagno, *Canoptum* (?) sp., *Praewilliriedellum convexum* (Yao), *Ristola turpicula* Pessagno & Whalen, *Striatojaponocapsa synconexa* O'Dogherty, Goričan & Dumitrica, *Transhsuum* sp., *Williriedellum yaoi* (Kozur).

PR-SB23 (Table 6; Plate 6)

This sample includes the following radiolarian association: *Angulobracchia* sp., *Archaeodictyomitra* aff. *rigida* Pessagno, *Archaeodictyomitra patricki* Kocher, *Eucyrtidiellum unumaense* s.l. (Yao), gen. et sp. indet., *Levileugeo ordinarius* Yang & Wang, Nassellaria gen. et sp. indet., *Parahsuum* (?) sp., *Praewilliriedellum convexum* (Yao), *Praewilliriedellum robustum* (Matsuoka), *Stichomitra* (?) sp., *Striatojaponocapsa synconexa* O'Dogherty, Goričan & Dumitrica, *Svinitzium kamoense* (Mizutani & Kido), *Transhsuum maxwelli* gr. (Pessagno), *Triversus* (?) sp., *Williriedellum yaoi* (Kozur), *Xitus* sp.

Sample PR-SB24 (Table 7; Plate 6)

This outcrop (coordinates N18°00′13.5″ W067°07′41.2″) is located 100 m upstream from outcrop PR-SB14 (Fig. 2), and 80 m upstream from outcrop PR-SB21 and may correspond to outcrop 7919-21 from Mattson and Pessagno (1979).

This sample yielded a radiolarian association comprising: *Archaeodictyomitra* aff. *rigida* Pessagno, *Archaeodictyomitra* sp., *Canoptum* (?) sp., *Emiluvia* sp., *Eucyrtidiellum unumaense* s.l. (Yao), *Parahsuum* sp., *Praewilliriedellum convexum* (Yao), *Praewilliriedellum japonicum* (Yao), *Transhsuum* cf. *hisuikyoense* (Isozaki & Matsuda), *Transhsuum* cf. *maxwelli* gr. (Pessagno), *Triactoma parablakei* Yang & Wang.

Samples PR-SB26, PR-SB27 and PR-SB28

The outcrop (coordinates N17°59′31.2″ W67°07′50.6″) is located about 1.2 km north–north-east from the village of Las Palmas along the track called "Camino El Zapato" (Fig. 2).

PR-SB26 (Table 8; Plate 7)

This sample includes the following radiolarian association: *Acaeniotyle* cf. *umbilicata* (Rüst), *Acanthocircus* sp., *Archaeodictyomitra* spp., *Crucella* sp., *Crucella* sp. (with five rays), *Emiluvia* sp., *Napora* sp., *Nassellaria* gen. et sp. indet., *Obeliscoites* cf. *vinassai* (Squinabol), *Obesacapsula* sp., Pantanelliidae gen. et sp. indet., *Parvicingula* sp., *Praeconocaryomma* sp., *Pseudoeucyrtis corpulentus* Dumitrica, *Pseudoeucyrtis hanni* (Tan), *Thanarla* sp.

PR-SB27 (Table 8; Plate 8)

This sample yielded a radiolarian association comprising: *Archaeodictyomitra* cf. *gracilis* (Squinabol), *Archaeodictyomitra* cf. *immenhauseri* Dumitrica, *Archaeodictyomitra montisserei* (Squinabol), *Archaeodictyomitra* spp., *Archaeospongoprunum* sp., *Halesium* (?) cf. *palmatum* Dumitrica, *Pantanellium* sp., *Quadrigastrum lapideum* O'Dogherty, Spumellaria gen. et sp. indet., *Stichomitra* (?) spp., *Thanarla* aff. *veneta* (Squinabol), *Thanarla brouweri* (Tan), *Thanarla* sp., *Stylosphaera* spp.

PR-SB28 (Table 8; Plate 9)

This sample includes the following radiolarian association: *Archaeodictyomitra gracilis* (Squinabol) gr., *Archaeodictyomitra* sp., Neosciadiocapsidae Pessagno gen. et sp. indet., *Squinabollum* aff. *fossile* (Squinabol), *Stichomitra* (?) sp.

PR-SB30 (Table 9; Plate 9)

The outcrop (coordinates N17°59′32.5″ W67°07′50.2″) is located approximately 50 m north of outcrop PR-SB26 on the track called "Camino El Zapato" (Fig. 2).

This sample yielded a radiolarian association comprising: *Archaeodictyomitra* sp., *Hiscocapsa* aff. *asseni* (Tan), *Hiscocapsa* (?) spp., *Hiscocapsa uterculus* (Parona), *Praeconocaryomma* sp., *Pseudocrucella* (?) *elisabethae* (Rüst), *Pseudodictyomitra leptoconica* (Foreman), *Pseudodictyomitra* sp., *Syringocapsa* (?) *limatum* Foreman, *Tuguriella* sp., *Zhamoidellum* cf. *testatum* Jud.

Appendix C: Species list

Acaeniotyle cf. *umbilicata* (Rüst): PR-SB26 (Plate 7, Fig. 12)

Acanthocircus spp.: PR-SB02 (Plate 1, Figs. 26, 27), PR-SB11 (Plate 4, Fig. 14), PR-SB26 (Plate 7, Fig. 14)

Alievium cf. *longispineum* Yang & Wang: PR-SB14 (Plate 4, Fig. 37)

Amuria sp.: PR-SB01 (Plate 1, Fig. 16)

Angulobracchia sp.: PR-SB23 (Plate 6, Fig. 30)

Archaeodictyomitra aff. *rigida* Pessagno: PR-SB21 (Plate 6, Fig. 1), PR-SB23 (Plate 6, Fig. 9), PR-SB24 (Plate 6, Fig. 31)

Archaeodictyomitra cf. *chalilovi* (Aliev): PR-SB02 (Plate 1, Fig. 18), PR-SB07 (Plate 2, Fig. 13)

Archaeodictyomitra cf. *gracilis* (Squinabol): PR-SB27 (Plate 8, Fig. 3)

Archaeodictyomitra cf. *immenhauseri* Dumitrica: PR-SB27 (Plate 8, Figs. 1, 2.)

Archaeodictyomitra cf. *pseudomulticostata* (Tan): PR-SB12 (Plate 4, Fig. 17)

Archaeodictyomitra cf. *tumandae* Dumitrica: PR-SB01 (Plate 1, Fig. 3), PR-SB02 (Plate 1, Fig. 19), PR-SB11 (Plate 4, Fig. 3)

Archaeodictyomitra cf. *vulgaris* Pessagno: PR-SB11 (Plate 4, Fig. 1)

Archaeodictyomitra gracilis (Squinabol) gr.: PR-SB28 (Plate 9, Figs. 1, 2)

Archaeodictyomitra immenhauseri Dumitrica: PR-SB11 (Plate 4, Fig. 4), PR-SB12 (Plate 4, Fig. 20)

Archaeodictyomitra mitra gr. Dumitrica: PR-SB02 (Plate 1, Fig. 20), PR-SB12 (Plate 4, Figs. 18, 19)

Archaeodictyomitra montisserei (Squinabol): PR-SB07 (Plate 2, Fig. 15), PR-SB27 (Plate 8, Figs. 4, 5)

Archaeodictyomitra patricki Kocher: PR-SB17 (Plate 5, Fig. 1), PR-SB23 (Plate 6, Fig. 10)

Archaeodictyomitra prisca Kozur & Mostler: PR-SB14 (Plate 4, Fig. 27)

Archaeodictyomitra pseudomulticostata (Tan): PR-SB01 (Plate 1, Fig. 2)

Archaeodictyomitra spp.: PR-SB01 (Plate 1, Figs. 4, 5), PR-SB02 (Plate 1, Fig. 21), PR-SB07 (Plate 2, Fig. 14), PR-SB08 (Plate 3, Figs. 1–5), PR-SB11 (Plate 4, Fig. 2), PR-SB14 (Plate 4, Fig. 26), PR-SB17 (Plate 5, Figs. 2, 3),

PR-SB24 (Plate 6, Fig. 32), PR-SB26 (Plate 7, Figs. 1, 2), PR-SB27 (Plate 8, Figs. 6, 7), PR-SB28 (Plate 9, Fig. 3), PR-SB30 (Plate 9, Fig. 9)

Archaeospongoprunum elegans Wu: PR-SB17 (Plate 5, Fig. 41)

Archaeospongoprunum spp.: PR-SB11 (Plate 4, Fig. 13), PR-SB27 (Plate 8, Figs. 13–15)

Caneta (?) sp.: PR-SB01 (Plate 1, Fig. 1)

Canoptum (?) spp.: PR-SB21 (Plate 6, Fig. 3), PR-SB24 (Plate 6, Fig. 38)

Cinguloturris cf. *cylindra* Kemkin & Rudenko: PR-SB01 (Plate 1, Fig. 6)

Crucella sp. (with five rays): PR-SB26 (Plate 7, Fig. 17)

Crucella sp.: PR-SB26 (Plate 7, Fig. 15)

Cryptamphorella spp.: PR-SB01 (Plate 1, Fig. 12), PR-SB02 (Plate 1, Figs. 23–25), PR-SB07 (Plate 2, Figs. 20–23), PR-SB08 (Plate 3, Figs. 13–17), PR-SB11 (Plate 4, Fig. 12), PR-SB12 (Plate 4, Figs. 21, 22, 24), PR-SB17 (Plate 5, Fig. 29)

Deviatus diamphidius hipposidericus (Foreman): PR-SB17 (Plate 5, Fig. 35)

Emiluvia (?) sp.: PR-SB17 (Plate 5, Fig. 33)

Emiluvia cf. *ordinaria* Ozvoldova: PR-SB01 (Plate 1, Fig. 14)

Emiluvia chica Foreman: PR-SB01 (Plate 1, Fig. 13)

Emiluvia ordinaria Ozvoldova: PR-SB17 (Plate 5, Fig. 32)

Emiluvia spp.: PR-SB24 (Plate 6, Fig. 40), PR-SB26 (Plate 7, Fig. 13)

Eucyrtidiellum ptyctum (Riedel & Sanfilippo): PR-SB17 (Plate 5, Fig. 16)

Eucyrtidiellum unumaense s.l. (Yao): PR-SB14 (Plate 4, Figs. 30 and 31), PR-SB23 (Plate 6, Fig. 25), PR-SB24 (Plate 6, Figs. 41, 42)

Eucyrtidiellum unumaense pustulatum Baumgartner: PR-SB14 (Plate 4, Fig. 32)

gen. et sp. indet.: PR-SB14 (Plate 4, Fig. 29), PR-SB07 (Plate 2, Fig. 19), PR-SB08 (Plate 3, Fig. 20), PR-SB23 (Plate 6, Fig. 27), PR-SB23 (Plate 6, Fig. 28)

Halesium (?) cf. *palmatum* Dumitrica: PR-SB27 (Plate 8, Fig. 18)

Hexasaturnalis nakasekoi Dumitrica & Dumitrica-Jud: PR-SB05 (Plate 2, Fig. 11)

Hiscocapsa cf. *asseni* (Tan): PR-SB07 (Plate 2, Figs. 28, 30, 31)

Hiscocapsa pseudouterculus (Aita & Okada): PR-SB07 (Plate 2, Figs. 24–26, 29)

Hiscocapsa (?) spp.: PR-SB12 (Plate 4, Fig. 25), PR-SB17 (Plate 5, Fig. 23), PR-SB30 (Plate 9, Figs. 11, 15)

Hiscocapsa aff. *asseni* (Tan): PR-SB30 (Plate 9, Fig. 12)

Hiscocapsa cf. *campana* (Kiessling): PR-SB08 (Plate 3, Fig. 21)

Hiscocapsa cf. *kitoi* (Jud): PR-SB01 (Plate 1, Fig. 11)

Hiscocapsa cf. *kaminogoensis* (Aita): PR-SB01 (Plate 1, Fig. 10)

Hiscocapsa lugeoni O'Dogherty, Goričan & Dumitrica: PR-SB05 (Plate 2, Fig. 4)

Hiscocapsa cf. *subcrassitestata* Aita: PR-SB08 (Plate 3, Fig. 22)

Hiscocapsa cf. *uterculus* (Parona): PR-SB07 (Plate 2, Fig. 27)

Hiscocapsa uterculus (Parona): PR-SB30 (Plate 9, Fig. 13)

Homeoparonaella sp.: PR-SB14 (Plate 4, Figs. 35, 36)

Homoeoparonaella cf. *irregularis* (Squinabol): PR-SB02 (Plate 1, Fig. 31)

Levileugeo ordinarius Yang & Wang: PR-SB23 (Plate 6, Fig. 29)

Loopus aff. *primitivus* (Matsuoka & Yao): PR-SB08 (Plate 3, Figs. 8, 9)

Loopus sp.: PR-SB08 (Plate 3, Fig. 10)

Loopus primitivus (Matsuoka & Yao): PR-SB08 (Plate 3, Figs. 6, 7)

Mictyoditra sp.: PR-SB11 (Plate 4, Figs. 5, 6)

Napora spp.: PR-SB07 (Plate 2, Figs. 34, 35), PR-SB08 (Plate 3, Figs. 18, 19), PR-SB17 (Plate 5, Figs. 18, 19), PR-SB26 (Plate 7, Fig. 10)

Nassellaria gen. et sp. indet.: PR-SB17 (Plate 5, Figs. 30, 31), PR-SB23 (Plate 6, Fig. 26), PR-SB26 (Plate 7, Fig. 11), PR-SB26 (Plate 7, Fig. 9)

Neosciadiocapsidae Pessagno gen. et sp. indet.: PR-SB28 (Plate 9, Fig. 6)

Obeliscoites (?) sp.: PR-SB07 (Plate 2, Figs. 32, 33)

Obeliscoites cf. *vinassai* (Squinabol): PR-SB26 (Plate 7, Fig. 8)

Obesacapsula (?) cf. *cetia* (Foreman): PR-SB12 (Plate 4, Fig. 23)

Obesacapsula bullata Steiger: PR-SB01 (Plate 1, Fig. 15)

Obesacapsula sp.: PR-SB26 (Plate 7, Fig. 6)

Pantanelliidae gen. et sp. indet.: PR-SB26 (Plate 7, Fig. 16)

Pantanellium karinae Bandini, n. sp.: PR-SB17 (Plate 5, Figs. 38–40)

Pantanellium ranchitoense Pessagno & Macleod: PR-SB17 (Plate 5, Fig. 36)

Pantanellium spp.: PR-SB11 (Plate 4, Fig. 16), PR-SB17 (Plate 5, Fig. 37), PR-SB27 (Plate 8, Figs. 19, 20)

Pantanellium squinaboli (Tan): PR-SB01 (Plate 1, Fig. 17), PR-SB02 (Plate 1, Figs. 28–30), PR-SB11 (Plate 4, Fig. 15)

Parahsuum (?) sp.: PR-SB23 (Plate 6, Fig. 16)

Parahsuum spp.: PR-SB05 (Plate 2, Fig. 3), PR-SB24 (Plate 6, Fig. 33)

Parvicingula sp.: PR-SB26 (Plate 7, Fig. 4)

Parvicingula vera Pessagno & Whalen: PR-SB17 (Plate 5, Fig. 10)

Parvicingulidae gen. et sp. indet.: PR-SB17 (Plate 5, Figs. 8, 9, 11)

Praeconocaryomma spp.: PR-SB17 (Plate 5, Fig. 34), PR-SB26 (Plate 7, Fig. 18), PR-SB30 (Plate 9, Fig. 18), PR-SB08 (Plate 3, Fig. 24)

Praewilliriedellum convexum (Yao): PR-SB05 (Plate 2, Figs. 5, 7), PR-SB17 (Plate 5, Fig. 22), PR-SB21 (Plate 6, Fig. 5), PR-SB23 (Plate 6, Figs. 18, 19), PR-SB24 (Plate 6, Fig. 37)

Praewilliriedellum japonicum (Yao): PR-SB05 (Plate 2, Fig. 6), PR-SB24 (Plate 6, Fig. 36)

Praewilliriedellum robustum (Matsuoka): PR-SB23 (Plate 6, Fig. 20)

Praewilliriedellum sp. aff. *robustum* (Matsuoka): PR-SB17 (Plate 5, Fig. 21)

Pseudocrucella (?) *elisabethae* (Rüst): PR-SB30 (Plate 9, Fig. 17)

Pseudodictyomitra (?) sp.: PR-SB17 (Plate 5, Fig. 12)

Pseudodictyomitra aff. *leptoconica* (Foreman): PR-SB11 (Plate 4, Fig. 9)

Pseudodictyomitra carpatica (Lozyniak): PR-SB01 (Plate 1, Fig. 9)

Pseudodictyomitra cf. *suyarii* Dumitrica: PR-SB02 (Plate 1, Fig. 22)

Pseudodictyomitra leptoconica (Foreman): PR-SB30 (Plate 9, Fig. 7)

Pseudodictyomitra spp.: PR-SB11 (Plate 4, Fig. 10), PR-SB17 (Plate 5, Fig. 13), PR-SB30 (Plate 9, Fig. 8)

Pseudodictyomitrella (?) sp.: PR-SB17 (Plate 5, Fig. 4)

Pseudoeucyrtis corpulentus Dumitrica: PR-SB26 (Plate 7, Fig. 5)

Pseudoeucyrtis hanni (Tan): PR-SB26 (Plate 7, Fig. 7)

Quadrigastrum lapideum O'Dogherty: PR-SB27 (Plate 8, Fig. 21)

Ristola turpicula Pessagno & Whalen: PR-SB21 (Plate 6, Fig. 4)

Spinosicapsa (?) sp.: PR-SB08 (Plate 3, Figs. 11, 12), PR-SB14 (Plate 4, Fig. 33)

Spumellaria gen. et sp. indet.: PR-SB17 (Plate 5, Fig. 42), PR-SB27 (Plate 8, Fig. 22)

Squinabollum aff. *fossile* (Squinabol): PR-SB28 (Plate 9, Fig. 5)

Stichomitra (?) *doliolum* Aita gr.: PR-SB17 (Plate 5, Figs. 14, 15)

Stichomitra (?) spp.: PR-SB11 (Plate 4, Fig. 7), PR-SB23 (Plate 6, Fig. 13), PR-SB28 (Plate 9, Fig. 4), PR-SB17 (Plate 5, Figs. 5–7), PR-SB27 (Plate 8, Figs. 8, 9)

Stylosphaera spp.: PR-SB27 (Plate 8, Fig. 16)

Striatojaponocapsa (?) sp.: PR-SB14 (Plate 4, Fig. 34)

Striatojaponocapsa plicarum (Yao): PR-SB17 (Plate 5, Fig. 20)

Striatojaponocapsa synconexa O'Dogherty, Goričan & Dumitrica: PR-SB05 (Plate 2, Figs. 8, 9), PR-SB21 (Plate 6, Figs. 6, 7), PR-SB23 (Plate 6, Figs. 23, 24)

Svinitzium (?) *mizutanii* Dumitrica: PR-SB11 (Plate 4, Fig. 11)

Svinitzium depressum (Baumgartner): PR-SB01 (Plate 1, Fig. 8)

Svinitzium kamoense (Mizutani & Kido): PR-SB05 (Plate 2, Fig. 1), PR-SB23 (Plate 6, Fig. 15)

Syringocapsa (?) *limatum* Foreman: PR-SB30 (Plate 9, Fig. 16)

Tethysetta boesii (Parona): PR-SB01 (Plate 1, Fig. 7)

Tetraditryma sp.: PR-SB05 (Plate 2, Fig. 12)

Thanarla aff. *veneta* (Squinabol): PR-SB27 (Plate 8, Fig. 10)

Thanarla brouweri (Tan): PR-SB27 (Plate 8, Fig. 11)

Thanarla cf. *conica* (Aliev): PR-SB11 (Plate 4, Fig. 8)

Thanarla sp.: PR-SB26 (Plate 7, Fig. 3), PR-SB27 (Plate 8, Fig. 12)

Theocampe (?) sp.: PR-SB07 (Plate 2, Figs. 16–18)

Transhsuum cf. *hisuikyoense* (Isozaki & Matsuda): PR-SB24 (Plate 6, Fig. 34)

Transhsuum cf. *maxwelli* gr. (Pessagno): PR-SB24 (Plate 6, Fig. 35)

Transhsuum maxwelli gr. (Pessagno): PR-SB23 (Plate 6, Figs. 11, 12)

Transhsuum spp.: PR-SB14 (Plate 4, Fig. 28), PR-SB21 (Plate 6, Fig. 2)

Triactoma parablakei Yang & Wang: PR-SB24 (Plate 6, Fig. 39)

Triactoma spp.: PR-SB08 (Plate 3, Fig. 23)

Triversus (?) sp.: PR-SB05 (Plate 2, Fig. 2), PR-SB23 (Plate 6, Fig. 14)

Tuguriella sp.: PR-SB30 (Plate 9, Fig. 10)

Vallupus hopsoni Pessagno & Blome: PR-SB17 (Plate 5, Fig. 17)

Williriedellum carpathicum Dumitrica: PR-SB17 (Plate 5, Figs. 24, 25)

Williriedellum formosum (Chiari, Marcucci & Prela): PR-SB17 (Plate 5, Figs. 27, 28)

Williriedellum sp.: PR-SB17 (Plate 5, Fig. 26)

Williriedellum tetragona (Matsuoka): PR-SB05 (Plate 2, Fig. 10)

Williriedellum yaoi (Kozur): PR-SB21 (Plate 6, Fig. 8), PR-SB23 (Plate 6, Figs. 21, 22)

Xitus sp.: PR-SB23 (Plate 6, Fig. 17)

Zhamoidellum cf. *testatum* Jud: PR-SB30 (Plate 9, Fig. 14)

References

Abelmann, A., & Gowing, M. M. (1997). Spatial distribution pattern of living polycystine radiolarian taxa—baseline study for paleoenvironmental reconstructions in the southern ocean (Atlantic sector). *Marine Micropaleontology, 30*, 3–28.

Bandini, A. N., Flores, K., Baumgartner, P. O., Jackett, S.-J., & Denyer, P. (2008). Late cretaceous and Paleogene Radiolaria from the Nicoya Peninsula, Costa Rica: a tectonostratigraphic application. *Stratigraphy, 5*(1), 3–21.

Bartok, P. E., Renz, O., & Westermann, G. E. G. (1985). The Siquisique ophiolites, Northern Lara State, Venezuela: A discussion on their Middle Jurassic ammonites and tectonic implications. *Geological Society of America Bulletin, 96*, 1050–1055.

Baumgartner, P. O. (1987). Age and genesis of Tethyan Jurassic radiolarites. *Eclogae geologicae Helvetiae, 80*, 831–879.

Baumgartner, P. O., Bartolini, A., Carter, E. S., Conti, M., Cortese, G., Danelian, T., et al. (1995). Middle Jurassic to Early Cretaceous Radiolarian biochronology of Tethys based on Unitary Associations. In: P. O. Baumgartner, L. O'Dogherty, S. Gorican., E. Urquhart, A. Pillevuit & P. De Wever (Eds.), *Middle Jurassic to Lower Cretaceous Radiolaria of Tethys: Occurrences, systematics, biochronology* (Vol. 23, pp. 1013–1048). Lausanne: Mémoires de Géologie.

Baumgartner, P. O., & Denyer, P. (2006). Evidence for middle cretaceous accretion at Santa Elena Peninsula (Santa Rosa Accretionary Complex), Costa Rica. *Geologica Acta, 4*(1–2), 179–191.

Baumgartner, P. O., Flores, K., Bandini, A. N., Girault, F., & Cruz, D. (2008). Upper Triassic to Cretaceous Radiolaria from Nicaragua and Northern Costa Rica—the Mesquito Composite Oceanic Terrane. *Ofioliti, 33*(1), 1–19.

Baumgartner, P. O., & Matsuoka, A. (1995). New radiolarian data from DSDP Site 534, Blake Bahama Basin, Central Northern Atlantic. In: P. O. Baumgartner, L. O'Dogherty, S. Gorican, E. Urquhart, A. Pillevuit & P. De Wever (Eds.), *Middle Jurassic to Lower Cretaceous Radiolaria of Tethys: Occurrences, systematics, biochronology* (Vol. 23, pp. 709–715). Lausanne: Mémoires de Géologie.

Bill, M., O'Dogherty, L., Guex, J., Baumgartner, P. O., & Masson, H. (2001). Radiolarite ages in Alpine–Mediterranean ophiolites: Constraints on the oceanic spreading and the Tethys–Atlantic connection. *Geological Society of America Bulletin, 113*, 129–143.

Boltovskoy, D., Uliana, E., & Wefer, G. (1996). Seasonal variations in the flux of microplankton and radiolarian assemblage compositions in the northeastern tropical Atlantic at 2195 m. *Limnology and Oceanography, 41*, 615–635.

Bortolotti, V., & Principi, G. (2005). Tethyan ophiolites and Pangea break-up. *The Island Arc, 14*, 442–470.

Bosch, D., Gabriele, P., Lapierre, H., Malfere, J.-L., & Jaillard, E. (2002). Geodynamic significance of the Raspas metamorphic complex (SW Ecuador): Geochemical and isotopic constraints. *Tectonophysics, 345*, 83–102.

Burke, K. (1988). Tectonic evolution of the Caribbean. *Annual Reviews of Earth and Planetary Science, 16*, 201–230.

Carter, E. S., Gorican, S., Guex, J., O'Dogherty, L., De Wever, P., Dumitrica, P., et al. (2010). Global radiolarian zonation for the Pliensbachian, Toarcian and Aalenian. *Palaeogeography, Palaeoclimatology, Palaeoecology, 297*, 401–419.

Chiari, M., Dumitrica, P., Marroni, M., Pandolfi, L., & Principi, G. (2006). Radiolarian biostratigraphic evidence for a Late Jurassic age of El Tambor Group ophiolites (Guatemala). *Ofioliti, 31*(2), 141–150.

Cordey, F., & Cornée, J.- J. (2009). New radiolarian assemblages from La Désirade Island basement complex (Guadeloupe, Lesser Antilles Arc) and Caribbean tectonic implications. *Bulletin de la Societé géologique de France, 180*(5), 399–409.

Cox, D. P., Marvin, R. F., M'Gonigle, J. W., McIntyre, D. H., & Rogers, C. L. (1977). Potassium-argon geochronology of some metamorphic, igneous, and hydrothermal event in Puerto Rico and the Virgin Islands. U.S. Geological Survey. *Journal of Research, 5*, 689–703.

Danelian, T. (2008). Diversity and biotic changes of Archaeodictyomitrid Radiolaria from the Aptian/Albian transition (OAE1b) of southern Albania. *Micropaleontology, 54*(1), 3–13.

De Wever, P., Azema, J., & Fourcade, E. (1994). Radiolarians and radiolarite: Primary production, diagenesis and paleogeography. *Bulletin des Centres de Recherche et Exploration-Production d'Elf-Aquitaine, 18*, 315–379.

De Wever, P., Azema, J., Tournon, J., & Desmet, A. (1985). Découverte de matériel océanique du Lias-Dogger inférieur dans la péninsule de Santa Elena (Costa Rica, Amérique Centrale). *Comptes Rendus de l'Académie des Sciences de Paris, 300*, 759–764.

De Wever, P., Dumitrica, P., Caulet, J.-P., Nigrini, C., & Caridroit, M. (2001). *Radiolarians in the sedimentary record* (p. 533). Amsterdam: Gordon and Breach Science Publishers.

Denyer, P., & Baumgartner, P. O. (2006). Emplacement of Jurassic–Lower Cretaceous radiolarites of the Nicoya Complex (Costa Rica). *Geologica Acta, 4*(1–2), 203–218.

Dumitrica P. (1995). Upper Jurassic and Lower Cretaceous Radiolarians at Svinita (Romania). In: P. O. Baumgartner, L. O'Dogherty, S. Gorican, E. Urquhart, A. Pillevuit & P. De Wever (Eds.), *Middle Jurassic to Lower Cretaceous Radiolaria of Tethys: Occurrences, systematics, biochronology* (Vol. 23, pp. 897–905). Lausanne: Mémoires de Géologie.

Dumitrica, P., Immenhauser, A., & Dumitrica-Jud, R. (1997). Mesozoic Radiolarian Biostratigraphy from Masirah Ophiolite, Sultanate of Oman Part I: Middle Triassic, Uppermost Jurassic and Lower Cretaceous Spumellarians and Multisegmented Nassellarians. *Bulletin of the national Museum of natural Science, Taiwan, 9*, 1–106.

Dumitrica-Jud, R. (1995). Early Cretaceous Radiolarian biostratigraphy of Umbria-Marche Apennines (Italy), Southern Alps (Italy and Switzerland) and Hawasina Nappes (Oman). In: P. O. Baumgartner, L. O'Dogherty, S. Gorican, E. Urquhart, A. Pillevuit & P. De Wever (Eds.), *Middle Jurassic to Lower Cretaceous Radiolaria of Tethys: Occurrences, systematics, biochronology* (Vol. 23, pp. 751–797). Lausanne: Mémoires de Géologie.

Empson-Morin, K. (1984). Depth and latitude distribution of Radiolaria in Campanian (Late Cretaceous) tropical and subtropical oceans. *Micropaleontology, 30*, 87–115.

Favre, P., & Stampfli, G. M. (1992). From rifting to passive margin: The example of the Red Sea, central Atlantic and Alpine Tethys. *Tectonophysics, 215*, 69–97.

Favre, P., Stampfli, G., & Wildi, W. (1991). Jurassic sedimentary record and tectonic evolution of the northwestern corner of Africa. *Palaeogeography, Palaeoecology, Palaeoclimatology, 87*, 53–73.

Ferrari, O. M., Hochard, C., & Stampfli, G. M. (2008). An alternative plate tectonic model for the Palaeozoic–Early Mesozoic Palaeotethyan evolution of the Southeast Asia (Northern Thailand–Burma). *Tectonophysics, 451*, 346–365.

Flores, K. (2009). *Mesozoic oceanic terranes of southern Central America—geology, geochemistry and geodynamics*. Unpublished PhD thesis, Université de Lausanne, Lausanne.

Gordon, W. A. (1974). Physical controls on marine biotic distribution in the Jurassic Period. In: C. A. Ross (Ed.), *Paleogeographic*

provinces and provinciality. S.E.P.M. (Vol. 21, 136–147) Tulsa: Society for Sedimentary Geology, Special Publication.

Gradstein, F. M., Ogg, J. G., Smith, A. G., Agterberg, F. P., Bleeker, W., Cooper, R. A., et al. (2004). *A geologic time scale 2004*. Cambridge: Cambridge University Press.

Guex, J. (1991). *Biochronological correlations* (p. 250). Berlin: Springer.

Gursky, H. J. (1994). The oldest sedimentary rocks of southern Central America: The radiolarian cherts of the Nicoya Ophiolite Comples (?Early Jurassic to Late Cretaceous). *Profil, 7*, 265–277.

Hochard, C. (2008). *GIS and geodatabases application to global scale plate tectonics modelling*. Unpublished PhD Thesis, Université de Lausanne, Lausanne.

Hoernle, K., van den Bogaard, P., Werner, R., Lissinna, B., Hauff, F., Alvarado, G., et al. (2002). Missing history (16–71 Ma) of the Galápagos hotspot: Implications for the tectonic and biological evolution of the Americas. *Geology, 30*(9), 795–798.

Huon, S., Cornée, J. J., Piqué, A., Rais, N., Clauer, N., Liewig, N., et al. (1993). Mise en évidence d'un métamorphisme statique d'âge triassico—liasique lié à l'ouverture de l'Atlantique. *Bulletin de la Societé Géologique de France, 164*, 165–176.

Iturralde-Vinent, M. A. (2006). Meso-cenozoic Caribbean paleogeography: Implications for the historical biogeography of the region. *International Geology Review, 48*, 791–827.

James, K. H. (2009). In situ origin of the Caribbean: Discussion of data. In: K. H. James, M. A. Lorente & J. L. Pindell (Eds.), *The origin and evolution of the Caribbean Plate* (Vol. 328, pp. 77–125). London: Geological Society, Special Publications.

Jenkyns, H., & Winterer, E. (1982). Palaeoceanography of Mesozoic ribbon radiolarites. *Earth and Planetary Science Letters, 60*, 351–375.

Johnston, S. T., & Borel, G. D. (2007). The odyssey of the Cache Creek terrane, Canadian Cordillera: Implications for accretionary orogens, tectonic setting of Panthalassa, the Pacific superwell, and break-up of Pangea. *Earth and Planetary Science Letters, 253*, 415–428.

Jolly, W. T., Lidiak, E. G., Schellekens, J. H., & Santos, H. (1998). Volcanism, tectonics, and stratigraphic correlations in Puerto Rico. In: E. G. Lidiak & D. K. Larue (Eds.), *Tectonics and geochemistry of the Northeastern Caribbean* (Vol. 322, pp. 1–34). Boulder: Geological Society of America, Special Paper.

Jud, R. (1994). Biochronology and systematics of Early Cretaceous Radiolarian of the Western Tethys. *Mémoires de Géologie (Lausanne), 19*, 1–147.

Kiessling, W. (1999). Late Jurassic Radiolarians from the Antarctic Peninsula. *Micropaleontology special issues, 45*, 1–96.

Matsuoka, A. (1995). Late Jurassic tropical Radiolaria: Vallupus and its related forms. *Palaeogeography, Palaeoclimatology, Palaeoecology, 119*, 359–369.

Mattinson, J. M., Pessagno, E. A. Jr., Montgomery, H., & Hopson, C. A. (2008). Late Jurassic age of oceanic basement at La Désirade Island, Lesser Antilles arc. In: J. E. Wright & J. W. Shervais (Eds.), *Ophiolites, arcs, and batholiths: A tribute to Cliff Hopson* (Vol. 438, pp. 175–190). Boulder: Geological Society of America, Special Paper.

Mattson, P. H. (1960). Geology of the Mayaguez Area, Puerto Rico. *Bulletin of the Geological Society of America, 71*, 319–362.

Mattson, P. H. (1964). Petrography and structure of serpentinite from Mayaguez, Puerto Rico. In: C. A. Burke (Ed.), *A study of serpentinite* (pp. 7–24). NAS-NRC publication no. 1188.

Mattson, P. H. (1973). Middle Cretaceous nappe structures in Puerto Rican ophiolites and their relation to the tectonic history of the Greater Antilles. *Geological Society of America Bulletin, 84*, 21–38.

Mattson, P. H., & Pessagno, E. A, Jr. (1979). Jurassic and early Cretaceous radiolarians in Puerto Rican ophiolite; tectonic implications. *Geology, 7*(9), 440–444.

Molina-Cruz, A., Welling, L., & Caudillo-Bohorquez, A. (1999). Radiolarian distribution in the water column, southern Gulf of California, and its implication in thanatocoenose constitution. *Marine Micropaleontology, 37*, 149–171.

Montgomery, H., & Kerr, A. C. (2009). Rethinking the origins of the red chert at La Désirade, French West Indies. In: K. H. James, M. A. Lorente & J. L. Pindell (Eds.), *The origin and evolution of the Caribbean Plate* (Vol. 328, pp. 457–467). London: Geological Society, Special Publications.

Montgomery, H. A., Pessagno, E. A., Jr., Lewis, J. A., & Schellekens, J. H. (1994a). Paleogeography of the Jurassic fragments of the Caribbean. *Tectonics 13*, 725–732.

Montgomery, H., Pessagno, E. A. J., & Muñoz, I. M. (1992). Jurassic (Tithonian) Radiolaria from La Désirade (Lesser Antilles): Preliminary paleontological and tectonic implications. *Tectonics, 11*, 1426–1432.

Montgomery, H., Pessagno, E. A, Jr, & Pindell, J. L. (1994b). A 195 Ma Terrane in a 165 Ma Sea: Pacific Origin of the Carribbean Plate. *GSA Today, 4*(1), 2–6.

O'Dogherty, L. (1994). Biochronology and Paleontology of Mid-Cretaceous Radiolarians from Northern Apennines (Italy) and Betic Cordillera (Spain). *Mémoires de Géologie (Lausanne), 21*, 1–415.

O'Dogherty, L., Carter, E. S., Dumitrica, P., Gorican, S., De Wever, P., Bandini, A. N., et al. (2009a). Catalogue of Mesozoic radiolarian genera. Part 2: Jurassic-Cretaceous. *Geodiversitas, 31*(2), 271–356.

O'Dogherty, L., Carter, E. S., Dumitrica, P., Gorican, S., De Wever, P., Hungerbuehler, A., et al. (2009b). Catalogue of Mesozoic radiolarian genera. Part 1: Triassic. *Geodiversitas, 31*(2), 213–270.

Pessagno, E. A., Blome, C. D., Hull, D. M., & Six, W. M. (1993). Jurassic Radiolaria from the Josephine ophiolite and overlying strata, Smith River subterrane (Klamath Mountains), northwestern California and southwestern Oregon. *Micropaleontology, 39*, 93–166.

Pessagno, E. A., Longoria, J., MacLeod, N., & Six, W. (1987). Studies of North American Jurassic Radiolaria; Part I, Upper Jurassic (Kimmeridgian-upper Tithonian) Pantanelliidae from the Taman Formation, east-central Mexico; tectonostratigraphic, chronostratigraphic, and phylogenetic implications. *Cushman Foundation for Foraminiferal Research Special Publication, 23*, 1–51.

Pessagno, E. A. Jr., & Blome, C. D. (1986). Faunal affinities and tectonogenesis of Mesozoic rocks in the Blue Mountains of eastern Oregon and western Idaho. In: T. L. Wallier & H. C. Brooks (Eds.), *Geologic implications of paleozoic and Mesozoic paleontology and biostratigraphy* (Vol. 1435, pp. 65–78). Blue Mountains Province: U.S. Geological Survey, Professional Paper.

Pessagno, E. A., Whalen, P., & Yeh, K. Y. (1986). Jurassic Nassellariina (Radiolaria) from North American geologic terranes. *Bulletins of American Paleontology, 9*, 1–75.

Pindell, J. L., & Kennan, L. (2007). *Rift models and the salt-cored marginal wedge in the northern Gulf of Mexico: implications for deep water Paleogene Wilcox deposition and basinwide maturation*. In: L. Kennan, J. L. Pindell & N. C. Rosen (Eds.), Transactions of the 27th GCSSEPM Annual Bob F. Perkins Research Conference. The Paleogene of the Gulf of Mexico and Caribbean Basins: Processes, Events and Petroleum Systems (pp. 146–186).

Pindell, J. L., & Kennan, L. (2009). Tectonic evolution of the Gulf of Mexico, Caribbean and northern South America in the mantle

reference frame: An update. In: K. H. James, M. A. Lorente & J. L. Pindell (Eds.), *The origin and evolution of the Caribbean Plate* (Vol. 328, pp. 1–55). London: Geological Society, Special Publications.

Pindell, J. L, Kennan, L., Maresch, W. V., Stanek, K. P., Draper, G., & Higgs, R. (2005). Plate-kinematics and crustal dynamics of circum-Caribbean arc-continent interactions: Tectonic controls on basin development in Proto-Caribbean margins. In: H. G. Avé Lallemant & V. B. Sisson (Eds.), *Caribbean–South American plate interactions, Venezuela* (Vol. 394, pp. 7–52). Boulder: Geological Society of America, Special Paper.

Price, G. D. (1999). The evidence and implications of polar ice during the Mesozoic. *Earth-Science Reviews, 48*, 183–210.

Pszczolkowski, A. (1978). Geosynclinal sequences of the Cordillera de Guaniguanico in western Cuba; their lithostratigraphy, facies development, and paleogeography. *Acta Geologica Polonica, 28*(1), 1–96.

Pszczolkowski, A. (1999). The exposed passive margin of North America in western Cuba. In: P. Mann (Ed.), *Caribbean basins. Sedimentary basins of the world* (Vol. 4, pp. 93–121). Amsterdam: Elsevier Science B.V.

Pszczolkowski, A., & Myczynski, R. (2003). Stratigraphic constraints on the Late Jurassic–Cretaceous paleotectonic interpretations of the Placetas Belt in Cuba. In: C. Bartolini, R. T. Buffler & J. F. Blickwede (Eds), *The circum-Gulf of Mexico and the Caribbean; hydrocarbon habitats, basin formation, and plate tectonics* (Vol. 79, pp. 545–581). Memoir: American Association of Petroleum Geologists.

Racki, G., & Cordey, F. (2000). Radiolarian palaeoecology and radiolarites: Is the present the key to the past? *Earth-Science Reviews, 52*, 83–120.

Schellekens, J. H., Montgomery, H. M., Joyce, J., & Smith, A. L. (1990). *Late Jurassic to Late Cretaceous development of island-arc crust in southwestern Puerto Rico*. In: D. K. Larue & G Draper (Eds.), *Transactions of 12th Caribbean Geological Conference* (pp. 268–281), St. Croix, U.S. Virgin Islands.

Sisson, V. B., Avé Lallemant, H. G., Ostos, M., Blythe, A. E., Snee, L. W., Copeland, P., Wright, J. E., Donelick, R. A., & Guth, L. R. (2005). Overview of radiometric ages in three allochthonous belts of northern Venezuela: Old ones, new ones, and their impact on regional geology. In: H. G. Avé Lallemant & V. B. Sisson (Eds.), *Caribbean–South American plate interactions, Venezuela* (Vol. 394, pp. 91–117). Boulder: Geological Society of America, Special Paper.

Stampfli, G. M., & Borel, G. D. (2002). A plate tectonic model for the Palozoic and Mesozoic constrained by dynamic plate boundaries and restored synthetic oceanic isochrones. *Earth and Planetary Science Letters, 196*, 17–33.

Stampfli, G. M., & Hochard, C. (2009). Plate tectonics of the Alpine realm. In: J. B. Murphy, J. D. Keppie & A. J. Hynes (Eds.), *Ancient orogens and moderns analogues* (Vol. 327, pp. 89–111). London: Geological Society, Special Publications.

Steiner, C., Hobson, A., Favre, P., Stampfli, G. M., & Hernandez, J. (1998). Mesozoic sequence of Fuerteventura (Canary Islands): Witness of Early Jurassic sea-floor spreading in the central Atlantic. *Geological Society of America Bulletin, 110*, 1304–1317.

Tobisch, O. T. (1968). Gneissic amphibolite at Las Palmas, Puerto Rico, and its significance in the early history of the Greater Antilles island arc. *Geological Society of America Bulletin, 79*, 557–574.